

# Lawrence Berkeley National Laboratory

## Recent Work

### Title

ISOTHERMAL TRANSFORMATION STUDIES ON THE EFFECT OF ALLOYING ELEMENTS (Mo, Ni, Cr, Mn, AT, Si, Co) IN STEELS ON THE KINETICS OF THE AUSTENITE TO BAINITE TRANSFORMATION

### Permalink

<https://escholarship.org/uc/item/3b06k3hx>

### Author

Llopis, Ana Maria.

### Publication Date

1976-12-01

UC-25

LBL-6068

c1

ISOTHERMAL TRANSFORMATION STUDIES ON THE  
EFFECT OF ALLOYING ELEMENTS  
(Mo, Ni, Cr, Mn, Al, Si, Co) IN STEELS ON THE  
KINETICS OF THE AUSTENITE TO  
BAINITE TRANSFORMATION

Ana Maria Llopis  
(Ph. D. thesis)

December 1976

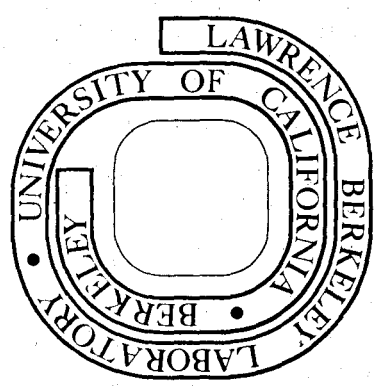
RECEIVED  
LAWRENCE  
BERKELEY LABORATORY

NOV 8 1977

LIBRARY AND  
DOCUMENTS SECTION

Prepared for the U. S. Department of Energy  
under Contract W-7405-ENG-48

**For Reference**  
Not to be taken from this room



LBL-6068

c1

## DISCLAIMER

This document was prepared as an account of work sponsored by the United States Government. While this document is believed to contain correct information, neither the United States Government nor any agency thereof, nor the Regents of the University of California, nor any of their employees, makes any warranty, express or implied, or assumes any legal responsibility for the accuracy, completeness, or usefulness of any information, apparatus, product, or process disclosed, or represents that its use would not infringe privately owned rights. Reference herein to any specific commercial product, process, or service by its trade name, trademark, manufacturer, or otherwise, does not necessarily constitute or imply its endorsement, recommendation, or favoring by the United States Government or any agency thereof, or the Regents of the University of California. The views and opinions of authors expressed herein do not necessarily state or reflect those of the United States Government or any agency thereof or the Regents of the University of California.

ISOTHERMAL TRANSFORMATION STUDIES ON THE EFFECT  
OF ALLOYING ELEMENTS (Mo, Ni, Cr, Mn, Al, Si, Co) IN  
STEELS ON THE KINETICS OF THE AUSTENITE TO BAINITE TRANSFORMATION

Contents

Abstract . . . . .		vii
I. Introduction . . . . .		1
II. Experimental Procedures . . . . .		5
A. Materials . . . . .		5
1. Choice of Alloy Compositions . . . . .		5
2. Preparation . . . . .		7
3. Chemical Analysis . . . . .		7
B. Experimental . . . . .		8
1. Apparatus Description . . . . .		8
2. A Typical Run . . . . .		10
C. Thermodilatometric Experiments . . . . .		11
1. Austenite Transformation Temperature . . . . .		11
2. $M_s$ Temperatures . . . . .		11
3. Isothermal Runs in the Bainite Reaction Range . . . . .		12
4. Graphical Examples of Two Typical Runs . . . . .		12
D. X-Ray Analysis . . . . .		13
1. Determination of Retained Austenite for the Saturation Level . . . . .		13
E. Hardness Testing . . . . .		14
F. Optical Microscopy . . . . .		14



III. Results and Discussion . . . . .	16
A. Austenite Transformation Temperature . . . . .	16
B. $M_S$ Temperature and Hardness Values . . . . .	18
1. Martensite Transformation Temperature . . . . .	18
2. Discussion of Some Available Empirical Formulae for $M_S$ Determination on the Basis of Alloy Content	19
3. Effect of Austenitizing Temperature on $M_S$ . . . . .	22
4. Hardness Data of $M_S$ Structures. Proposed Linear Relationship between Hardness and $M_S$ Temperature of the Alloys . . . . .	23
5. Effect of Quenching Rate of $M_S$ . . . . .	24
C. Bainite Transformation Data . . . . .	26
1. Isothermal Transformation for the Various Alloys .	26
2. TTT Diagrams of the Austenite to Bainite Transformation . . . . .	26
3. Effect of Alloying Elements . . . . .	30
4. Effect of Quenching Rate on the Kinetics and Reproducibility . . . . .	38
5. Retained Austenite Levels . . . . .	39
6. Discussion of the Effect of Austenitizing Temperature on the Bainite Transformation Kinetics	41
7. Determination of $B_S$ on the Basis of Some Existing Empirical Equations . . . . .	43
8. Hardness Data for Bainitic Structures . . . . .	44

D.	Analysis of the Available Empirical Rate Equations . . .	45
1.	Johnson-Mehl Equation . . . . .	45
2.	Austin-Ricket Equation . . . . .	49
3.	Proposed Generalized Equation . . . . .	51
4.	Considerations on Activation Energies . . . . .	53
E.	Optical Microscopy and ASTM Grain Size Characterization	56
1.	ASTM Grain Size of the Treatments Used . . . . .	56
2.	Effect of Austenitizing Temperature on the Grain Size . . . . .	56
3.	Optical Microscopy of the Martensitic Structures . .	57
4.	Optical Microscopy of the Bainitic Structures . . .	57
IV.	Conclusions . . . . .	61
	Acknowledgements . . . . .	64
	Appendix 1. Determination of Retained Austenite by Means of X-Ray Analysis . . . . .	66
	Appendix 2. Hardness vs $M_s$ Transformation Temperature Equation . . . . .	72
	Appendix 3. Activation Energy . . . . .	74
	References . . . . .	77
	Tables . . . . .	83
	Figure Captions . . . . .	122
	Figures . . . . .	128

ISOTHERMAL TRANSFORMATION STUDIES ON THE EFFECT  
OF ALLOYING ELEMENTS (Mo, Ni, Cr, Mn, Al, Si, Co) IN  
STEELS ON THE KINETICS OF THE AUSTENITE TO BAINITE TRANSFORMATION

Ana Maria Llopis

Materials and Molecular Research Division, Lawrence Berkeley Laboratory  
and  
Department of Materials Science and Engineering,  
University of California, Berkeley, California 94720

ABSTRACT

Thermodilatometric experiments were performed on seven Fe-C-X ternary systems (where X = Mo, Ni, Cr, Mn, Al, Si, Co) at different alloy concentrations. TTT diagrams for the isothermal decomposition of austenite in the bainite range were obtained. Extension of these experiments included combinations of some of the alloying elements such as Fe-C-Mo-Ni, Fe-C-Mo-Cr, Fe-C-Ni-Cr in order to determine what their interaction effects were in the bainite transformation.

All the alloying elements studied, accelerated the austenite decomposition for isothermal treatments just above the  $M_s$  giving for the reaction start curve an S-like curve.

Present results indicated that Mn, Ni, Cr and Al retarded the bainite reaction. The bainite reaction below 500°C was unaffected by Si when present by itself and was accelerated by the presence of Co, and by the presence of Mo to a lesser degree.

Combined additions had a synergistic effect on reaction start times for the isothermal decomposition of the austenite and suggested interaction effects (e.g., Ni-Cr, Mo-Cr, Mo-Ni systems). However, the effect of three combined additions on kinetics of further stages of transformation were less well defined.

Retained austenite levels for the bainite transformation were below 5% with the exception of the 2.93 Si alloy which for some temperatures was as high as 7%. Therefore, within 5% error, the saturation level for the reaction was 95% transformed.

Analysis of the kinetic data has been performed using well-known, empirical-rate equations such as the Johnson-Mehl, and the Austin-Rickett equations. A generalized empirical rate equation is proposed to satisfy all the boundary conditions not satisfied by the above two equations. Apparent activation energies obtained from the data could not be associated with the activation energies of carbon diffusion ferrite or austenite implying that there were other controlling processes in the bainite reaction.

Interpretation of the results for Cr, Ni, Mn, Si and Co were in good agreement with the "drag effect" produced by the segregation of certain alloying elements to austenite/ferrite boundaries.

## I. INTRODUCTION

The bainite transformation in steels was investigated and described for the first time 40 years ago by Davenport and Bain and this type of transformation was named after Bain.<sup>8</sup>

Even today, the bainite transformation is still the subject of debate and controversy.<sup>9</sup> There are several schools of thought on what metallographic and mechanistic features characterize it.

It has been proposed by Aaronson that a definition in terms of morphology should be accepted.<sup>10</sup> From a microstructural viewpoint, bainite is defined as a nonlamellar aggregate of ferrite and carbide with an acicular morphology. There have been observations, since the beginning of the bainitic studies, of two variants of bainite,<sup>8,11-16,52,53</sup> upper and lower bainite. In upper bainite the carbides precipitate along the lath boundaries of ferrite laths whereas for lower bainite the carbides precipitate within the ferrite plates at an angle of 55-65° to the major growth direction.

Differentiating these two structures is sometimes difficult and not always possible because morphology of bainite changes gradually with reaction temperature so no pronounced structural changes are observed over small temperature changes.<sup>13,16,17</sup>

The bainite reaction overlaps the proeutectoid ferrite and pearlite reactions at higher temperatures and the martensitic reaction at low temperatures. Bainite can be formed either by continuous cooling or by isothermal transformation.

In contrast to the pearlitic reaction, bainitic transformations can be characterized by a diffusion controlled growth in conjunction with martensitic crystallography. This is primarily based on the fact that at the temperatures of the formation of bainite, the iron and substitutional atoms transform mainly by a cooperative shear transformation from austenite into ferrite, while the carbon atoms diffuse individually so that changes in concentration and precipitation of carbide are possible (surface relief effects have been observed).<sup>57</sup>

The kinetics are predominantly determined by the diffusion of the faster diffusing component.

The "kinetic" definition describes bainite in terms of its own C-curve which is increasingly incomplete as the highest temperature of this curve is approached. Recent evidence indicates, however, that these phenomena (of separate C-curves for pearlite and bainite transformations) develop only in the presence of certain alloying elements that retard the kinetics of the proeutectoid ferrite reaction, particularly at intermediate transformation temperatures.<sup>56</sup>

Very little work has been done on the effect of alloying elements on the kinetics of the bainite reaction, as opposed to the work done on the pearlite and proeutectoid ferrite. Recent systematic studies<sup>17,18</sup> on commercial alloy steels with a magnetometric technique have shown that the various alloying elements affect the kinetics of the bainite reaction differently. A series of bainite reaction TTT diagrams were obtained for 4340 with alloying additions (Mo, Ni, Cr, Mn, Si). Previous results were published<sup>17,18,81</sup> on different alloy steels.

The commercial steels and in particular 4340 in which these systematic studies were performed may be characterized as multi-component systems (0.39C, 0.7Mo, 0.28Si, 0.76Cr, 1.7Ni, 0.2Mn, 0.22Cu). The results of additions of more than one alloying element showed complex, rather than additive, effects on the bainite hardenability kinetics.

Because so many alloying elements were present, it was difficult to assert what the actual influence on the kinetics was due to. Many possible interactions were involved.

The primary objective of this investigation was to follow a systematic experimental investigation by means of thermodilatometric studies. It was unfortunate that this was not possible in all the ternary Fe-C-X ternary systems because some of the reactions took place in fractions of a second. Nonetheless, several ternary systems could be studied (Mo, Ni, Cr, Mn, Si, Al, Co).

As a secondary objective, some quaternary systems were studied to indicate possible interaction effects. It is hoped that these studies will be continued in the future for a complete overview of the problem and to provide a statistical basis for the analysis of a multi-component system.

A fundamental knowledge was not expected from these studies because of the complexity of the systems but a qualitative understanding of interactions and their relative effectiveness on bainite hardenability was found.

The most recent work in the field of "steels" for the past years has focused on alloy design. It is well-known that the microstructure

of alloys has major influence on their mechanical properties. If theories that relate microstructures to mechanical properties are developed and then applied, the empiricism of alloy design can be reduced.<sup>1,27</sup>

The design of new alloys, or obtaining considerable improvements in the properties of the existing ones, largely involves achieving microstructural control through variations in chemical composition and heat treatment. An understanding of the kinetic mechanisms of formation and reaction product morphologies of the bainite transformation appears to be essential. Some commercial tempered martensitic steels have good pearlitic hardenability without good bainitic hardenability. In these steels significant amounts of ferrite, upper bainite, and lower bainite may form during quenching. In small amounts, either ferrite or upper bainite are generally considered to have detrimental effects on the fracture toughness. However, lower bainite has been considered comparable to tempered martensite,<sup>5-7</sup> although some conflicting evidence exists.<sup>2-4</sup>

It is hoped that future research on the factors that affect the kinetics, thermodynamic, chemical, and morphological aspects of the transformation, and the correlation of microstructure with mechanical properties and heat treatments, could lead to improved progress of alloy design.

Several reviews on the austenite to bainite transformations have been published during the past years. For a more complete list see Refs. 9, 13-15, 45, 50, 56, 76 and 80.



## II. EXPERIMENTAL PROCEDURES

### A. Materials

#### 1. Choice of Alloy Compositions

The choice of materials was made keeping in mind the need for a simple iron-base system that would permit the study of the bainite transformation. The binary system Fe-C was discarded because the austenite to pearlite transformation in these alloys is very fast interfering with kinetic studies of bainite and producing resulting mixed structures. One needed alloying elements that would improve the separation of the bainite and pearlite reactions, so that their reactions would not interfere. This was possible in most of the alloys chosen, and it was found for the different alloys that this was attained in different degrees.

The elements Mo, Cr, Ni, Mn were initially chosen. Ni and Mn are austenite stabilizers, Mo and Cr are ferrite formers.<sup>3,20,23</sup> In a second part of the investigation where the carbon content was higher, Al, Si, and Co were studied and of these elements Al and Si are ferrite formers.

All these elements behave differently with respect to their effects on carbon diffusion in austenite. On the basis of diffusion of carbon in austenite, it decreases with increasing contents of Cr, Mo, Mn, Al (in order of effectiveness), and increases in the presence of Ni and Si. So it is expected that they could have different effects on the transformation kinetics, especially in the upper bainite range which

seems to be a process controlled by nucleation and growth where diffusion plays an important role.<sup>56,76,80,17,57</sup>

Also, the diffusivities of these alloying elements in gamma ( $\gamma$ ) or alpha ( $\alpha$ ) iron are different, probably having some effect, if partitioning takes place at the interfaces, on the kinetics of growth.

The activation energies for diffusion of the alloying elements in  $\gamma$  and  $\alpha$  iron are given in Table I from data compiled by Blanter<sup>22</sup> and Krishtal.<sup>21</sup>

Considerations were also taken as to the data of existing studies in higher component low alloy steels. Examples are the bainite TTT diagrams given by Babu,<sup>17</sup> ASTM,<sup>19</sup> Irving and Pickering,<sup>24</sup> and Kinsman and Aaronson.<sup>25</sup> Ni, Cr, Mn, and Si seemed to retard the bainite reaction as opposed to Co and Mo which in some cases was found to accelerate it.

Therefore, it was most interesting to study what these elements would do in ternary Fe-C-X systems.

The compositions were chosen on the basis of amounts that seemed to affect the transformation most from results available on commercial and other alloy steels. It was found that Mn should be effective in the range (2-3) wt%, Ni and Cr in the (1-2) wt%, and Mo in the (0.3-0.5) wt% (Mo should not be higher than 0.4% to avoid undissolved carbides that would require going to higher austenitizing temperatures or holding much longer than 15 min at this temperature), Al(1-2)%, (not higher because at the austenitizing treatment chosen,  $\alpha + \gamma$  phase

would be stable instead of  $\gamma$  only for higher Al contents),  $^{54}\text{Co}$ (0.5-1)%, and Si(1-3)%.

The C content for the Al, Si, Co was higher at 0.4% instead of 0.3% in order to help retard the reaction a little bit further, especially since Co was expected to accelerate it. The variations from the nominal compositions of alloy or C content were due mainly to initial processing treatments.

A list of alloys prepared and their nominal compositions are given in Table II.

## 2. Preparation

A series of 20 lb ingots were cast following the specifications of alloy compositions given in Table II.

The homogenization procedure consisted of high temperature treatments either at 1100°C for 72 hr under vacuum or at 1400°C for 24 hr under vacuum. After the ingots had been homogenized, they were softened by holding at 500°C for 4 hr.

Dilatometer specimens were prepared by cutting from the cold rolled strips (according to specifications in Fig. 1).

## 3. Chemical Analysis

Chemical analyses were made in all cases by spectroscopic atomic absorption methods. This was done twice with very good consistency except for the low carbon values (e.g., alloys I, X) where there was a maximum relative variation of 8%. A LECO carbon analysis was also done for some specimens which showed good agreement with the average

absorption values. The average chemical compositions from all this analysis are given in Table II.

Emphasis was made on the chemical analysis due to the fact that it was most important to know what the actual alloy content was for the comparative studies on the kinetics of the reaction for future analyses.

It was known from previous works that the homogenizing treatment changed the chemical composition slightly, therefore, our results were taken after the homogenization.

As was pointed out previously,<sup>77,78</sup> it was most important to check at random for other alloying elements such as O, B, S, P, which if present even in very low concentrations would affect these experiments considerably. The concentrations of these elements were measured and was found to be less than 0.001 or 0.005% the limits of detection methods available (chemical spectroscopic atomic absorption). Therefore, it was concluded that the samples were free from these impurities (see Table IV).

## B. Experimental

### 1. Apparatus Description

The experimental apparatus is a Theta-dilatometer. It consists of a measuring module chamber (see Fig. 3), a vacuum system (Figs. 4 and 5) and a recording system, that can record as fast as 20 in./min corresponding to  $10^{-3}$  sec given a reading accuracy of 0.02 in.<sup>28</sup>

The recording, main power, and furnace control units can operate under manual or programmed operating conditions. The transformations

transformations were measured as a function of length changes which form as a consequence of the volume change between austenite and the several low temperature forms of the alloys. The specimens were mounted between the gap of two quartz holders with holes inside to let the quenching gas flow through the specimen (see Fig. 2).

In these studies the interest was not in the absolute volume changes or length changes but rather on where the transformation (volume changes) starts and proceeds with time at a given isothermal hold or temperature gradient. Nevertheless, the equipment was calibrated each time a new set of runs was made, and zeroed for each individual specimen.

The vacuum system consists of a mechanical and a diffusion pump which permitted vacua of  $10^{-5}$  to  $10^{-6}$  Torr range with addition of liquid nitrogen and otherwise in the  $10^{-5}$  to  $10^{-4}$  Torr range.

The experimental runs were done in the second range after it was found that there was no decarburization and improving the vacuum did not change the conditions (no oxidation) at the austenitizing temperature treatment of  $1080^{\circ}\text{C}$  for 15 min.

The measuring module chambers and the main parts are specified in Fig. 3. The schematic module shown in part in Fig. 2 slides in the furnace in such a way that the specimen is placed in the center of the induction coil before each treatment.

The equipment is designed in such a way that it is very sensitive to any length change giving an immediate signal in the recording system depending on the sensitivity level.

As in any horizontal dilatometer problems are introduced if the specimen is at any angle rather than aligned to the quartz holders because only the horizontal component of the length change would be recorded. Therefore, extra care was taken when mounting each specimen within the chamber.

The thermocouple used was a Pt, Pt-Rd thermcouple attached to the outer surface of the specimen. Of course, there is always going to be a temperature gradient with respect to the thickness, but since the specimens were thin, (1/16 in. wall thickness), the temperature gradient was neglected. Heat transfer calculations showed the worst case to be a 4-5°C difference between the inner and outer surface.<sup>29</sup>

## 2. A Typical Run

The main features of a typical run consist of heating the specimen under vacuum to the austenitizing temperature, 1080°C. Once the specimen was inside the induction furnace and under vacuum, a programmed controlled heating cycle started the heating process with typical heating rates of 6.7°/sec. The specimen was held at the austenitizing temperature of 1080°C for 15 min to allow for carbide dissolution. The next step was to quench the specimen to the desired temperature range with He gas flow (before this step, one must close the chamber from high vacuum and the chamber will remain closed for the rest of the run to avoid damaging the diffusion pump).

For the alloy compositions used, the kinetics of the reactions were sufficiently fast that it was desirable to have the quenching rates as fast as possible. Thus experimental runs were made, in

most cases, to use the maximum quenching rate capacity of the equipment. The maximum pressure of the He inlet was 30 pounds per minute which gave quenching rates depending on the final temperatures involved but the average values are given in Table V.

When isothermal runs were finished the specimen was again quenched to room temperature and finally (after using the ventilation valve to balance to atmospheric pressure) the specimen was removed, and the system was ready for the next run.

### C. Thermodilatometric Experiments

#### 1. Austenite Transformation Temperature

Each austenitizing run consisted of heating the sample from room temperature to the austenitizing temperature. In the temperature range where the austenite transformation occurred, the volume (therefore, length) changes associated with the transformation were recorded to attain the values of austenite start and finish temperatures. Many runs were made on each composition. The values tabulated in Table VI are averages of at least 8 runs.

#### 2. M<sub>s</sub> Temperatures

In a similar fashion, the specimen was quenched to room temperature and the martensite transformation was recorded. This was very useful information for the bainite studies in order to choose a temperature range above the M<sub>s</sub> for the kinetic investigation (results in Table VII).

### 3. Isothermal Runs in the Bainite Reaction Range

The specimen was quenched to the desired temperature and held until the reaction was complete or reached a value of saturation. For some cases, however, it was found that after a maximum increase in length and saturation of the reaction there was a very slow decrease in the length of the specimen. This was attributed to a relaxation effect of the quartz holders and was not considered as part of the transformation. In other experiments<sup>30</sup> for Nb, Al, Ni, that had no reactions at these ranges of temperatures, there was a similar slow decrease in length with time which was due to the relaxation of the quartz holders.

### 4. Graphical Examples of Two Typical Runs

The typical runs, as described previously, result in chart signals as indicated in Fig. 6 for the martensite transformation and Fig. 7 for a bainite transformation. It is worth pointing out that the temperature and length changes have a lag of (1/16 in.) so this must be considered when  $A_s$ ,  $A_f$ ,  $M_s$  and  $M_f$  are recorded.

The heating rate, quenching rate, and austenitizing treatments are pointed out for the martensitic transformation, in the case of continuous cooling (Fig. 6), and for the case of the bainite transformation in an isothermal run (Fig. 7). Changes in scale have been pointed out to give an idea of the time elapsed in the different regions and holds.



D. X-Ray Analysis

1. Determination of Retained Austenite for the Saturation Level.

When dealing with steels whether they are plain carbon or alloy steels, one of the major concerns is the amount of retained austenite present after a phase transformation or present after a sequence of heat treatments have been applied. When dealing with bainitic phase transformations, if we want to construct the corresponding TTT diagrams, we have to compare the level of saturation of each of the transformation reactions, hence the level of retained austenite still present (saturation does not necessarily mean 100% volume transformed) effects the appearance of the TTT diagram.

In order to obtain this information by X-ray means, relative intensity measurements were obtained by a radiation counting procedure discussed in Appendix A.

To avoid preferred orientation effects which would mask the actual volume fraction, several peaks were scanned for austenite, deciding finally on the choice of  $\gamma(220)$  and  $\gamma(311)$  to be compared with  $\alpha(211)$  planes. Other investigators have made this choice as well.<sup>59-61,64</sup>

Using an X-ray diffractometer with Cu radiation ( $K_{\alpha} = 1.542\text{\AA}$ ) source, a LiF monochromator, 40 kV voltage, and 14 Amps current, the corresponding peaks for those planes were located at:

(211)	2 $\theta$	83.5°
(220)	2 $\theta$	74.6°
(311)	2 $\theta$	91°

The amount of retained austenite for the carbon contents involved in the alloys was less than 5% but since the alloying elements could have an effect on this level, careful studies were made nonetheless to establish whether or not this was the case.

#### E. Hardness Testing

By means of a Leitz-Wetzlar microhardness testing unit, the Vickers microhardness values of heat treated specimens were determined. An applied load of 1,000 g was used in measuring the hardness of each specimen from metallographic samples polished and prepared for optical microscopy. Both diagonal indentations were measured and an average value (from five tests made on each specimen) is given as the hardness value (Table XII for the martensitic structures and Table XXXVIII for some of the bainitic structures). These tests were made to compare their relative hardness values and to see if there was any effect from the alloying elements.

#### F. Optical Microscopy

The limitations of optical microscopy are recognized for morphological considerations.<sup>51</sup> The best means of distinguishing the detailed structures would have been transmission electron microscopy, however, due to the size and shape of the specimens for dilatometric studies, it was not possible to prepare thin foils.

Some pictures where martensites and bainites are present are shown in a later section for the purpose of comparison and to see the possible differences due to the differences in alloying elements present.

After each run, most of the specimens were mounted in koldmount. Specimens were ground on Si-carbide papers to 600 grit, and polished on a  $1\mu$  abrasive diamond paste wheel followed by  $0.05\mu$  alumina slurry on a syntron.

All the specimens for structure observation were etched with 2% nital solution, and where prior austenite grain boundaries were desired, a saturated picral solution with a few drops of HCl was used.

The results of the ASTM austenite grain sizes for the heat treatment at  $1080^{\circ}\text{C}$  for 15 min showed that there were variations from specimens of different composition and in some cases with the same composition. The ASTM grain size was in the range of (3-4) or (4-5) which is a coarse grain size.

### III. RESULTS AND DISCUSSION

#### A. Austenite Transformation Temperature

In any hardening process on heat treatment, the heating temperatures and times involved for the steels are one of the most important steps. Careful considerations should be taken because the final properties are profoundly altered by the degree of carbide dissolution, also affected is the degree of homogenization of the alloying elements and carbon.

For many steels, specifically commercial steels, the optimum austenitizing temperature has been established by a long process of experience. However, even here the actual period of time during which diffusion may occur is not stressed (Bain, Paxton).<sup>26</sup>

"No useful diffusion occurs until austenite is established (at a certain minimum temperature) and, thereafter it occurs at a rate that increases very rapidly with increasing temperature of heating.

Furthermore, the different elements diffuse at such different velocities, that, in principle, at least each composition should be so heated as to assume the required homogeneity of austenite."

The ternary equilibrium systems for some elements have been studied and the results of those for Mo, Mn, Cr, Si,<sup>26</sup> Al,<sup>54</sup> will be compared with the present results.

Table VI shows the data from which, the  $Ae_1(A_s)$  eutectoid and  $Ae_3(A_f)$  temperatures, will be compared.

The results were obtained for the bcc to fcc austenite transformation on heating the specimen from room temperature to the austenitizing temperature (1080°C). For these data the heating rate was fixed by

-17-

a programmed heating treatment where 1080°C was reached in 2.63 min (read on chart as 5.25 in. on the 2 in./min scale). This implied a typical heating rate of 6.73°/sec.

The austenite start was detected from the initial slope change and the austenite finish from the final change before the pick up of the heating rate.

The validity of these results lie within the limits of how much austenite forms before any recordable signal occurs. For example, it must be understood that  $A_s$  is not 0.01% transformed, but more likely 3% transformed and similarly for  $A_f$ .

The values given in Table VI are averaged over 8 or more runs.

Comparative results showed that Cr, Mo, Al and Si restricted the austenite stable region, with Si and Mo being most effective (e.g., alloys XIV and XV with 0.87 wt% and 1.94 wt.% Al respectively, had corresponding  $A_s$ , 746°C and 753°C, and  $A_f$ , 889°C and 960°C, temperatures. One can see how the  $\alpha + \gamma$  region was expanded, therefore, restricting the  $\gamma$  stable region).

Manganese expanded the austenite stable range. (e.g., alloys XII and XIII with 1.67 wt.% and 2.59 wt.% Mn respectively; had corresponding  $A_s$ , 728°C and 715°C, and  $A_f$ , 770°C and 750°C, temperatures). One can see how the  $\alpha + \gamma$  region was restricted expanding the  $\gamma$  stable region slightly.

Finally, Ni and Co exerted little influence (e.g., alloys XIX and XX with 0.52 wt.% and 1.05 wt.% Co respectively; had corresponding  $A_s$ , 747°C and 746°C, with  $A_f$ , 863°C and 850°C). The slight variations in

$A_s$  and  $A_f$  probably correspond to the differences in the carbon contents 0.35 and 0.33 wt.% respectively.

These results were in agreement with published results.<sup>26,54</sup> It can be said according to Bain and Paxton's results and these results that the choice of 1080°C as an austenitizing temperature for carbon contents below 0.4 wt% was a good choice. This choice enables the carbon to be dissolved in austenite for all the alloys.

For steels that have two or more alloying elements, systematic studies have been done in very few instances so no comparison was made. It is suggested that if one element raises the transformation temperature and the other lowers the transformation temperature the effect is not additive or average.

Also note, for instance, the fact that Fe-C-Cr (VI) and Fe-C-Mo (VII), and Fe-C-Cr-Mo (X) showed that the interaction effect of Cr-Mo was less effective in raising  $A_{e1}$  ( $A_s$ ) than their independent effect.

#### B. $M_s$ Temperature and Hardness Values

##### 1. Martensite Transformation Temperature

The martensite transformation temperatures of the different alloys were obtained under the following experimental conditions. Heating rate 6.73°/sec with an average quenching rate of 85°/sec.\*

The same pressure of the He gas lead to slight variations from the average QR = 85°/sec. In order to be consistent in comparative

---

\* This quenching rate is an average over the whole temperature range. Actually, the first 600° of quenching have a much faster rate QR = 180°/sec which corresponded to a He pressure inlet of 30 LPM air.

studies we checked the effect of the quenching rate at these levels on the  $M_s$  values and the results indicated no change (as discussed in Section III-B-4). So we could place all of the  $M_s$  values from different compositions and different runs in the same comparative scale despite slight differences in quenching rates.

An  $M_f$  determination is very difficult to make. The martensite reaction is often incomplete even at absolute zero temperature.<sup>26</sup>

The transformation of the last traces of austenite is difficult and there is usually a small amount of retained austenite in the structure of overlapping martensite plates. The values of  $M_s$  and  $M_f$  temperatures for the different alloys studied are given in Table VII.

It is known that the  $M_s$  temperature is markedly affected by the composition of the austenite (being primarily determined by the carbon content and to a lesser extent by the alloy content).

There have been several formulae suggested for the determination of  $M_s$  which presuppose that all the carbides have been dissolved and are usually a result of statistical empirical averages on different alloy steels. They will be discussed in the following section.

## 2. Discussion of Some Available Empirical Formulae for $M_s$ Determination on the Basis of Alloy Content

These formulae in some cases have been discussed by their authors as being limited to a linear dependence approximation which in many cases is far from the actual case.

An equivalent determination of the temperature at which the reaction ends,  $M_f$ , is an extremely difficult task especially because even experimental determination is not consistent as it was pointed out earlier. There are indications as early as 1945 (Grange and Stewart)<sup>34</sup> that carbon depresses the  $M_f$  temperatures even more markedly than it does the  $M_s$  temperatures.

The formulae studied here for comparative purposes with experimental values are the following:

a. Additive types.

Payson and Savage<sup>35</sup>

$$M_s^{\circ}F = 930 - 570C - 60Mn - 50Cr - 30Ni - 20Si - 20Mo - 20W \quad (1)$$

Grange and Stewart<sup>34</sup>

$$M_s^{\circ}F = 1000 - 650C - 70Mn - 35Ni - 70Cr - 50Mo \quad (2)$$

Nehrenberg<sup>36</sup>

$$M_s^{\circ}F = 930 - 540C - 60Mn - 40Cr - 30Ni - 20Si - 20Mo \quad (3)$$

Rowland and Lyle<sup>37</sup>

$$M_s^{\circ}F = 930 - 600C - 60Mn - 50Cr - 30Ni - 20Mo - 20Si - 20W \quad (4)$$

Stevens and Haynes<sup>38</sup>

$$M_s^{\circ}F = 1042 - 853C - 60Mn - 30Cr - 30Ni - 38Mo \quad (5)$$

Andrews<sup>39</sup>

$$M_s^{\circ}C = 539 - 423C - 30.14Mn - 17.7Ni - 12.1Co - 7.5Mo \quad (6)$$

b. Product types. There have been some attempts to take into account second order and higher order terms using product formulae of the alloys and C content.



Carapellas<sup>40</sup>

$$M_S^{OF} = 925(1 - 0.61C)(1 - 0.092Mn)(1 - 0.033Si)(1 - 0.045Ni) \quad (7)$$

$$(1 - 0.070Cr)(1 + 0.120Co)(1 - 0.029Mo)(1 - 0.018W)$$

Andrews<sup>39</sup>

$$*M_S^{OC} = 512 - 453C - 16.9Ni + 15Cr - 9.5Mo + 217(C)^2$$

$$- 71.5(C)(Mn) - 67.6(C)(Cr) \quad (8)$$

The results from these calculations are shown in Table VIII and the variations involved with respect to the present experimental results are given in Table IX.

Results from these calculations showed that Nehrenberg's linear formula for  $M_S$  determination gave the best fit over the 21 alloys studied (previous results, including other alloys as well, gave similar results<sup>55</sup>), followed by Payson and Savage and the Andrews product formula considering interaction effects.

The problems with these formulae and their applicability is that in most of the cases they do not include the effect of Al and Co and some neglect the Si effect.

The major discrepancies of Nehrenberg's values coincided with the lower C contents with respect to the other alloys. Also the ones that included Co or Al deviated from the formula mainly because their effect is not considered by Nehrenberg's additive equation (3). Finally there were some discrepancies with Cr to lesser degree, but these are known to be due to strong interaction effects that are not linear.<sup>39</sup>

---

\* Tried to account for interaction effects and variation from linearity.

Carapella's formula attempting to consider the second order interaction effects in the present cases does not give improved values, on the contrary, it gave a  $\Delta M_S = 31.8^\circ$  against  $\Delta M_S = 11.8$  for Nehrenberg's formula. Also, Grange and Stewart's<sup>34</sup> formula that has been widely used does not give a good fit when compared with the others.

One thing is evident from these type of studies; that is: we are in need of formulae to determine transformation temperatures, but on more theoretical grounds where the factors involved in these determinations of transformation temperatures from the chemical composition should be explained from basic principles.

### 3. Effect of Austenitizing Temperature on $M_S$

The results of the experimental determination of  $M_S$  temperature showed that the austenitizing temperature affected the  $M_S$  values. It was observed that the higher the austenitizing temperature the higher the  $M_S$  (there was a distinct rise, see Table X). For alloy XXI austenitized at  $950^\circ\text{C}$  and  $1085^\circ\text{C}$  there was a  $20^\circ\text{C}$  increase in the  $M_S$  temperature obtained for austenitizing treatment at  $1085^\circ\text{C}$  with respect to that obtained for  $950^\circ\text{C}$  austenitizing temperature. Similarly, for alloys I and IV a change from  $950^\circ\text{C}$  to  $1200^\circ\text{C}$  in austenitizing temperature gave a corresponding  $20^\circ\text{C}$  increase in  $M_S$  (see Fig. 8).

These results are consistent with prior studies by Prakash Babu<sup>17</sup> and Ansell and Breinan<sup>32</sup> and Sastri and West<sup>33</sup> who observed an increase of  $20^\circ\text{C}$  in the  $M_S$  from  $800^\circ\text{C}$  to  $1200^\circ\text{C}$  change in the austenitizing temperature.

The increase in the  $M_s$  is believed to be due to the increase in grain size at higher austenitizing temperatures which could result in a decreased flow strength of the prior austenite. The decreased resistance of the austenite matrix to the deformation accompanying the formation of martensite caused this increase. The effect of austenitizing temperature on grain size is discussed in Section III-E-2 and Fig. 48 summarizes this effect.

4. Hardness Data of  $M_s$  Structures. Proposed Linear Relationship between Hardness and  $M_s$  Temperature of the Alloys.

The Vickers microhardness test for 1000 g load was used. Besides the available compositions three other plain carbon alloys were treated in the same way, with the resulting  $M_s$  average values given in the following table (for comparative purposes)

Alloy	Wt% C	$M_s$
A	0.32C	370°C
B	0.59C	255°C
C	0.88C	200°C

Results are tabulated in Table XII and a plot of microhardness vs carbon content is given in Fig. 9 where the different alloying elements involved are distinguished for each point. A plot of microhardness vs  $M_s$  temperature is also plotted in Fig. 10. A linear regression formula for these results is given in Appendix 2.

It has long been known that the effect of C is fundamental in determining the properties of martensite (i.e., hardness). Small additions at low concentrations are more effective than equal increments at higher

concentrations. A secondary factor is the composition of austenite in terms of alloying elements other than C where the C content is relatively low and the quench is to develop maximum hardness.

In the present case of low C contents (except for the plain C steels A, B, C for comparison) the alloy composition made some differences.

Results indicated that steels containing Mn, Si and Ni gave higher hardnesses than plain C steels while additions of Mo and Co gave lower hardnesses. The additions of Cr and Al resulted in variable hardness with respect to plain C steel.

A comparative curve for plain C steels for 15 kG load on Vickers test is given in Fig. 9.

A linear function was obtained to fit the microhardness vs  $M_s$  transformation temperature results. The lower the  $M_s$  the higher the hardness. Since  $M_s$  is a function of C and the alloying elements there is a relation between hardness and alloying elements (Fig. 10).

The approximate quantitative function gave the following results: (see Appendix 2 for detailed development of Eq. (9))

$$\text{VHN}(1000 \text{ gr}) = -1.913/^{\circ}\text{C} \times M_s(^{\circ}\text{C}) + 1240.9 \quad (9)$$

with coefficient of determination  $r^2 = 0.882$ .

##### 5. Effect of Quenching Rate of $M_s$

Quenching rates obtained for  $M_s$  determination from specimen to specimen were fairly reproducible. Figure 11 shows the average quenching rate values vs the time for quench as the specimens were taken from the austenitizing temperature (1080°C) to their martensite

transformation temperature regions. Figure 11 shows the results for Alloy XIV, similar results were found for other alloys.

Since the variations of the quenching rate were more pronounced in some cases, it was necessary to study the effect of quenching rate on  $M_s$  to see if it would affect the results for comparative purposes.

The results of the  $M_s$  measurements showed that the quenching rate range had no effect on the  $M_s$  temperature for the three alloys studied, see Tables X and XI.

This was also the case independent of the austenitizing temperature. It was found for example, in Alloy XXI that the  $M_s$  was 300°C for 1080°C austenitizing temperature for different quenching rates. Similarly it was 290°C for 950°C austenitizing treatments irrespective of quenching rates.

This result was consistent with a recent publication by Donachie and Ansell<sup>31</sup> where a study over a wide variation of quenching rates and its effect on  $M_s$  was made. According to their study, the  $M_s$  was a function of quenching rate indicated a nominal plateau for slow quenches (which was the present case). Also it indicated that the first changes in the  $M_s$  occur at a quench rate of 8300°C/sec (lower critical rate) and that changes in  $M_s$  ceased to occur at rates above 18,300°C/sec (upper critical quench rate) and that there was a maximum increase of 75°C for high C alloy and 40°C in the low C alloys.

Figure 12 shows where the present quenching rates lie (within a very low band of quenching rates of their study).

### C. Bainite Transformation Data

#### 1. Isothermal Transformation for the Various Alloys

The data are presented in a series of tables from Table XIII to Table XXXII where the run number, the corresponding temperature (in °C) and the times (in secs) for the initial part of the transformation (recordable reaction start), the successive amounts of transformation (i.e., 25%, 50%, and 75% transformed) and finally the saturation of the reaction are given. The corresponding TTT diagrams showing these results (in the usual form of temperature vs log time of transformation) were plotted and are given from Fig. 13 to Fig. 32 and will be discussed in the next section.

They were built on the basis of the dilatometric isothermal data for the austenite to bainite transformation. The specimens whose saturation was complete before 15 min still were held at the isothermal temperature chosen for 15 min. Exceptions were made for those specimens whose reaction completion was slower and required longer times to achieve the saturation levels which was on the  $(10-10^2)$  sec range for most specimens except for the higher temperature range where it could take as long as  $(10^3-10^4)$  sec for the compositions shown.

#### 2. TTT Diagrams of the Austenite to Bainite Transformation

According to Aaronson's review<sup>56</sup> the kinetic definition describes bainite in terms of the following behavior of the overall kinetics of the isothermal reaction.

"(1) On a TTT diagram, the bainite reaction has its own C-curve for the initiation of transformation. Most of this curve usually lies in the temperature range between the C curves for the pearlite reaction and the  $M_s$  temperature. In plain carbon steels the bainite and pearlite C-curves overlap extensively, whereas in steels containing an appreciable proportion of an alloying element that is a strong carbide former the curves can be quite well separated.

(2) The upper temperature of the bainite C-curve here denoted as the "kinetic-bainite start" or "kinetic  $B_s$ " temperature, represents the highest temperature at which bainite can form, and usually lies 100-300°C below the eutectoid temperature range.

(3) Austenite can be completely transformed to bainite at and below a characteristic temperature inappropriately termed the "bainite finish" or  $B_f$  temperature. At higher temperatures, transformation ceases entirely after the austenite matrix has been only partially decomposed. The proportion of the austenite transformed to bainite decreases with increasing temperature becoming zero at the kinetic  $B_s$ ."

It is important to keep this in mind because for some of the higher temperature studies mixed structures of bainite and degenerate pearlites were present. Calculations of  $B_s$  on the basis of empirical rate equations are given in Section C-7.

If one looks in general at the TTT diagrams obtained for the different alloys (I-XX) there are some features which are common to almost all of them. There was an acceleration of the austenite decomposition at isothermal temperature treatments just above the  $M_s$

giving as a result for the reaction start curves, S-shaped rather than a C-shaped curve (Figs. 13-22).

This decrease in the incubation period for the nucleation of lower bainite was observed consistently in all of the 20 alloys studied, and in some cases this effect was more pronounced in alloys containing Mo, Cr, Co.

S-shape curves for the bainite reaction have also been reported by other investigators<sup>17,19,41-43</sup> although their studies were mainly on commercial steels (where many alloying elements have been present).

It should also be pointed out that these curves were extrapolated from experimental data shown in Figs. 13-33. What happens in between these points could be different from these curves although big changes in nucleation times through small temperature ranges should not be expected. This was found in some instances in Co, Si, Cr alloys which from a thermodynamic point of view could be questionable.

In some cases separate C curves for lower and upper bainites start to show as for Fig. 17 (0.29C - 1.01Ni), Fig. 19 (0.17C - 1.0Cr), Fig. 26 (0.37C-0.87Al), Fig. 31 (0.33C - 0.52Co) and Fig. 32 (0.35C - 1.05Co).

As the transformation proceeded it was found that the 25% transformed kinetic curve had in some instances the same shape as the reaction start kinetic curve. This could also happen for further stages of the transformation up to the saturation transformed curve. This was not the case for Mn, Al, Si and Co where the shapes of the corresponding



temperature time curves could be drastically different (see Fig. 27 for Al for instance).

Also it was found that the rate of transformation was not constant and linear extrapolations of times for a certain percent transformed could not be made. It takes, for instance, 10 sec at  $T = 450^{\circ}\text{C}$  for alloy XIV (Fig. 26) to achieve 75% transformed, but to transform the remaining austenite, until saturation is attained, requires approximately 100 sec; therefore, the rate for completion is much slower. This could be due to impingement effects between the already formed bainite plates.

It was also noted as a characteristic, present in almost all cases, that as one went to higher temperatures of transformations ( $T = 550^{\circ}\text{C}$ ) the reaction kinetics became much slower for the start as well as the saturation stages.

Finally, to end up the discussion on general aspects of the TTT diagrams obtained in this investigation it must be said that with the exception of Si for which an upper-lower bainitic bay was not pronounced, there was an effective retardation of the austenite to bainite decomposition which created a bay type shape to the diagram (see Figs. 16, 23, 24, 26, 32 and others).

Since the lower bainitic structure has good mechanical properties it would be ideal to increase its range over that of upper bainite which has detrimental fracture toughness properties. Cr proved to be the most effective in expanding the range of lower bainite to higher temperatures; lower bainite appeared even at an isothermal treatment of  $460^{\circ}\text{C}$ . It has been pointed out through the literature that  $350^{\circ}\text{C}^{17}$  is the transition

temperatures for upper to lower bainite transformations for commercial alloy steels while other investigators<sup>75</sup> have found that it is over a range of temperatures that upper and lower bainite can be found overlapping in kinetics and structure. The present investigation indicated from the kinetics that for these ternary and quaternary systems this transition was in the 450°C neighborhood which was much higher than other authors have indicated but was in more agreement with Pickering's<sup>69</sup> results (see Fig. 34). For a detailed discussion see Section C-7.

The relative dominance of upper and lower bainite reaction is not only determined by the carbon diffusion rates but also by the nucleation rates of carbides and alloying elements present. The alloy composition plays a major role in determining these factors. Hehemann<sup>9</sup> claims that the rate at which precipitation of carbon occurs from the supersaturated ferrite is responsible for the difference in morphology between upper and lower bainite.

### 3. Effect of Alloying Elements

Though alloying components which form substitutionally in the crystals of iron phases cannot be partitioned according to the stable equilibrium in bainitic transformation, they can influence the kinetics of the transformation by means of two factors:<sup>57</sup> first they alter the metastable phase equilibrium and thus activate chemical energies,

G for the partial reaction, and secondly, alloy atoms at reaction fronts can be enriched and dragged thereby their mobility is diminished.

Hillert<sup>57</sup> considered this to be probably the main influence of the alloying elements.

Evidence of partitioning of alloying elements has been found by Scott and Famhan<sup>77</sup> where partitioning of certain elements, particularly Ni was determined for slowly cooled steels (the greater number containing 0.35% carbon). Approximately 3% of the Ni, 18% of the Mn, 33% of the Mo and 35% of the Cr occur in the carbide phase. It was also found that partitioning of one element is not much affected by the presence of another. Sarouson and Domain<sup>76</sup> found partitioning of Pt, Mn and Ni although none was found for Si, Mo, Co, Al, Cr and Cu steels.

Hultgren<sup>83</sup> based his explanation of the kinetic bainite phenomena entirely upon the proeutectoid ferrite reaction.<sup>56</sup> He proposed that the initial product of transformation at temperatures above that of the bay be termed "orthoferrite." This product contains equilibrium (with austenite) proportions of both carbon and alloying element. At lower temperatures it was postulated to be replaced by "paraferrite" which contains a nearly equilibrium concentration of carbon but inherits the full alloy content of the parent austenite. A bay in the TTT diagram is readily derived from such a reaction sequence.

However, electron beam microprobe analysis<sup>56</sup> of specimens of 3% Cr steels reacted at temperatures above and below that of the bay has disclosed no partition of chromium between austenite and ferrite in either the orthoferrite or the paraferrite temperature range. This explanation must accordingly be discarded.

With respect to the kinetics of the transformation the present results showed that (Mn, Al, Cr, Ni) shifted the bainite curves to longer times, increasing the incubation period and lowering the kinetic

bainite start. Different alloying elements affected this differently, Mn being the most effective for the compositions studied and Ni being the least.

Cobalt accelerated the reaction, shifting the bainite curves to shorter times. Here it is important to note that with respect to the simple Fe-C binary system that all of the alloying elements retarded the reaction, or in other words, increased the hardenability of bainite. The bainite reaction in Fe-C system would not be able to be studied with the present techniques due to the velocity at which the reaction would take place (mainly interfering with the very fast pearlite kinetics). Hence it is most important to keep in mind that what is discussed is a comparative analysis for ternary or quaternary systems and when it is said that Co accelerates the reaction it means that further additions of Co decreases the incubation period to shorter times.

Molybdenum accelerated and retarded the reaction. It retarded the reaction for the lower bainite range for further additions of Mo (i.e., 0.29 wt% Mo, 0.39 wt% Mo, 0.49 wt% Mo) where the kinetics of the reaction start were slower. But in the upper bainite range this was not the case; 0.39 wt% Mo was faster than 0.29 wt% but 0.49 wt% Mo was slower. The evidence in this case was not that clear (see Figs. 14 and 15).

Silicon retarded the reaction for higher temperatures while further additions had little influence on the transformation below 500°C. Not only was there a good matching for the kinetics of the transformation start between 0.94 wt% Si, 1.91 wt.% Si, and 2.93 wt% Si, (see Figs. 30-32) but there was also good matching for 25, 50 and 75% transformed.

To emphasize this effect, the three cases for the bainite transformation start are plotted together in Fig. 23.

Some general observations of the bainite reaction kinetics follow:

- i. If one concentrates in observations on the upper bainite nose for the different alloys, then
  - a. Mo additions lowered the nose temperature and accelerated the reaction start,
  - b. Ni additions lowered the nose temperature despite the fact that the C content was higher for the 1.01 wt% than for the 2.04 wt% Ni alloy,
  - c. Al, Cr and Mn behaved similarly to Ni but in order of effectiveness Mn was more effective followed by Ni and Cr (when alone),
  - d. Si reduced the temperature of the nose and decreased the reaction start time, but decreased slightly the saturation time involved,
  - e. Co accelerated the transformation but the data did not seem to fit a smooth S curve and was scattered. Maybe this scattering was due to experimental error because the times involved were so short,
  - f. Combined additions of 1 wt% Cr + 1 wt% Ni was much more effective than 1 wt% Cr and/or 1 wt% Ni alone implying that the interaction was very strong in retarding the bainite reaction, which turned out not be an additive but a synergistic effect. With respect to lowering the  $B_s$ , results showed the effect was not as marked, but rather seems to be additive.
  - g. For combined additions of 0.48 wt% Mo + 1 wt% Ni and 0.99 wt% Cr + 0.47 wt% Mo, the Mo-Ni combination was more effective than

Mo-Cr and again the retardation of bainite was not an additive effect. However, the  $B_s$  decrease suggested additive interactions.

h. For the C-Cr-Ni-Mo combined effect, unfortunately the C content resulting from the initial melting procedure was very low. Nonetheless, for such a low C content the presence of Cr-Ni-Mo and their interaction was strong enough to bring it into the detectable ranges of the equipment.

ii. If one concentrates in observations on the lower bainite region for the different alloys, then

a. Mo additions retarded the kinetics and lowered the reaction temperatures. Since the martensitic transformation temperature was lowered with increasing Mo content, the  $B_s$  was also lowered.

b. Ni did not show an appreciable effect with further additions in retarding the lower bainite kinetics (or increasing its lower bainitic hardenability).

c. Cr raised the temperatures for lower bainite formation expanding the range. This effect was also noted when in addition to Cr other alloys like Mo and Ni were added (Figs. 20 and 21). This effect not present in a Ni-Mo combined steel (see Fig. 22).

d. Mn and Al additions retarded the initial stages of the lower bainite transformation but had negligible effect on subsequent stages or saturation levels compared to unmodified Fe-C alloys.

e. Si as was pointed out earlier did not affect the hardenability of lower bainite when further additions of Si were considered (see Fig. 33). This was also the cases for further stages of transformation.

f. Co was not effective in accelerating the kinetics of lower bainite as if was in upper bainite.

iii. Comparison of other investigations with the present study.

The closest systematic study done in the field was that followed by Prakash Babu<sup>17</sup> with his magnetic permeability technique on 4340 steels with alloying elements added. It was found in that study as well as in the present investigation that the lowering of the  $B_s$  temperature range seemed to be additive whereas the rate of bainite formation was not. Moreover, Babu found that the bainite reaction was retarded by increasing amounts of alloying elements such as (Cr, Ni, Mn, Si) with the exception of Mo when added alone.<sup>17</sup>

In the present investigation the retardation effect was not linear with alloy addition. If simple increasing additions of one element were considered, then, as an example, Ni additions had a negligible effect upon the position of the bainite nose (see Figs. 16 and 17). If combined, interaction effects played a major role, then the order of effectiveness was Ni + Cr followed by Mo + Ni and Mo + Cr in retarding the bainite reaction. Ni was more effective in the presence of Cr which was in agreement with that of Prakash Babu<sup>17</sup> and that of Brophy and Miller.<sup>44</sup>

The fact that Co accelerated the reaction was pointed out by Davenport<sup>8</sup> 40 years ago on additions to commercial alloyed steels.

It is recognized that these are qualitative interferences from the data. But the effects of combination of two or more alloying elements on the bainite transformation were too complex to infer what extent

the effects of one element had on the presence of another element (i.e., weakened or strengthened).

It was not expected that the results would be similar to those done on a 4340 alloy which contained 0.39 wt% C, 0.7 wt% Mn, 0.28 wt% Si, 0.76 wt% Cr, 1.7 wt% Ni, 0.2 wt% Mo, and 0.11 wt% Cu, because other interaction effects were believed to be present. Nonetheless the results were surprisingly similar to simple Fe-C-X systems.

What these results seem to indicate is that the other alloying elements present (such as Cu and Al) might play a minor role in this reaction or that their individual interaction effects cancel each other, and such alloys as Cr, Ni, Mo and Mn significantly affect the bainite kinetics.

"The special effect of alloying elements<sup>56</sup> upon growth kinetics has been interpreted in terms of a "drag effect" produced by the segregation of certain alloying elements to austenite/ferrite boundaries.<sup>84</sup>

Alloying elements that reduce the activity of carbon in austenite should be particularly prone to such segregation. The tendency for segregation ought to increase with decreasing temperature, partly because of the declining importance of the entropy factor but specially because of the rapid rise of the carbon concentration in austenite at austenite/ferrite boundaries. The special effect should begin to appear when the drag effect becomes sufficiently large relative to the driving force if the drag is sufficiently large an "upper nose" will develop in the TTT diagram high above the temperature of the single nose normally



formed. Conversely as the drag effect approaches saturation in such a steel, a bay will begin to develop in the TTT diagram as the driving force for growth begins to overcome this effect.

The successively smaller reductions in the activity of carbon in austenite produced by Cr, Mn and Ni are consistent with the declining effectiveness of a given proportion of these elements in producing a bay in the TTT diagram."<sup>56</sup> This has been the case for other investigations as well (for references see Aaronsons review<sup>56</sup>).

"Conversely Si and Co raise the activity of carbon in austenite and should not give rise to the kinetic-bainite phenomena."<sup>56</sup>

Aaronson concludes that this effect of Si and Co could probably be seen in high purity Fe-C-X alloys.

These Arguments are in agreement with our results. If we consider the case of Cr, Mn and Ni when combined as discussed previously, we had Cr being the most effective and Ni being least effective (when added to Fe-C-Mo system) in producing a bay. On the contrary, it was also discussed previously how Si alloys did not have a pronounced bay, which is also expected according to this "drag effect." Also in good agreement was the fact that further additions of Co accelerated the reaction and eliminated the pronounced bay present in lower alloy contents (see Figs. 31 and 32).

The inclination is to believe in the interpretation of the present results in terms of a "drag effect" produced by the segregation of certain alloying elements to austenite/ferrite boundaries. Other attempts were made to correlate the present results with C content, alloy content,

lattice parameter mismatch, and C diffusion and how it is affected by different alloys present in austenite and in ferrite with no success. These results were difficult to rationalize and are just presented as empirical facts within the limits of the experimental technique.

#### 4. Effect of Quenching Rate on the Kinetics and Reproducibility

The effect of the quenching rate was studied in three alloys (I, IV, XVI) in order to see if there were any changes in the kinetics and also how the variation of the quenching rate affected the reproducibility.

The data was divided in two parts; for that purpose it will be tabulated in Tables XXXIII and XXXIV.

From these data, although the evidence is not conclusive, it suggests that with slower quenching rates the kinetics of the reaction are faster at the initial stages of the transformation but not necessarily so for further progress of the reaction (see Figs. 35-37).

The fact that for alloy IV, the slower quenching rate (12.9°/sec) gave slower reaction kinetics could be explained from the fact that the austenitizing temperature was slightly higher 1095°C for that run as opposed to 1090°C for the other cases of alloy IV.

With slight variations in the quenching rate the reproducibility was good. The results would be clearer when interpreted from Figs. 35 and 36, which give an idea of the errors involved by assuming reproducibility.

When the quenching rate was not varied outside the 130-150°C/sec range, the change in amount of saturated bainite was almost negligible as the

data shows (for I, IV, V see Fig. 38), where the same quenching rate for five runs at two different isothermal temperature treatments (560°C and 415°C) were used.

#### 5. Retained Austenite Levels

The amounts of retained austenite in steels seems to be mainly affected by the carbon content and the presence of some alloying elements (Si, Mn, Ni, Cu and others).<sup>26,59-64</sup>

For low carbon (less than 0.4 wt% for instance) plain C steels, large amounts of retained austenite were not expected; specifically less than 4% was expected.<sup>59</sup> Nevertheless when there are alloying elements present such as Si the retained austenite level changes drastically.<sup>17</sup>

For optical microscopy determinations below 10%, limitations appear when one wants a quantitative reliable estimate of retained austenite. The situation would improve very much by the use of electron microscopy but preparing thin foils should assume uniform distribution and random orientation which is not always the case.<sup>59,60</sup>

In view of the factors discussed above it was chosen to use X-ray analysis for the determination of retained austenite levels considering that if any retained austenite was found it would be present in small percentages.

If the levels are lower than 0.4-0.5% then from statistical considerations the signal-background noise ratio in these analyses loses meaning and the error is quite large.

A relative intensity radiation counting technique was used (see Appendix 1).

The results of the present investigation indicated that within 5% error, all the alloys Mo, Ni, Cr, Mn, Al, and Co for all heat treatments used and all isothermal temperature holds, achieved saturations where the level of retained austenite was below 5%. Hence it can be said that saturation for these alloys was at least 95% transformed (value used when studying kinetic aspects). Silicon was the critical alloy, because higher levels of retained austenite were expected. Other investigators results for commercial alloy steels had given higher austenite levels when Si was present (e.g., on the order of 20% for 2% Si 4340 steel).<sup>17</sup>

The present investigation dealt with just a simple ternary Fe-C-Si system not a commercial alloy steel. Different Si compositions were obtained at percentages of 0.94, 1.91, and 2.93 in alloys XVI, XVII, XVIII respectively. Results indicated no retained austenite above 4% for alloys XVI, XVII and small amounts for alloy XVIII. The temperatures of formation of most of the retained austenite were those below the upper bainite nose where the upper-lower bainite bay would be located although the bay was not pronounced for the Si steels from the kinetic TTT diagram (kinetics).

It was expected that higher levels of retained austenite would be obtained in the previously mentioned temperature range because the kinetics of the transformation start were much slower than for higher temperatures. Also higher temperatures were of interest because close to the  $B_s$  temperature the reaction may not be complete.

Results for some of the temperatures (e.g., 580°C, 480°C and 460°C) for alloy XVIII for the percentage of retained austenite was less than

4%, the limit of the experimental technique (see Appendix I). Other temperatures for this same alloy gave the following: for 440°C,  $\gamma \approx 5.6\%$ ; for 420°C,  $\gamma \approx 7.5\%$ ; and 400°C,  $\gamma \approx 4.3\%$ .

Hence only for alloy XVIII was there evidence of retained austenite higher than 5% and just a maximum of 7.5% for 420°C was found, so the claim that for all the alloys, the saturation level was achieved approximately when 95% was transformed, was correct within the limits of accuracy of retained austenite determination.

#### 6. Discussion of the Effect of Austenitizing Temperature on the Bainite Transformation Kinetics

The effect of the austenitizing temperature was studied on alloys I and IV, with consistent results obtained for both alloys. The results of the effect of austenitizing temperature showed that the lower the austenitizing temperature the faster the reaction start (nucleation) and the faster the reaction completed or saturated.

Partial results are given in Table XXXV and Figs. 39(a) and (b). In Fig. 39a the effect of austenitizing temperature on the formation of lower bainite in alloy IV was studied and similarly the effect upon upper bainite in alloy I is shown in Fig. 39b.

The times for different percentages of saturation level of the reaction are given as well as the corresponding isothermal holds and quenching rates (see Table XXXV).

Figures 40(a) and (b) show the effect of austenitizing temperature on the bainite kinetics and the time for progressive stages of the transformation as a function of the austenitizing temperature for alloys I and IV respectively. For alloy I the relation, % transformed

vs austenitizing temperature, suggested linearity up to 75% of the saturation level.

Present results showed that the austenitizing temperature had more effect in the incubation time for upper bainite formation than for lower bainite (although more data should be required to assure this). There is conflicting data in the literature as to what the effect of austenitizing temperature is on the bainite reaction. Those who found that increasing the grain size (higher austenitizing temperature) did not affect the reaction rate were Davenport, et al.,<sup>46</sup> while others found that the reaction rate was increased: Cottrel and Ko<sup>47</sup> and Graham and Axon.<sup>49</sup> Fujimura and Muramatsu<sup>58</sup> found that the reaction rate was increased for lower bainite. Finally those who found the reaction was slower: Barford and Owen<sup>48</sup> and Prakash Babu.<sup>17</sup>

It is difficult to separate the effect of the increased austenite grain size and the increased chemical homogeneity within the austenite grains.

These results from Fig. 40 also show that the non-linearity of percent transformed vs time is maintained for any austenitizing temperature. Notice that the 1250°C treatment (higher austenitizing temperature) renders this effect more pronounced.

At 950°C it is possible that for 15 min the specimen will not be fully austenitic. So some sites for preferred inhomogeneous nucleation might be present at this temperature (inhomogeneities). Also the grain size is smaller hence there are more grain boundary surfaces contributing to the nucleation of bainite, therefore, it should be a faster reaction.

At 1200°C for instance the grain size is larger so the available grain boundary surface for nucleation is reduced which is consistent with a slower reaction.<sup>55</sup> These results are in agreement with the fact that upper bainite nucleates at the grain boundaries but lower bainite can also nucleate within the grain, therefore, the effect should be less for the latter.

7. Determination of  $B_s$  on the Basis of Some Existing Empirical Equations

It was observed that combined additions of alloying elements to Fe-C-X-Y systems gave an additive effect in lowering the bainite temperature ranges. The results showed that the C content also played a major role.<sup>38,17</sup>

Two equations were studied (based on additive effects) to determine the  $B_s$ .

Steven and Haynes<sup>38</sup>

$$B_s^{\circ}\text{C} = 830 - 270\text{C} - 90\text{Mn} - 37\text{Ni} - 70\text{Cr} - 83\text{Mo} \quad (10)$$

Prakash Babu<sup>17</sup>

$$B_s^{\circ}\text{C} = 839 - 300\text{C} - 60\text{Mn} - 33\text{Ni} - 63\text{Cr} - 130\text{Mo} - 45\text{Si} \quad (11)$$

Results are given in Table XXXVI.

At temperatures near the  $B_s$  the austenite did not completely transform and part of the retained austenite<sup>9</sup> transformed to martensite during cooling to lower temperature. Examples of this behavior were alloy X at 600°C and alloy XII at an isothermal hold of 650°C.

It was noticed that both Stevens and Haynes, and Prakash Babu's empirical equation gave relatively high  $B_s$  values (less in the latter case). From microstructural observation it was determined that above

approximately 560°C the structures did not look bainitic. In any case it was not the attempt of this investigation to do a microstructural study of this kind, but it is suggested as a necessary problem to look into for the future. There is need of a careful electron microscopic study on the Pearlite-Bainite frontier; as well as a  $B_s$  determination and with changes of alloy contents.

Table XXXVI also contains information on the kinetic values for the location of the Upper-Lower Bainitic Bay.

A plot of the position of the Bay (from kinetic data) with respect to the carbon content is given in Fig. 34 where it was compared with a previous study by Pickering.<sup>69</sup> It shows that the tendency was maintained although as was expected, the data points lie below in temperature scale because the kinetic location of the bay does not indicate the start of the lower bainite transformation but an overlap of both upper and lower bainite kinetics. Comparison with previous studied on commercial steels showed consistency with these results.

#### 8. Hardness Data for Bainitic Structures

To study the effect of alloying elements on hardness of different bainite structures, seven alloys were studied containing Fe-C-X where X = Mo, Ni, Cr, Mn, Al, Si or Co.

Vickers hardness values were obtained (average of 5 measurements on each specimen) for some of the bainite structures at different temperatures.

Results tabulated in Table XXXVII are given in Fig. 41. Where it was possible to compare alloys with similar carbon content. The



C content was very critical in establishing the ultimate hardness values of these structures.

Figure 41 shows that the hardness decreased with increasing transformation temperature for all the alloys although for any individual alloy the hardness could be lower or higher. The results suggested that the decrease of hardness with increasing isothermal reaction temperature was asymptotic in nature.

Except for the case of Si (alloy XVII) which seemed to be consistently higher than the rest of the alloys, no alloying element drastically changed this effect; their presence had little influence on the hardness of the structures. It was believed that the scattering of the data was probably a function of the differences in C content of the alloys considered (0.27, 0.29, 0.29, 0.41, 0.37, 0.38, 0.33) for (II, V, VI, VII, XIV, XVII, XX) respectively. Hardness values for the different bainite structures decreased with increasing temperature of transformation. Present results did not give a linear function but seemed to be consistent with prior results on tensile strength vs different transformation temperatures<sup>2</sup> for low carbon steels.

#### D. Analysis of the Available Empirical Rate Equations

##### 1. Johnson-Mehl Equation

Heterogeneous systems consist of a mixture of phases, and reactions in such a system, occurs by the growth of one or more phases at the expense of others.<sup>71,85</sup> In general, each phase is not found as one single entity but as a dispersion of smaller domains. That is the case of bainite (ferrite and carbides). The transformation of the new product,

bainite, involves formation of new domains referred to as nucleation, and the advancement of the phase boundaries termed growth.

The rate of bainite transformation will depend on the rate of nucleation and growth of the ferrite and carbides and the effect of mutual interference of neighboring domains either through direct impingement or by ion range competition of solute atoms.

It was found empirically that an equation of the general form

$$\frac{dy}{dt} = k^n t^{n-1} (1 - y) \quad (12)$$

describes the isothermal kinetics of a wide variety of reactions in metals. Rate curves that in general conform to this equation are shown for alloy IV in Figs. 6, 9 and 42. The factor  $(1 - y)$  may be regarded as an allowance for the retardation in reaction rate due to impingement.  $K$  has time dimensions but is not a free rate constant (i.e.,  $k = 0$ ). In practice, if  $k = 1$ , the reaction is too fast to be followed experimentally and very fast quenching rates are necessary.  $K$  fixes the position on the time axis of the fraction transformed vs log time. The shape of the curve is determined by the index  $n$ .

If one assumes  $k$  and  $n$  to be true constants of time, then Eq. (12) can be integrated

$$\ln \frac{1}{1 - y} = (kt)^n \quad (13)$$

$$y = 1 - e^{-(kt)^n} \quad \text{Johnson-Mehl}^{73} \quad (14a)$$

This equation (Eq. (14a)) is the generalized form of the Johnson and Mehl equation derived for the particular case of transformation of austenite to pearlite with  $n = 4$ . It was first derived for recrystallization of a cold worked metal for the kinetics of the nucleation and growth of pearlite at constant temperature and no composition change:

$$x_t = 1 - \exp\left[-(\pi/3) u^3 I t^4\right] \quad (14b)$$

$U$  is a vector growth rate and  $I$  the nucleation frequency. It should be remembered that  $U$  and  $I$ , when Eq. (14b) was derived, were assumed independent of time, and the nucleation sites were considered to be located at random.

Occasionally Eq. (14a) is written

$$y = 1 - \exp\left[-kt^n\right] \quad \text{Zener}^{72} \quad (15)$$

Activation energies derived from Zener's equation cannot be compared directly with values derived from constants having dimensions  $t^{-1}$ .

It is preferred to use the Johnson-Mehl generalized equation to avoid that difficulty.

For the bainite reaction, the transformation had an incubation or induction period during which no detectable transformation occurred (see Fig. 42(a)). In these cases one should measure  $t$  from the end of the incubation period. "However, in practice, it is very difficult to establish a reaction "start" time precisely and it is more meaningful and convenient to measure  $t$  from one common zero usually the time the specimen attains the reaction temperature. Apart from slight dis-

tortions of the curve initially, this causes negligible error.<sup>71</sup> The times for the transformation start are given in Tables XIII-XXXII and Figs. 13-32 were obtained in the latter way described by Burke.<sup>71</sup>

If a reaction follows the Johnson-Mehl generalized equation, a graph of  $\log \left[ \log \left( \frac{1}{1-y} \right) \right]$  vs  $\log t$  should be linear where the values of  $n$  and  $k$  can be obtained from the slope and the intercept respectively

$$\log \left[ \log \left( \frac{1}{1-y} \right) \right] = n \log k + n \log t - \log 2.3 \quad (16)$$

One can see from Figs. 43(a-d) that the curves were not linear. The deviation from linearity was pronounced after 75% transformed for the lower bainitic transformation temperatures, and for lower amounts transformed for higher temperatures. Those where bainite and pearlite mixtures were formed in the 600°C range, were especially deviant. Figures 42(a-d) illustrate this for alloys I, VII, XIV and XVII. For other alloys studied, the deviation from linearity was even worse. The average correlation factor ( $r^2$ ) was 0.915 for all the alloys which was not too bad although worse than the one obtained for the Austin-Rickett Equation.

Studies of this kind were done for all the alloys, a sample of which is given for alloy III in table (Table XXXVIII). From these results we can say that  $N$  and  $k$  were not constant and that they vary with transformation temperature. The fit was not good; a perfect fit would be  $(r)^2 = 1$  and there were many instances where  $(r)^2 = 0.8$ .

Analysis of the constant  $N$  from the Johnson-Mehl equation and the experimental data for different transformation temperatures showed

that  $N$  was not a constant of the reaction for each and every alloy.  $N$  varied with bainitic transformation temperatures and this could be due to the different product structures and their mechanism of formation not being the same in all the temperature ranges studied.  $N$  varying at different temperatures and for the same temperature as the transformation proceeds could reflect the fact that  $(1 - y)$  is not necessarily the proper impingement factor for the reaction kinetics.

## 2. Austin-Rickett Equation

When the Johnson-Mehl graph of

$$\log \log(1/1-y)$$

against  $\log t$  shows a pronounced negative curvature as in Figs. 43(a-d) a better agreement is frequently obtained by replacing the impingement factor  $(1 - y)$  by  $(1 - y)^2$  and in this case the rate becomes

$$\frac{dy}{dt} = (1 - y)^2 R_A^{n_A} t^{n_A - 1} \quad (17)$$

which integrates to

$$y/1-y - (kt)^{n_A} \quad (18)$$

This integrated rate equation was used for the first time by Austin and Rickett to analyze the kinetics of austenite decomposition.

A plot of  $\log(y/1 - y)$  against  $\log t$  again should give a straight line and the Austin-Rickett equation should then describe the kinetics of these bainitic transformations. It was found that this was not

the case. Figure 44(a-d) show that there is a deviation from linearity implying that just the change in the impingement factor  $(1 - y)$  by  $(1 - y)^2$  in the rate equation was not sufficient.

Analysis of  $N_A$  as a function of percent transformation for different temperatures was done. Results are given in Fig. 45 for six of the alloys studied: I, III, IV, VI, XII, IX. Notice how  $N_A$  (labeled N average in the graphs) varies with temperature and with the degree of transformation that has elapsed. What was striking was the shape of  $N_A$  as a function of temperature. It was the same for all the alloys demarking two regions of the peaks, which suggested a dependence probably not on temperature itself but on the reaction product structures (e.g., lower bainite, upper bainite and pearlite).

Similar analysis was made of  $N_A$  as a function of the time elapsed (to see variations of  $N_A$  as the reaction proceeded) at the different isothermal holds for some of the alloys. Results are given for alloys XII, III, X and VII in Fig. 46. Notice that there was a slight increase of  $N_A$  as the transformation proceeded until a certain point was reached where  $N_A$  decreased. The lower temperatures and higher upper bainite temperatures close to the pearlite range, did not follow this behavior for most alloys. Again, from the present results, it was found that  $N_A$  and  $k_A$  were not constants.

The values of N given by other investigations have been from 0.5 up to as high as 6. Radcliffe and Rollason<sup>41</sup> have found N values of (1.8-2.6) for the upper bainite kinetics and (3.0-4.0) for the lower bainite. Prakash Babu<sup>17</sup> found (1.0-2.0) for the upper bainite

and (2.0-3.0) for the lower bainite. From the present results it can be seen (Figs. 45(a-f)) that one cannot make similar conclusions. It can be said, nonetheless, that as a whole, upper bainite can have the same order of  $N_A$  as lower bainite with  $N_A$  being a minimum for temperatures where upper and lower bainite overlap (e.g., 1.5 for alloy III), and a maximum where upper bainite and pearlite overlap (e.g., 4.6 for alloy III).

### 3. Proposed Generalized Equation

From the present results on the kinetic investigation of bainite it was found that for the bainitic transformation there was an incubation period. During the incubation period even at time different from zero the percent transformed and the rate were still zero. This possibility was not included in any of the two previously discussed equations. The only equation found where this condition could be satisfied was that given by Hillert<sup>70</sup> in reference to some other aspects (activation energy considerations, see Appendix 3 for detailed explanation):

$$\left(\frac{1}{y}\right) \left(\frac{\partial y}{\partial t}\right) = k(1-y)^i y^{-1/n} \exp\left[-Q^*(y)/RT\right] \quad (19)$$

Then

$$\frac{\partial y}{\partial t} = k(1-y)^i y^{-1-1/n} \exp\left[-Q^*(y)/RT\right] \quad (20)$$

which would mean that even when  $t \neq 0$  one can have  $dy/dt = 0$ . It is proposed here that a more general equation of the types described in Section D-1 and D-2 be developed in the future.

The equation would be

$$\frac{dy}{dt} = nk^n t^{n-1} y^{1-\alpha} (1-y)^{1-\beta} \quad (21)$$

Experiments show that

(i)  $\frac{dy}{dt} \rightarrow 0$  when  $y = 0$ , even at  $t \neq 0$

(ii)  $\frac{dy}{dt} \rightarrow 1$  when  $y = 1$

and (iii)  $F(y,t) = t^{n-1} y^{1-\alpha} (1-y)^{1-\beta} f(y,t)$

Notice we have the possibility of different  $\beta$  eliminating the restriction on impingement being  $(1 - \beta) = 1$  for the Johnson-Mehl equation and  $1 - \beta = 2$  for the Austin Rickett equation. Because the impingement factor may change from one isothermal treatment to the next, and since there are differences in the product structures and their growth rates,  $(1 - \beta)$  might take different values for different reaction temperature ranges. The parameters  $n$ ,  $\alpha$ ,  $\beta$  would be determined, while  $f(y,t)$  varies smoothly and  $f(y,t) = nk^n$  where  $k$  is a constant in the less generalized form<sup>22</sup> associated with activation energy.

Hence

$$k^n n t^{n-1} dt = dy y^{\alpha-1} (1-y)^{\beta-1} \quad (22)$$

and

$$(kt)^n = \int_0^y dx x^{\alpha-1} (1-x)^{\beta-1} \quad (23)$$



It is hoped that future development of this equation (presently investigated by the author) could lead to constant  $n$ , and  $\alpha$  and  $\beta$  related to the special structural degrees of freedom for the nucleation and growth processes in the austenite to bainite transformation.

#### 4. Considerations on Activation Energies

In the past 25 years authors have tried to associate an activation energy for the upper and lower bainite reactions and have correlated them with the activation energies for diffusion of carbon in austenite and ferrite.<sup>17,41,66-69</sup>

The results available in the literature regarding this aspect are conflicting. There has been work done on hot stage microscopy<sup>68,69</sup> and it appears to indicate an activation energy for upper bainite of (3-8)kcal/mole and for lower bainite of (17-22)kcal/mole correlating them to C diffusion in ferrite and austenite respectively.

However, electrical resistivity measurements indicated<sup>41,44,67</sup> the reverse. Radcliffe and Rollason<sup>41</sup> reported (18-32)kcal/mole for upper bainite and (7-13)kcal/mole for lower bainite. They concluded that these activation energies were respectively those of C diffusion in austenite and ferrite (for comparison refer to Table I ( $Q_{c\gamma} = 36$ ,  $Q_{c\alpha} = 19.6$  kcal/mole)).

The magnetic method gave (Prakash Babu<sup>17</sup>) activation energies for upper bainite 10 kcal/mole and for lower bainite 5 kcal/mole which were too low to be related to carbon diffusion processes in austenite. Results from the present investigation did not show consistently high or low values for upper and lower bainite activation energies. In

some cases for upper bainite the values were higher than those for lower bainite, but the contrary was also true in other cases. It was also noted that in some cases the slopes in an Arrhenius plot were negative and in others positive. It was questionable whether the activation energies obtained in this fashion are meaningful. A controversy is raised. These results seem to show that the interpretation of these activation energies is not simple and there are other controlling processes besides the role played by C diffusion.

Arrhenius type plots discussed in Appendix 3 with data in the form  $-\ln t$  vs  $1/T$  are shown in Figs. 47(a-g) for different alloys: Mo III, Ni IV, Cr VIII, Mn XIII, Al XIV, Si XVI and Co XIX. These graphs revealed in all cases that the activation energy  $E_A$  was not independent of temperature, or transformation products, in as much as the processes involved the bainite transformation.

Detailed calculation of activation energies for different combinations of points taken into consideration for all the alloys revealed variations from temperature to temperature of the following kind: for instance, 9.42, 19.04, 42.2, 5.56, 14.25 kcal/mole for alloy VI. No fixed pattern emerged, which did not seem to bring light into the controversy. One thing was clear though, and that was: the problem was more complex than just simple association of an apparent average activation energy with C diffusion.

It is relevant to quote Warlimont's<sup>57</sup> enumeration of the partial reactions involved to understand why it is a difficult task to associate a physical meaning to activation energies obtained in this manner.

"From the description of the microstructures of the bainite transformation products and from the thermodynamic relations it follows that the transformation kinetics depends on numerous partial reactions."

Except for the growth velocity of  $\alpha$  plates in the direction of the edges, none of the partial reactions has been satisfactorily treated quantitatively, and that is in no way astonishing. If it is analyzed how many partial reactions will influence the increase in volume fraction of the bainite product, which is what is measured for production of TTT diagrams, there are the following considerations:

1. The nucleation rate of the ferrite
2. The nucleation rate of the cementite during carbon enrichment of the austenite (upper bainite)
3. The nucleation rate of cementite that is  $\epsilon$ -carbide in ferrite (upper and lower bainite)
4. Growth velocity of ferrite plate in the direction of their edges
5. Growth velocity of ferrite plate in the direction of their thickness,
  - a. without coupled cementite precipitation in the austenite plates (UB)
  - b. with coupled carbide precipitation (bainite ferrite)
  - c. with coupled cementite precipitation in the ferrite (UB)
  - d. with coupled  $\epsilon$ -carbide precipitation in the ferrite (LB)
6. Influences from interface structures on the growth kinetics
7. Influences of alloying elements in the mobility of the interface.

## E. Optical Microscopy and ASTM Grain Size Characterization

### 1. ASTM Grain Size of the Treatments Used

The austenitizing temperatures for all the diagrams was 1080°C +5°C. The specimens were held at that temperature for 15 min for reasons discussed previously. The corresponding ASTM grain size for all the alloys studied were within the range (3-4) and (4-5). Exceptions were found for some alloys: VII, X, and XI where the ASTM numbers were (2-3, 2-3, 1-2) respectively coinciding with the low carbon content (0.17, 0.24, 0.14 respectively) which was responsible for the large grain size. Except for these three cases one could say that all the austenitizing treatments gave essentially the same initial grain size for the reactions involved.

### 2. Effect of Austenitizing Temperature on the Grain Size

The grain size showed a distinct increase with higher austenitizing temperatures; a change of austenitizing temperature from 950° to 1080°, or 1200°C gave corresponding ASTM numbers of (6-7) to (3-4), or (1-2), respectively which implies an increase in all equivalent spherically shaped grains from a diameter of (1-2) x 10<sup>-3</sup> in. to (4-5) x 10<sup>-3</sup> in. to (8-10) x 10<sup>-3</sup> in. respectively. The respective surface areas were 1.57 x 10<sup>-6</sup> in.<sup>2</sup>, 3.18 x 10<sup>-5</sup> in.<sup>2</sup>, and 1.27 x 10<sup>-4</sup> in.<sup>2</sup>.

The results<sup>55</sup> were tabulated for two cases studied. Alloys I and IV are shown in Table XXXIX; they were also plotted in Fig. 48 where 'd' means the diameter of the corresponding spherically shaped grains.

All these results were derived from holding at the austenitizing range, for an equal holding time of 15 min so the variables involved for the grain growth were temperature and composition.

### 3. Optical Microscopy of the Martensitic Structures

Some optical microscopy studies were made. In no way was this an attempt of a morphological study, but it was done to obtain an overview of the different alloy's martensitic and bainitic structures. As was discussed previously the limitations of optical microscopy for these purposes was recognized.

The structures were taken at 1000x magnification. Figures 49 to 55 show the martensitic structures of 7 of the cast and treated alloys (II Mo, V Ni, VII Cr, XII Mn, XIV Al, XVIII Si, XX Co). They all showed the martensitic needle type plate structure.

### 4. Optical Microscopy of the Bainitic Structures

These are shown only for seven of the alloys studied (II,V, VII, XII, XIV, XVIII, XX) which correspond to the Fe-C-Mo, Fe-C-Ni, Fe-C-Cr, Fe-C-Mn, Fe-C-Al, Fe-C-Si, Fe-C-Co systems.

Different bainitic transformation temperatures and their resulting structures are shown for each alloy.

Figures 56-60 correspond to alloy V at isothermal holds of 660°C, 512°C, 489°C, 460°C, 400°C. Figures 61-63 correspond to alloy II at 610°C, 512°C, and 435°C. Figures 64-67 correspond to alloy VI at 600°C, 555°C, 490°C and 460°C. Figures 68-71, correspond to alloy XII at 610°C, 560°C, 400°C and 350°C. Figures 72-77 correspond to alloy XIV at 400°C, 440°C, 460°C, 500°C, 540°C, and 620°C. Figures 78-80

correspond to alloy XVIII at 400°C, 440°C, 460°C and 540°C. Finally, Figs. 82-85 correspond to alloy XX at 400°C, 440, 460 and 540°C.

It was attempted to have both types of bainite showing upper and lower bainite. In some cases the structures were mixed and a distinction was not possible with optical microscopy resolution. A brief discussion of the figures for each alloy will be given

i. In the case of Fe-C-Ni, Fig. 56 shows a structure similar to pearlite but it was not, it was a very degenerate form of pearlite at 660°C. Figure 57 shows another degenerate structure that tries to be bainite at 512°C; just below, at 489°C we can see a definite upper bainite structure (Fig. 58). In Figure 59 (450°C) there is a mixture of upper and lower bainite structure followed by Fig. 60 where lower bainite predominates.

ii. In the case of Fe-C-Mo at 610°C (Fig. 61) again a very degenerate type of structure, that tries to be pearlite forms. At a lower temperature of 512°C upper bainite formed (Fig. 62); and at 435°C a mixture of upper and lower bainite was formed in the corresponding microstructure (Fig. 63).

iii. In the case of Fe-C-Cr at 600°C, proeutectoid ferrite and the corresponding expected eutectoid matrix was present see Fig. 64, and at 555°C again a degenerate type of pearlite appeared characteristic of some Cr-steels. At 490°C and 440°C one can see upper bainite structures (Figs. 66 and 67) at lower temperatures a mixture of upper and lower bainite structures was observed.

iv. In the case of Fe-C-Mn at 610°C proeutectoid ferrite and the corresponding expected eutectoid matrix is shown in Fig. 68 and at 560°C a partially transformed upper bainite appears (Fig. 69). At 400°C a mixture of upper and lower bainite with upper bainite predominating is present see Fig. 70; the reverse (lower bainite predominating) occurred at 350°C shown in Fig. 71.

v. In the case of Fe-C-Al at 620°C a degenerate pearlite is shown in Fig. 77. At 540°C upper bainite appeared (Fig. 76). At 460°C (and 500°C) upper bainite was present. Notice the Windmastaten ferrite present (Fig. 75). At 440°C a mixture of upper and lower bainite was present (Fig. 73). At 400°C lower bainite is shown (Fig. 72).

vi. In the case of Fe-C-Si at 540°C upper bainite and some pearlitic eutectoid matrix is shown (Fig. 81). At 460°C upper bainite was present (Fig. 80). At 440°C and 400°C lower bainite was present (Figs. 78 and 79).

vii. In the case of Fe-C-Co at 540°C degenerate pearlitic and upper bainite structures appeared (Fig. 85). At 460°C upper bainite is shown in Fig. 84. Lower bainite is shown in Figs. 82 and 83 for corresponding transformation temperatures of 400°C and 440°C respectively.

From this sampling of microstructures one could say that although the temperature ranges of the bainites were not the same for the different ternary systems, the overall optical features of the bainites were similar.

To be able to see the differences in morphology, carbide distribution, alloy segregation (if any) one should go to higher resolutions as discussed before.

It should be pointed out though that at lower magnifications it was observed that upper bainite nucleated at the grain boundaries but lower bainite did it also within the grains which was consistent with very many other investigations.

There was no clear cut temperature of transition for upper and lower bainite and optical microscopy showed a range of temperatures where lower and upper bainite were both present. This was in agreement with the belief that morphology of bainite changes gradually with reaction temperature so no pronounced structural changes were observed over small temperature changes.<sup>13,16,17,56</sup>



## IV. CONCLUSIONS

Based on the various results of this investigation, the following conclusions are drawn:

1. Comparative results showed that Cr, Mo, Al and Si restricted the austenite stable region with Si and Mo being most effective. Mn expanded the austenite stable range slightly while Ni and Co exerted little influence. Their interaction effect was not additive or average on the transformation temperatures  $Ae_1$  and  $Ae_3$ .

2. Results of the  $M_s$  transformation temperatures showed,  
 a) that the quenching rate differences within the available range had no effect on the  $M_s$ , b) that the higher the austenitizing temperature the higher was the  $M_s$  (from 950-1200°C there was a corresponding increase of 20°C on the  $M_s$ ), c) that the comparison of experimental  $M_s$  values and existing empirical formulae indicated that for these low C alloy steels, Nehremberg's linear formula, Eq. (8), gave the best fit:

$$M_s^{\circ}C = 1000 - 650C - 70Mn - 35Ni - 70Cr - 50Mo \quad , \quad (8)$$

d) that a linear function approximated the microhardness vs  $M_s$  transformation temperature results:

$$VHN(1000 \text{ gr}) = \left[ -1.913/^{\circ}C \times M_s (^{\circ}C) + 1240.9 \right] \quad (9)$$

3. Hardness values for the different bainite structures decreased with increasing temperature of transformation, results indicated non-linearity for the seven alloys studied.

4. In the present studies there was an acceleration of the austenite decomposition at isothermal treatments just above the  $M_s$  giving, for the reaction start curves, an S-shaped rather than a C-shaped curve.

5. Present results indicated Mn, Ni, Cr, and Al retarded the bainite reaction. The bainite reaction below 500°C was unaffected by Si when alone; and was accelerated by the presence of Co, and Mo but to a lesser degree.

6. Combined additions had a multiplicative effect (synergistic) on reaction start times for the isothermal decomposition of the austenite suggesting interaction effects (e.g., Ni-Cr, Mo-Cr, Mo-Ni systems). However, the effect of additions on kinetics of further stages of transformation was less defined.

7. Some of the alloying elements lowered the temperature of shortest incubation time in the nose. Further addition suggested an additive effect even for mixed additions as Cr + Ni, Mo + Cr and Mo + Ni.

8. The effect of austenitizing temperature on the kinetics of the transformation showed that the lower the austenitizing temperature the faster the bainite reaction (this effect being slightly stronger for upper bainite).

9. Retained austenite levels for the bainite transformation were below 5% with the exception of 2.93 Si alloy which for some temperature was as high as 7%, concluding that with 5% error the saturation level for the reaction was 95% transformed.

10. Analysis of the kinetic data was performed using well known empirical-rate equations such as the Johnson-Mehl, and the Austin-Rickett equations. A generalized empirical rate equation was proposed to satisfy all the boundary conditions not satisfied by the above two equations.

11. Activation energy considerations for this investigation could not be associated with activation energies of carbon diffusion in ferrite or austenite implying that there are other controlling processes in the bainite reaction.

12. Interpretation of these results for Cr, Ni, Mn, Si, Co were in good agreement with the "drag effect" produced by the segregation of certain alloying elements to austenite/ferrite boundaries.

#### ACKNOWLEDGEMENTS

The author is deeply grateful to Professor Earl Parker for his continued guidance and encouragement throughout the course of this investigation. She would also like to express here gratitude to Professors Victor Zackay, Jack Washburn, and Iain Finnie for reviewing the manuscript.

The author wishes to express her thanks in general to the students and the members of the "P and Z" group for their discussion, encouragement, and support. Special thanks are given to M. Shanthidas Bhat, Janet Conn, Glenn Haddick, Ron Horn, Larry Thompson and John Wert for their help and numerous discussions. Special thanks to Glenn Haddick for his help in the manuscript preparation.

Thanks are also due to the technical support staff of the Materials and Molecular Research Division, in particular, Brian Pope and John Holthius (alloy preparation), J. A. Patenaude (machinery), Lee Johnson (metallography), Jim Sevrens (electronics), Phila Witherall (photography), Sandy Stewart (purchases and an open door), Gloria Pelatowsky (preparation of line drawings), Jenni Ingraham and Jean Wolslegel (for their patience in typing the manuscript), and John Dillon, Laura Lindberg and Kent Carey (research helpers).

Last but not least, the author is thankful to her family whose love and support through the years has made this step possible, to Felix, Regina, and Toni, whose love and encouragement helped smooth the difficult moments and made life beautiful at Berkeley; to my friends

Josefa, Yougindra, and Maureen whose human warmth and encouragement kept me going when loneliness was a problem.

This work was done under the U. S. Energy Research and Development Administration through the Materials and Molecular Research Division of the Lawrence Berkeley Laboratory.

Very special thanks are extended to CONICIT (Consejo Nacional de Investigaciones Cientificas y Tecnologicas, Venezuela) for financially supporting the author while undergoing this investigation.

APPENDIX 1. DETERMINATION OF RETAINED AUSTENITE BY MEANS OF X-RAY ANALYSIS

Relative Intensity Radiation Counting

The relative advantage of relative intensity measurements as opposed to those based on height or width of the peaks has been discussed by Miller<sup>61</sup> exposing the latter problems (such as Bain distortion and line broadening, particle size effects and others).

It was chosen to determine the relative intensities on the basis of the radiation counts on a determined angular interval that includes the peak, scanning over it and comparing with a similar scan for the background on both sides of the peak.

Of course as in any radiation counting technique<sup>63</sup> there is a limitation as to when the intensity (I) measurement is valid. The criteria of  $I > \sqrt{SA}$  was chosen where

$$I = SA - \left( \frac{B_1 + B_2}{2} \right) \quad (24)$$

and where

background on oneside =  $B_1$

background on the otherside =  $B_2$

signal peak scan = SA

Otherwise it will be within the mean deviation value and will have no significance over the background.

In alloy steels with different C concentrations, the presence of C distorts the lattice parameters and will shift the angles of the peaks.

Main Peaks for standard  $\alpha$ -Fe at 400 cps range with Cu radiation and conditions specified in Section II-D.

Planes	Degrees = $2\theta$	Signal	Strength Decreasing Order
(100)	44.7	98	1
(200)	65.2	16	3
(211)	83.5	47.5	2
(220) doublets	100.2	13	4
(310) doublets	116.5	16	3

Peaks for Standard Austenite 3.6 - L, 1000 cps Range.

Planes	Degrees = $2\theta$	Signal	Strength Decreasing Order
(111)	43.6	67	1
(200)	50.8	25.5	2
(220)	74.6	25	4
(311)	91	19	3
(222) doublet	96	5	5
(400) doublet	118.3	2	6

The peaks that were used for relative intensity measurements were  $\gamma(220)$ ,  $\gamma(311)$ ,  $\alpha(211)$ . See Dietchie,<sup>64</sup> Miller,<sup>61</sup> Cullity<sup>62</sup> in order to consider effects of preferred orientation.

Quantitative Analysis Theoretical Considerations

If we want to find out the relation between concentration and intensity one must go back to the basic equation for the diffracted intensity.<sup>5</sup>

$$I = \left( \frac{I_0 e^4}{m^2 c^4} \right) \left( \frac{\lambda^3 A}{32\pi r} \right) \left( \frac{1}{v} \right) \left[ |F|^2 p \left( \frac{1 + \cos^2 2\theta}{\sin^2 \theta \cos \theta} \right) \right] \left( \frac{e^{-2M}}{2\mu} \right) \quad (25)$$

where  $I$  = Integrated intensity per unit length of diffraction line

$I_0$  = Intensity of incident beam

$e, m$  = charge and mass of the electron

$c$  = speed of light

$\lambda$  = wavelength of the incident radiation

$r$  = radius of diffractometer circle

$A$  = cross sectional area of the incident beam

$v$  = volume of unit cell

$F$  = structure factor

$p$  = multiplicity factor

$\theta$  = Bragg angle

$e^{-2M}$  = temperature factor (function of  $\theta$ )

$\mu$  = linear absorption coefficient.



Lets define

$$k = \left( \frac{I_o e^4}{m^2 c^4} \right) \left( \frac{\lambda^3 A}{32\pi r} \right) \quad (26)$$

$$R = \frac{1}{v^2} \left[ |F|^2 p \left( \frac{1 + \cos^2 2\theta}{\sin^2 \theta \cos \theta} \right) \right] \quad (27)$$

$$I = kR/2\mu \quad (28)$$

One can simplify the problem in the alloys where C content is low assuming the volume fraction of carbides is negligible and one mainly can characterize the  $\gamma$  as the fcc structure present and the bainite as the bcc  $\alpha$  structure present. Then for a particular diffraction line of each phase we have

$$I = \frac{KR C_{\gamma}}{2\mu} \quad (28a)$$

$$I_{\alpha} = \frac{KR C_{\alpha}}{2\mu} \quad (28b)$$

$$C_{\gamma} + C_{\alpha} = 100 \quad (29)$$

$$C_{\gamma} = \frac{100}{1 + \left( \frac{I_{\alpha}}{I_{\gamma}} \right) \left( \frac{R_{\gamma}}{R_{\alpha}} \right)} \quad (30)$$

Computing  $R_{\alpha}/R_{\gamma}$  Ratios the Following Considerations Had to be Made

Generally in the literature discussed<sup>4</sup> and the work by Miller it was found that  $R_{\alpha}/R_{\gamma}$  for steels is approximately 1.4, Miller gave a theoretical explanation for this factor for a Te-Ni alloy using Mo radiation. For a rough estimate one could use this 1.4 value or  $R_{\gamma}/R_{\alpha} = 0.71$ . But in the present work, considerations have been made on these ratios for the (220) and (311) planes and the effect of the C content in distorting the lattice parameters. Hence, corrections to this factor should be made in each case according to the C content, the experimental X-ray arrangement, the type of radiation and the effect on the atomic scattering factor.

For instance "when the incident wavelength  $\lambda$  is nearly equal to the wavelength  $\lambda_k$  of the k absorption edge of the scattering element, then the atomic scattering factor of that element may be several units lower than it is when  $\lambda$  is very much shorter than  $\lambda_k$ " (see pg. 373).<sup>5</sup>

Since  $\text{Cu}^k$  radiation is near  $\text{Fe}^k$  of k absorption edge

$$\text{Cu}^k = 1.541\text{A} \quad \text{then} \quad \lambda/\lambda_k = 1.256$$

$$\text{Fe}^k = 1.937\text{A}$$

which implies a correction of  $\Delta f = -2$ .

It would also be ideal if we had available information to correct for the different alloying elements present. However, since they are substitutional we assume the strains on the lattice are much less than

from interstitials like C and so for this type of calculation can be neglected.

It was found that for 0.4 wt% C the  $R_{\gamma}/R_{\alpha}$  ratio was

$$\frac{R_{\gamma}(220)}{R_{\alpha}(211)} = 0.669$$

$$\frac{R_{\gamma}(311)}{R_{\alpha}(211)} = 0.7969$$

## APPENDIX 2. HARDNESS VS $M_s$ TRANSFORMATION TEMPERATURE EQUATION

In order to derive the linear equation discussed previously in Section III-B-4 a linear regression program (using the least square method of the hardness (y) vs  $M_s$ (x) temperature data) was used, where

$$VHN = aM_s + b \quad (9) \text{ and } (31)$$

$$a = \frac{\Sigma y \Sigma x^2 - \Sigma x \Sigma xy}{n \Sigma x^2 - (\Sigma x)^2} \quad (32)$$

$$b = \frac{n \Sigma yx - \Sigma x \Sigma y}{n \Sigma x^2 - (\Sigma x)^2} \quad (33)$$

with coefficient of determination

$$r^2 = \frac{n \Sigma xy - \Sigma x \Sigma y}{n(n-1) S_x S_y} \quad (34)$$

Where  $S_x, S_y$  are the standard deviation of x and y given by

$$S_x = \sqrt{\frac{\Sigma x^2 - (\Sigma x)^2/n}{n-1}} \quad (35)$$

$$S_y = \sqrt{\frac{\Sigma y^2 - (\Sigma y)^2/n}{n-1}} \quad (36)$$

for data given in Table XII

$$a = -1.913/^{\circ}\text{C}$$

$$b = 1240.9$$

$$r^2 = 0.882$$

where a perfect fit would imply  $r^2 = 1$ .

### APPENDIX 3. ACTIVATION ENERGY

With a few exceptions reaction rates increase rapidly with increasing temperature. Furthermore, provided that the temperature range is not too great the temperature dependence of the rates of most heterogeneous reactions of this type (bainitic, pearlitic) obeys an Arrhenius type equation.<sup>71</sup>

Under these circumstances it is always possible to define an empirical activation energy  $E_A$  and a frequency factor  $A$  by equation

$$k = Ae^{-E_A/RT} \quad (37)$$

where  $E_A$  = activation

$A$  = frequency factor

$R$  = gas constant

$T$  = absolute temperature.

There are various methods to determine  $E_A$  and  $A$ . The appropriate in our case is the time to a given fraction method.

In this way variations of  $E_A$  or  $A$  with temperatures will show up as curvatures in the Arrhenius plot. The value  $E_A$  at a particular temperature is obtained from the gradient at that temperature.

"For a reasonably narrow temperature range the curvature if any is likely to be so small as to justify taking an average value" (Burke<sup>71</sup>).

From the general rate equation

$$dy/dt = kf(y) \quad (38)$$

Provided that  $f(y)$  does not vary over the temperature range studied (which is unlikely in our case (see Section D-4))

$$ty \propto k^{-1} \quad \text{for a fraction transformed } y$$

$$ty \propto A^{-1} e^{E_A/RT}$$

$$\ln ty = C + E_A/RT - \ln A \quad (39)$$

Results of this type analysis are given in Section D-4 there was no point in including the data for activation energies since the scatter had no correlation and varied widely. An attempt was made using a different approach described by Hillert<sup>70</sup> with no improved results.

He suggested that instead of computing the activation energy

$$\frac{Q(t_1)}{R} = - \left[ \frac{\partial \ln f}{\partial 1/T} \right]_{t_1}$$

for any degree of transformation  $f = f_1$  where

$$1/t = F(f, T)$$

to use a definition of another activation energy which is of a somewhat more fundamental nature

$$\frac{Q^*(f_1)}{R} = - \left[ \frac{\partial \ln (\partial f / \partial t)}{\partial 1/T} \right]_{f_1}$$

Both activation energies are identical  $Q$  and  $Q^*$  when independent of  $f$ . Sometimes, however, the experimental data may not be accurate enough for an evaluation of  $\partial f/\partial t$  and the use of the second equation is not justified.



## REFERENCES

1. E. Parker and V. Zackay, Fundamentals of Alloy Design, LBL-2706 May 1974.
2. K. J. Irvine and F. B. Pickering, J. Iron Steel Inst. 201, 518 (1973).
3. J. S. Pascover and S. J. Matas, ASTM Special Technical Publication No. 370 (1963), p. 30.
4. Y. H. Liu, Trans. ASM 62, 55 (1959).
5. J. H. Holloman, L. D. Jaffe, D. E. McCarthy and M. R. Norton, Trans. ASM 38, 801 (1947).
6. S. A. Herres and C. H. Losig, Trans. ASM 40, 775 (1948).
7. Der-Hung Huang and G. Thomas, Met. Trans. 2, 1587 (1971).
8. E. S. Davenport and E. C. Bain, Trans. AIME 90, 117 (1930).
9. R. F. Hehemann, K. R. Kinsman and H. I. Aaronson, Met. Trans. 3, 1077 (1972).
10. H. I. Aaronson, The Mechanism of Phase Transformation in Crystalline Solids, IM Monograph Report 33, 270 (1969).
11. Electron Microstructure of Bainite in Steel. II-Progress Report ASTM Proc. 52, 543 (1952).
12. H. I. Aaronson and W. Wells, J. of Metals, Sept. 1955, p. 1002.
13. K. J. Irvine and F. P. Pickering, J. Iron Steel Institute, Feb. 1958, p. 101.
14. D. N. Shackelton and P. M. Kelly, Iron Steel Institute Spec. Report 93, 126 (1965).

15. G. R. Strinivasan and C. M. Wayman, *Acta Met.* 16, 609, 621 (1968).
16. Der-Hung Huang, Ph. D. Thesis, *Bainitic Transformation in Steels*, May 1975.
17. Naga Prakash Babu, D. Eng. Thesis, *An Investigation of Bainite Transformation in Medium Carbon Low Alloy Steels*, Aug. 1974.
18. C. E. Ericsson, M. S. Thesis, *An Isothermal Study of Bainitic and Martensitic transformations in Some Low Alloy Steels Using a New Magnetic Permeability Technique*, December 1973.
19. *Atlas of Isothermal Transformation Diagrams* (United States Steel Corporation, 1963, p. 103).
20. E. C. Rollason, *Fundamental Aspects of Molybdenum on Transformation of Steel* (Climax Molybdenum of Europe, Limited).
21. M. A. Krishtal, *Diffusion Process in Iron Alloys*, Metallurgizdat Moskva, 1963 (English translation Jerusalem, 1970).
22. K. Blanter, *Diffusion in Austenite and Hardenability of Alloy Steels*, Author's summary of thesis MIS, 1949.
23. K. W. Andrews, *JISI* 184, 414 (1956).
24. K. J. Irvine, F. B. Pickering, W. C. Hesllwood and M. Atkins, *JISI* 186, 54 (1957).
25. K. R. Kinsmann and H. I. Aaronson, *Met. Trans.* 3, 1106 (1972).
26. E. Bain and H. Paxton, *Alloying Elements in Steels*, ASM 1966.
27. V. F. Zackay, E. R. Parker, J. W. Morris, Jr. and G. Thomas, LBL-2261.
28. R. Clark, *Simplified Operations Manual for Theta-Dilatometers*, April 1975.

29. H. S. Carslaw and C. J. Jeager, Conduction of Heat in Solids, Oxford University Press, 1959.
30. Private communication from George Gordon--Lawrence Berkeley Laboratory, MMRD.
31. S. J. Donachie and G. S. Ansell, Met. Trans. 6A, 1863 (1975).
32. G. S. Ansell and E. M. Breinan, Met. Trans. 1, 1513 (1970).
33. A. S. Sastri and D. R. Wert, JISI 203, 1138 (1965).
34. R. A. Grange and H. M. Stewart, Trans AIME 167, 467 (1945).
35. P. Payson and C. H. Savage, Trans ASM 33, 261 (1944).
36. A. E. Nehrenberg, Trans. AIME 167, 494 (1946).
37. E. S. Rowland and S. R. Lyle, Trans ASM 37, 37 (1945).
38. W. Stevens and A. G. Haynes, Trans ASM 183, 349 (1956).
39. K. W. Andrews, JISI, July, 721 (1965).
40. L. A. Carapella, Met. Prog. 46, 108 (1964).
41. S. V. Radcliffe and E. C. Rollason, JISI 191, 56 (1959).
42. R. T. Howard and M. Cohen, Trans. AIME 176, 384 (1948).
43. O. Schaaber, J. Metals 7, 559 (1955).
44. G. R. Brophy and A. J. Miller, Trans. AIME 167, 654 (1946).
45. F. B. Pickering, Transformation and Hardenability in Steels, Climax Molybdenum Co., Ann Arbor, Michigan, 1967, p. 109.
46. A. S. Davenport, et al., Trans. AIME 145, 301 (1941).
47. S. A. Cottrel and T. Ko, JISI 173, 114 (1953).
48. J. Barford and W. S. Owen, JISI 197, 146 (1953).
49. L. W. Graham and H. Axon, JISI 191, 361 (1959).
50. R. F. Hehemann, Phase Transformation, ASM Ohio, 1970, p. 409.

51. G. Thomas, *Iron and Steel Intern.*, 451 (October 1973).
52. R. F. Mehl, Hardenability of Alloy Steels, ASM 1 (1939).
53. J. M. Oblak and R. F. Hehemann, *Transformation and Hardenability in Steels*, Climax Molybdenum Co., 1967.
54. A. S. Kenneford, V. D. Rance and S. Turner, *J. Iron and Steel Inst.*, 665 (June 1967).
55. A. M. Llopis, M. S. Thesis, LBL-4555, December 1975.
56. H. Aaronson, Institute of Metals 1966, Monograph and Report Series No. 33, Proceedings of an Intern. Symp., Univ. of Manchester, July 1968.
57. Warlimont Transformation in Bainite, 1976, to be published (in German).
58. Y. Fujimura and K. Muratsu, *Nippon Kinzoku* 36(1), 85-90 (1972).
59. C. S. Roberts, *Trans. AIME* 197, 203 (1953).
60. Hilliard Cahn, *Trans. AIME* 221, 344 (1961).
61. R. L. Miller, *Trans. ASM* 57, 892 (1964).
62. Cullity, Elements of X-Ray Diffraction, Addison Wesley, 1967).
63. Mellissinos, *Experiments in Modern Physics*, Academic Press, 1966.
64. L. Dietche, U. S. Steel Corporation Research Laboratory, unpublished work.
65. Reedhill, *Physical Metallurgy Principles*.
66. J. S. White and W. S. Owen, *J. Iron Steel Inst.* 197, 241 (1961).
67. J. Barford, *J. Iron and Steel Inst.* 204, 609 (1966).
68. R. H. Goodenow, S. J. Matas and R. F. Hehemann, *Trans. AIME* 227, 651 (1963).

69. F. B. Pickering, Transformation and Hardenability in Steel, Climax Molybdenum Co., Ann Arbor, 1967, p. 109.
70. M. Hillert, *Acta Metallurgica*, 7, 653 (1959).
71. J. Burke, The Kinetics of Phase Transformations in Metals, Pergamon Press, 1965.
72. C. Zener, *Trans. ASM* 41, 1057 (1949).
73. W. A. Johnson and R. F. Mehl, *Trans. AIME* 135, 416 (1939).
74. J. B. Austin and R. L. Ricketts, *Trans. AIME* 135, 396 (1939).
75. Traian Dumitescu, Constantin Inoescu and Maria Solacolu, *Studii si Cercetari de Metalurgie, Acad RPR* 8, 2 (1963).
76. H. Aaronson and H. Domian, *Transaction of the Metallurgical Society of AIME* 236, 731 (1966).
77. D. A. Scoll and G. S. Faruhan, *J. of Metals*, 541 (1953).
78. Discussion Bo treated steels, *Trans of ASM* 37, 180 (1943).
79. R. H. Hehemann and J.M. Oblak, *Symposium Iron and Hardenability in Steels*, Feb. 17, 1967.
80. R. Honeycombe and F. Pickering, *Met. Trans.* 3, 1099 (1972).
81. B. N. Babu, M. S. Bhat, E. R. Parker, and V. F. Zackay, *Met. Trans. A* 7A, 17 (1976).
82. G. F. Melloy, P. R. Slimmon and P. P. Podgersky, *Met. Trans.* 4, 2279 (1973).
83. A. Hultgren, *Trans. Amer. Soc. Metals*, 39, 195 (1974).
84. K. R. Kinsman and H. I. Aaranson, Transformation and Hardenability of Steels, Climax, Molybdenum Co., Ann Arbor, 1967, p. 39.

85. M. E. Fine, Phase Transformations in Condensed Systems (McMillan Co., New York, 1964).

Table I. Diffusion data for iron of some of the elements used.

Alloying Element	Q kcal/mole		D <sub>0</sub> cm <sup>2</sup> /sec.	
	γFe	αFe	γ	α
Fe	67	59	1.3	5.8
C	36	19.6	0.49	0.167
Mo	59	57	114.0	0.068
Ni		67	1.25	66.8
Cr	97.5	82		
Mn	57	59	0.48	0.38
Si	48	52.6		0.44
Al		57.7		5.9
Co	80	54		0.77

Table II. List of Alloys and Their Nominal Composition Given in Wt% before Casting.

Alloy No.	Spec. No.	Casting No.	Alloy Composition								
			C	Cr	Ni	Mn	Si	Al	Co	Mo	
I	4	7412-1	0.3								0.3
II	5	7412-2	0.3								0.4
III	6	7412-3	0.3								0.5
IV	7	7412-4	0.3		2.0						
V	8	7412-5	0.3		1.0						
VI	10	7412-7	0.3	1.0							
VII	11	7412-8	0.2	1.0							
VIII	12	7412-9	0.3	1.0	1.0						
IX	13	7412-10	0.3		1.0						0.5
X	14	7412-11	0.3	1.0							0.5
XI	16	7412-13	0.3	1.0	1.0						0.5
XII	17	747-6	0.4			2.0					
XIII	20	747-9	0.4			2.7					
XIV	21	765-1	0.4					1.0			
XV	22	765-2	0.4					2.0			
XVI	24	765-4	0.4				1.0				
XVII	25	765-5	0.4				2.0				
XVIII	26	765-6	0.4				3.0				
XIX	27	765-7	0.4							0.5	
XX	28	765-8	0.4							1.0	
XXI	18	747-7	0.4			2.2					



Table III. Results of Chemical Analysis (given in Wt%) of Cast Alloys.

Alloy No.	Casting No.	Composition of Analyzed Elements							
		C	Cr	Ni	Mn	Si	Al	Co	Mo
I	7412-1	0.24							0.29
II	7412-2	0.27							0.39
III	7412-3	0.3							0.49
IV	7412-4	0.23		2.04					
V	7412-5	0.29		1.01					
VI	7412-7	0.29	1.0						
VII	7412.8	0.17	1.0						
VIII	7412-9	0.27	1.01	1.1					
IX	7412-10	0.25		1.0					0.48
X	7412-11	0.24	0.99						0.47
XI	7412-13	0.14	0.97	1.05					0.47
XII	747-6	0.41			1.67				
XIII	747-9	0.39			2.59				
XIV	765-1	0.37					0.87		
XV	765-2	0.39					1.94		
XVI	765-4	0.39				0.94			
XVII	765-5	0.38				1.91			
XVIII	765-6	0.39				2.93			
XIX	765-7	0.35						0.52	
XX	765-8	0.33						1.05	
XXI	747-7	0.4			2.13				

Table IV. Results of chemical analysis of other elements that could be present and affect this investigation (given in wt %).

Specimen No.	Composition of the analyzed elements			
	B	O	P	S
1	----	*0.001	----	----
2	----	*0.001	----	----
3	----	*0.001	----	----
7	----	*0.001	----	----
5	*0.001	*0.001	*0.005	*0.005

\* less than

Table V. Typical Run Experimental Conditions.

Typical heating rates	6.7 °/sec
Typical time resolution	( $10^{-2}$ - $10^{-1}$ ) sec
Typical quenching rates	50 - 150 °/sec Martensite runs 150 - 300 °/sec Lower Bainite runs 300 - 450 °/sec Upper Bainite runs
Typical gas pressures (He)	(20-35) LMP Air
Typical Vacuums	( $10^{-4}$ - $10^{-5}$ ) Torr.

Table VI. Austenite Transformation Temperatures

Alloy No.	Spec. No.	As (°C)	Af (°C)
I	4	760	930
II	5	765	920
III	6	742	830
IV	7	715	819
V	8	730	840
VI	10	760	850
VII	11	744	905
VIII	12	753	857
IX	13	749	875
X	14	736	848
XI	16	747	853
XII	17	728	770
XIII	20	715	750
XIV	21	746	889
XV	22	753	960
XVI	24	760	873
XVII	25	743	902
XVIII	26	739	928
XIX	27	747	863
XX	28	746	850
XXI	18	720	765

Table VII. Martensitic Transformation Temperatures.

Alloy No.	Ms (°C)	Mf (°C)	Quenching Rate (°C/sec)
I	445	307	83.3
II	416	355	53.3
III	396	310	60.7
IV	403	270	111.6
V	390	210	148.2
VI	377	280	133.3
VII	350	250	102.5
VIII	380	224	58.9
IX	405	276	58.9
X	405	290	70.5
XI	428	310	84.0
XII	330	185	133.0
XIII	300	113	121.0
XIV	367	252	127.3
XV	368	180	121.6
XVI	364	206	117.3
XVII	368	192	137.9
XVIII	340	183	102.35
XIX	390	253	139.8
XX	390	327	140.5
XXI	298	130	133.0

Table VIII.  $M_n$  as determined by some calculations from existing formulae and comparison with observed experimental value in °C.

Alloy No.	$M_n$ Experimental	Linear (Additive)					Product		
		Payson and Savage	Grange and Stewart	Nehrenberg	Rowland and Lyle	Stevens and Haynes	Andrews	Carapella	Andrews
I	445	420	450	423	416	441	435	416	413
II	416	409	437	414	405	425	421	406	402
III	395	398	424	403	393	409	408	387	391
IV	403	392	421	395	388	417	407	382	385
V	390	390	422	395	385	406	398	385	382
VI	377	379	402	390	374	407	404	454	394
VII	350	417	442	426	414	463	455	497	445
VIII	380	367	387	377	363	391	393	441	384
IX	405	398	422	402	394	415	412	391	391
X	405	390	406	400	386	421	422	466	408
XI	428	405	419	413	403	450	446	499	429
XII	330	314	336	320	307	312	315	307	314
XIII	300	289	307	296	283	291	295	279	294
XIV	367	382	404	388	376	386	383	378	374
XV	368	376	397	382	369	376	374	372	368
XVI	364	364	392	371	359	376	374	359	368
XV.I	368	357	401	364	351	380	378	350	371
XVIII	340	363	397	349	336	376	374	334	368
XIX	390	388	411	393	382	395	385	408	388
XX	390	393	418	399	389	404	387	442	388
XXI	298	301	322	308	295	301	288	281	304

Table IX.  $\Delta M_g$  as determined from the formulae in OC.

Alloy No.	$M_g$ Exp.	$\Delta M_g$ (°C)							
		Payson and Savage	Grange and Stewart	Nehrenberg	Rowland and Lyle	Stevens and Haynes	Andrews	Carapella	Andrews
I	445	-25	5	-22	-29	-4	-10	-29	-32
II	416	-7	21	-2	-11	9	5	-10	-14
III	395	3	29	8	-2	13	13	-8	-4
IV	403	-11	18	-8	-19	14	3	-21	-18
V	390	0	32	5	-5	16	8	-5	-8
VI	377	2	25	+13	-3	30	27	77	17
VII	350	67	92	76	64	113	105	147	95
VIII	380	-13	7	-3	-17	11	13	61	4
IX	405	-7	17	-3	-11	10	7	-14	-14
X	405	-15	1	-5	-19	16	17	61	1
XI	428	-23	-9	-15	-25	22	18	71	1
XII	330	-16	6	-10	-23	-28	-15	-23	-16
XIII	300	-11	7	-4	-17	-9	-5	-21	-4
XIV	367	+15	+37	+21	+9	+19	+16	+11	+7
XV	368	+8	+29	+14	+1	+8	+6	+4	0
XVI	364	0	+28	+7	-5	+12	+10	-5	+4
XVII	368	-11	+33	-4	-17	+12	+10	-18	+3
XVIII	340	+23	+57	+9	-4	+36	+34	-6	+28
XIX	390	-2	+21	+3	-4	+5	-5	+18	-10
XX	390	+3	+28	+9	-1	+14	-3	+52	-4
XXI	398	3	24	10	-3	3	-12	-17	6
$\Sigma  \Delta M_g $		265	526	251	286	404	342	679	290
$\overline{\Delta M_g}$		12.6	25.1	11.9	13.6	19.2	16.3	32.3	13.8

00004708641

Table X. Effect of Austenitizing Temperature on Ms.

Alloy No.	Quenching Rate (°C/sec)	Austenite Temp. (°C)	Ms (°C)
IV	80.3	950	390
IV	133.3	1080	400
IV	73.7	1210	410
I	74.0	955	410
I	43.1	1085	418
I	63.1	1090	420
I	49.1	1200	430
XXI	52.7	950	280
XXI	126.2	950	280
XXI	60.9	1090	300
XXI	126.2	1085	298
XXI	133.3	1085	300



Table XI. Effect of Quenching Rate on Ms.

Alloy No.	Austenitizing Temp. (°C)	Quenching Rate °/sec	Ms (°C)
IV	1080	58.3	400
IV	1080	83.3	400
IV	1080	111.6	400
IV	1080	133.3	400
VII	1080	84.12	350
VII	1080	100.9	350
VII	1080	102.5	350
XXI	1090	50.92	300
XXI	1085	126.19	300
XXI	1085	133.0	298
XXI	950	52.7	280
XXI	950	126.2	280

Table XII. Microhardness Vickers test with 1000g load.

Alloy No.	Ms °C	VHN	C Wt%
I	445	396	0.24
II	416	440	0.27
III	396	533	0.3
IV	403	453	0.23
V	390	528	0.29
VI	377	422	0.29
VII	350	398	0.17
VIII	380	490	0.27
IX	405	464	0.25
X	405	470	0.24
XI	428	399	0.14
XII	330	575	0.41
XIII	300	716	0.39
XIV	367	581	0.37
XV	368	571	0.39
XVI	364	571	0.39
XVII	368	660	0.38
XVIII	340	636	0.39
XIX	390	460	0.35
XX	390	446	0.33
XXI	298	655	0.4

Table XIII. Isothermal data for alloy I.

Run No.	Temp. °C	t start	t25	t50	t75	t saturation
1	450	0.36	1.5	2.4	2.9	5.2
2	450	0.36	1.5	2.4	2.9	5.2
3	480	1.1	2.2	2.9	3.7	6.9
4	496	0.6	1.2	1.7	2.3	5.7
5	500	0.54	1.4	1.8	2.4	6.0
6	518	0.72	1.5	2.1	2.6	5.6
7	538	1.6	3.5	4.3	5.3	7.6
8	540	1.56	2.9	3.8	4.5	7.4
9	542	1.26	1.8	2.2	2.7	5.0
10	600	4.32	5.9	7.4	9.9	26.0
11	650	8.76	15.2	26.3	67.7	934.0

Table XIV. Isothermal data for Alloy II

Run No.	Temp. °C	t start	t25	t50	t75	t saturation
1	418	0.6	2.04	2.8	3.6	14.5
2	438	0.36	2.3	3.1	4.6	10.0
3	460	0.56	3.0	4.2	5.4	12.2
4	490	0.6	3.1	5.0	6.7	12.6
5	515	0.48	3.0	4.8	6.6	10.7
6	555	0.71	2.3	5.2	5.9	8.4
7	610	1.41	3.8	9.4	19.7	40.1
8	640	24.4	84.4	116.1	177.0	452.0

Table XV. Isothermal data for Alloy III

Run No.	Temp. °C	t start	t25	t50	t75	t saturation
1	407	1.2	2.6	3.4	4.2	14.8
2	423	1.38	2.2	2.9	3.5	17.7
3	445	2.52	4.3	5.7	7.1	19.3
4	470	1.8	5.2	6.7	8.8	18.4
5	487	1.92	4.9	6.5	8.4	16.1
6	520	2.7	4.7	5.8	6.8	16.1
7	555	5.4	8.5	9.9	11.4	45.0
8	595	11.2	16.2	22.2	37.2	593.0
9	640	81.4	537.6	777.6	1152.0	3402.0

Table XVI. Isothermal Data for Alloy IV.

Run No.	Temp. °C	t start	t25	t50	t75	t saturation
1	420	0.24	1.6	3.1	5.5	14.6
2	435	1.68	4.7	5.8	6.8	16.1
3	440	0.72	3.8	5.6	7.6	16.8
4	450	2.69	5.7	3.9	9.5	28.0
5	470	4.26	10.3	13.0	15.5	28.3
6	480	0.84	3.8	5.2	6.9	13.9
7	500	0.6	4.3	6.6	9.0	15.6
8	550	0.48	2.5	3.2	3.8	8.2
9	600	0.96	2.4	3.4	4.0	12.6
10	645	33.1	57.6	93.6	166.0	886.0

Table XVII. Isothermal data for alloy V.

Run No.	Temp. °C	t start	t25	t50	t75	t saturation
1	415	0.56	2.95	4.5	6.5	17.0
2	425	0.36	2.4	3.7	4.9	21.0
3	440	0.56	3.8	6.1	8.4	18.9
4	460	1.5	10.4	15.8	20.9	42.1
5	489	1.73	5.0	7.0	9.0	19.0
6	512	1.79	4.2	5.8	8.9	18.2
7	530	0.93	2.1	2.6	3.5	12.5
8	560	0.48	1.73	2.3	2.9	3.6
9	610	0.94	2.2	2.7	3.4	5.9
10	660	3.7	5.2	6.4	10.1	23.2

Table XVIII. Isothermal data for alloy VI

Run No.	Temp. °C	t start	t25	t50	t75	t saturation
1	385	0.2	0.9	1.5	2.9	14.8
2	400	0.24	1.4	2.3	3.4	15.9
3	425	0.42	2.2	4.2	5.8	19.2
4	440	0.56	3.9	5.8	8.1	20.0
5	450	0.63	4.2	6.3	8.5	23.4
6	460	0.84	4.6	6.3	9.0	23.5
7	490	1.62	5.1	7.2	9.6	22.8
8	495	1.56	4.1	5.8	9.5	18.9
9	510	2.64	7.5	9.8	12.5	32.0
10	530	3.6	7.6	10.6	14.1	39.6
11	555	0.6	4.8	9.0	13.2	37.2
12	605	0.9	9.6	16.2	24.0	63.0
13	650	1.8	12.0	14.4	17.7	44.0



Table XIX. Isothermal Data for Alloy VII

Run No.	Temp. °C	t start	t25	t50	t75	t saturation
1	365	0.36	0.72	0.84	1.1	3.0
2	410	0.48	0.96	1.3	1.6	9.5
3	420	0.72	1.1	1.4	2.3	9.4
4	450	1.2	2.5	3.3	4.2	15.1
5	476	0.45	2.1	3.2	6.9	16.6
6	480	0.42	0.96	1.9	2.4	10.8
7	495	0.42	1.9	2.9	3.8	10.2
8	505	2.1	4.0	5.4	6.9	14.4
9	545	2.8	4.9	6.5	8.2	20.0
10	600	4.32	8.5	12.2	17.3	215.0
11	650	8.3	13.5	18.1	24.0	70.0

Table XX. Isothermal Data for Alloy VIII.

Run No.	Temp. °C	t start	t25	t50	t75	t saturation
1	410	4.8	9.1	12.4	16.3	46.0
2	435	6.4	12.6	15.9	20.9	48.7
3	460	7.1	13.1	16.6	21.0	51.6
4	480	8.9	15.0	21.2	24.9	60.9
5	500	4.8	9.7	13.4	17.9	42.0
6	540	11.1	21.0	31.9	45.1	153.6
7	600	28.1	56.4	71.9	88.1	185.0
8	650	26.1	42.4	49.4	58.2	117.4

Table XXI. Isothermal data for alloy IX.

Run No.	Temp. °C	t start	t25	t50	t75	t saturation
1	420	2.28	4.9	6.8	9.8	27.0
2	438	7.26	12.0	14.6	17.6	36.5
3	440	9.0	18.0	21.5	24.8	39.0
4	460	4.32	7.9	10.7	13.8	38.0
5	480	2.7	8.4	11.8	15.0	31.3
6	495	3.96	7.1	9.0	18.0	30.0
7	540	8.64	14.5	17.7	21.9	39.0
8	544	13.2	16.9	25.2	32.0	56.5
9	600	20.04	33.9	50.4	116.0	1196.0
10	640	388.0	793.1	1333.0	2458.0	7858.0
11	645	426.9	832.0	1372.0	2497.0	7897.0

Table XXII. Isothermal data for alloy X

Run No.	Temp. °C	t start	t25	t50	t75	t saturation
1	415	2.3	5.2	7.4	10	31.1
2	440	4.1	7.2	9.6	11.5	32.3
3	460	5.6	9.9	13.1	17.0	47.5
4	480	6.6	11.7	12.9	19.2	53.6
5	490	2.4	5.4	7.5	10.0	31.4
6	540	8.5	16.2	23.1	32.7	74.7
7	600	21.7	183.7	1700.0	2671.0	$5.3 \times 10^3$
8	645	156.0	1386.0	2790.0	$3.6 \times 10^4$	$5.9 \times 10^4$

Table XXIII. Isothermal data for all XI

Run No.	Temp. °C	t start	t25	t50	t75	t saturation
1	420	0.12	0.6	1.1	1.9	2.8
2	440	0.24	0.7	1.4	2.2	4.9
3	460	0.96	1.4	1.9	2.9	13.2
4	480	0.36	0.6	1.8	4.4	20.4
5	500	1.36	1.3	2.6	6.1	27.0
6	518	3.8	9.9	17.2	26.5	74.5
7	530	55.6	5768.0	8294.0	54294.0	62394.0

Table XXIV. Isothermal data for alloy XII

Run No.	Temp. °C	t start	t25	t50	t75	t saturation
1	350	13.2	142.0	228.0	337.0	765.0
2	400	24.0	41.8	52.8	65.7	594.0
3	455	3.0	48.9	84.9	125.0	854.0
4	500	4.2	37.9	61.9	92.0	634.0
5	560	7.0	15.3	19.5	24.3	696.0
6	610	37.5	75.7	121.0	155.0	317.0

Table XXV. Isothermal data for alloy XIII

Run No.	Temp. °C	t start	t25	t50	t75	t saturation
1	328	45.0	304.0	434.0	600.0	1250.0
2	350	43.6	336.5	460.0	529.0	611.0
3	372	48.8	144.0	200.0	268.0	534.0
4	400	26.1	87.8	120.0	156.0	289.0
5	425	15.0	63.3	90.0	121.0	210.0
6	455	12.2	39.9	57.4	77.0	1414.0
7	505	12.7	63.9	163.0	206.0	1379.0
8	550	38.9	152.0	251.0	372.0	692.0
9	600	78.0	510.0	597.0	837.0	1617.0

Table XXVI. Isothermal data for alloy XIV

Run No.	Temp. °C	t start	t25	t50	t75	t saturation
1	390	3.5	6.8	9.1	11.8	26.1
2	410	3.1	6.3	8.3	10.8	22.7
3	430	1.9	4.9	6.9	9.3	27.7
4	445	3.8	7.0	9.3	12.5	59.9
5	470	3.3	5.9	8.5	11.2	60.9
6	490	1.7	2.7	3.5	4.05	14.4
7	510	1.5	2.1	2.4	2.7	15.9
8	530	0.6	1.6	1.9	2.2	11.1
9	600	1.3	2.3	2.8	3.5	5.7
10	620	2.3	3.1	3.6	4.1	37.7
11	630	7.3	11.9	17.7	51.6	68.4



Table XXVII. Isothermal data for alloy XV

Run No.	Temp. °C	t start	t25	t50	t75	t saturation
1	380	2.1	3.8	4.9	6.5	41.1
2	400	3.6	6.0	7.5	9.5	40.3
3	420	3.5	5.3	6.7	8.4	28.5
4	440	2.1	3.1	4.1	5.7	22.3
5	470	1.9	3.1	4.0	5.2	142.0
6	485	3.1	4.1	5.3	6.5	475.0
7	490	2.6	3.7	4.7	6.6	255.6
8	520	2.0	3.2	3.9	4.7	261.0
9	540	2.8	3.8	4.4	5.2	249.6
10	560	3.1	4.0	4.7	5.5	555.0
11	580	2.6	3.4	4.1	4.8	242.3
12	600	1.6	2.9	3.4	4.1	232.7
13	620	1.7	2.6	3.4	4.3	402.9
14	640	2.0	3.4	4.3	5.6	499.5
15	660	3.0	4.3	5.1	6.3	537.9

Table XXVIII. Isothermal data for alloy XVI

Run No.	Temp. °C	t start	t25	t50	t75	t saturation
1	380	3.9	7.5	10.1	14.7	73.2
2	400	4.7	8.8	11.3	15.2	61.8
3	420	5.9	10.8	13.9	17.8	111.6
4	450	6.1	10.7	13.4	16.9	59.6
5	485	6.4	11.0	14.1	18.6	146.9
6	505	6.7	10.7	13.2	15.5	258.3
7	520	4.2	5.8	6.5	7.5	33.18
8	538	3.5	8.0	10.7	14.0	37.1
9	560	1.1	4.6	7.6	10.9	27.4
10	575	1.4	2.9	4.5	6.0	27.8
11	600	2.0	3.3	4.1	4.7	30.9
12	620	1.9	3.4	4.2	4.9	26.4
13	660	3.1	4.7	5.8	7.0	25.7

Table XXIX. Isothermal data for alloy XVII

Run No.	Temp. °C	t start	t25	t50	t75	t saturation
1	380	1.7	7.6	10.1	13.9	74.0
2	400	4.3	9.4	12.1	15.5	95.5
3	418	4.4	7.9	10.4	13.7	63.8
4	440	4.7	12.3	15.9	20.0	40.0
5	460	4.9	10.5	14.0	18.6	56.4
6	480	7.5	12.6	15.7	19.9	39.0
7	500	5.6	11.1	14.2	17.9	39.5
8	520	2.9	6.3	9.1	11.7	28.1
9	530	4.8	8.9	11.4	14.0	25.1
10	560	5.8	10.4	13.2	15.6	33.9
11	570	4.0	6.4	7.7	9.0	22.1
12	590	2.9	4.7	5.3	6.1	19.0
13	620	3.3	5.8	6.9	7.9	11.6
14	635	2.9	4.6	5.2	6.1	9.9
15	660	4.9	6.1	7.4	8.3	15.2

Table XXX. Isothermal data for alloy XVIII

Run No.	Temp. °C	t start	t25	t50	t75	t saturation
1	380	5.1	8.4	10.6	13.6	42.5
2	400	5.6	9.7	12.6	16.4	292.4
3	420	5.1	9.8	12.3	16.7	150.4
4	440	7.5	11.1	13.8	17.5	59.1
5	460	7.6	11.9	14.6	19.4	65.2
6	480	9.7	13.7	16.7	21.5	57.5
7	500	6.6	10.8	13.9	18.3	47.7
8	520	5.3	9.7	12.5	16.4	41.7
9	535	6.6	11.4	13.7	17.2	41.2
10	560	5.5	9.2	11.7	14.5	34.4
11	570	6.6	11.4	14.2	16.5	31.4
12	590	4.5	6.0	6.7	7.5	21.6
13	620	3.3	5.3	6.1	6.9	19.9
14	640	2.6	3.9	4.7	5.4	12.3
15	660	2.1	4.4	5.5	6.5	10.4

Table XXXI. Isothermal data for Alloy XIX.

Run No.	Temp. °C	t start	t25	t50	t75	t saturation
1	380	0.24	0.9	1.6	3.0	20.6
2	400	0.3	1.74	3.2	5.3	27.8
3	420	0.18	1.2	2.3	3.6	24.3
4	440	0.42	1.14	1.9	2.8	28.1
5	460	0.36	0.63	0.8	0.9	14.5
6	500	0.54	0.9	1.3	1.7	2.0
7	520	0.3	0.66	0.8	1.1	1.6
8	535	0.15	0.54	0.7	0.9	2.1
9	560	0.36	0.57	0.7	0.8	1.5
10	575	0.24	0.54	0.7	0.9	3.6
11	600	0.72	1.56	1.7	2.2	3.0
12	618	0.54	0.63	0.8	1.5	7.2
13	635	0.54	1.53	1.7	2.0	4.3
14	640	0.9	1.32	1.5	1.9	68.4
15	660	0.45	1.26	1.9	3.7	643.3

Table XXXII. Isothermal data for Alloy XX

Run No.	Temp. °C	t start	t25	t50	t75	t saturation
1	380	0.24	0.72	1.3	2.1	36
2	400	0.3	1.14	1.9	2.5	33.3
3	420	0.36	1.5	2.4	3.6	34.2
4	440	0.24	1.8	3.6	5.2	28.0
5	460	2.58	4.2	5.4	7.3	20.6
6	480	1.5	2.5	3.2	4.3	31.5
7	500	0.72	1.6	2.3	6.9	30.0
8	520	0.54	1.9	3.0	4.1	23.9
9	540	0.45	1.1	1.3	1.7	20.7
10	560	0.3	0.96	1.3	1.6	145.8
11	580	0.3	0.78	1.2	1.7	162.6
12	600	0.6	0.9	1.3	1.6	230.5
13	618	0.3	0.84	1.4	1.7	559.9
14	640	0.42	1.9	3.2	69.5	1179.5
15	660	4.35	6.3	12.8	69.0	1388.9

Table XXXIII. Reproducibility with same Quenching Rate.

Alloy No.	Isoth. Temp. °C	Aust. Temp.	t start	t25	t50	t75	t saturation (Sec)
IV	450	1080	2.52	6.0	7.6	9.6	26.0
IV	450	1080	2.85	5.46	7.23	9.3	30.0
I	538	1080	1.6	3.5	4.3	5.3	7.6
I	540	1080	1.56	2.9	3.8	4.5	7.4
V	415	1080	0.564	2.9	4.26	6.2	15.1
V	415	1080	0.55	3.0	4.68	6.7	19.6
V	512	1080	1.78	5.0	7.0	9.5	17.5
V	512	1080	1.8	3.4	4.7	8.5	22.0
V	560	1080	0.39	1.9	2.34	3.14	3.5
V	560	1080	0.5	1.65	2.34	2.7	3.9
V	560	1080	0.5	1.62	2.22	2.7	3.84
VI	450	1080	0.66	3.7	5.7	7.7	21.5
VI	450	1080	0.6	4.6	6.9	9.3	25.2
VII	545	1080	2.7	4.6	5.9	7.4	17.2
VII	545	1080	2.88	5.1	6.9	8.8	22.8
XVI	560	1080	1.26	6.0	11.34	12.3	34.78
XVI	560	1080	2.08	5.0	8.76	12.45	30.6

00004708653

Table XXXIX. Effect of Quenching Rate on the Bainite Kinetics and Reproducibility

Alloy No.	QR °C/sec	Aust. Temp.	Isoth. Temp. °C	t0 sec	t25 sec	t50 sec	t75 sec	t saturation
IV	12.9	1095	450	0.28	1.16	1.6	2.2	8.72
IV	118.0	1090	450	0.36	0.74	0.98	1.3	3.36
IV	148.0	1090	450	0.34	0.54	0.86	1.22	3.34
IV	118.0	1090	450	0.29	0.52	0.75	1.05	3.27
I	69.26	1090	520	0.78	1.22	1.41	1.72	2.58
I	70.1	1085	520	0.52	0.83	1.12	1.37	2.58
I	70.1	1085	520	0.7	1.1	1.3	1.56	2.3
I	133.0	1085	520	0.9	1.38	1.62	1.92	2.56
I	148.0	1085	520	0.95	1.34	1.6	1.9	2.5
XVI	39.4	1080	560	1.08	2.79	5.13	8.61	25.9
XVI	43.3	1080	560	1.14	4.14	6.66	10.08	28.26
XVI	165.0	1080	560	1.26	6.0	11.34	12.3	24.78
XVI	180.6	1080	560	1.08	5.1	8.76	12.45	30.6



Table XXXV. Effect of austenitizing temperature on the bainite kinetics

Alloy	Aust. Temp. °C	Trans. Temp. °C	QR %/sec	t <sub>0</sub> sec	t <sub>25</sub> sec	t <sub>50</sub> sec	t <sub>75</sub> sec	t <sub>8</sub> sec
IV	1215	450	197.2	.42	.84	1.1	1.37	3.58
IV	1090	450	148.1	.27	.52	.75	1.05	3.27
IV	950	450	154.3	.1	.4	.56	.74	2.76
I	1200	520	94.4	1.02	1.44	1.78	2.12	4.04
I	1090	520	61.7	.78	1.22	1.41	1.72	2.58
I	955	520	68.4	.26	.62	.98	1.25	1.86

00104708654

Table XXXVI. Comparisons of temperatures at which the upper-lower bainite bay is located with  $B_s$  on the basis of empirical formulae.

Alloy	Spec. No.	Bainitic Bay Start Diagram	Stevens and Haynes (°C) $B_s$	Prakash Babu (°C) $B_s$
I	4	500	729	741
II	5	450	707	724
III	6	445	685	708
IV	7	450	702	692
V	8	470	718	714
VI	10	450	659	681
VII	11	450	725	714
VIII	12	480	660	645
IX	13	440	701	653
X	14	475	643	656
XI	16	460	640	646
XII	17	400	615	569
XIII	20	380	569	495
XIV	21	440	730	728
XV	22	430	723	722
XVI	24	*—	723	681
XVII	25	—	727	639
XVIII	26	—	723	690
XIX	17	435	736	734
XX	28	450	741	740

\* The three Si alloys did not have a marked Bay region below the upper and lower bainite temperature ranges.

TABLE XXXVII. Hardness of some bainitic structures.

C wt%	Alloy No.		Isothermal Transformation Temperature °C		Vickers Hardness at 1.000 gr Load								
			Temp °C	M <sub>s</sub>									
0.27	II	(Mo)	Temp °C	M <sub>s</sub>	416	435	460	490	512	610			
			VHN		495	309	311	261	243	187			
0.29	V	(Ni)	Temp °C	M <sub>s</sub>	390	415	440	460	489	512	560	520	660
			VHN		499	309	260	244	228	204	195	163	155
0.29	VI	(Cr)	Temp °C	M <sub>s</sub>	277	400	425	450	475	500	550	600	
			VHN		422	422	481	326	264	262	212	198	
0.4	XII	(Mn)	Temp °C	M <sub>s</sub>	330	350	400	455	500	560	610		
			VHN		575	459	374	300	263	239	220		
0.37	XIV	(Al)	Temp °C	M <sub>s</sub>	367	400	440	460	500	540	580	620	
			VHN		581	368	272	261	273	242	221	219	
0.38	XVII	(Si)	Temp °C	M <sub>s</sub>	368	400	440	460	500	540	580	620	
			VHN		660	432	325	330	272	254	257	254	
0.33	XX	(Co)	Temp °C	M <sub>s</sub>	390	400	460	500	540	580	620		
			VHN		460	353	263	245	201	214	193	182	

0000470855

Table XXXVIII. Austin-Pickett generalized equation values of n and k for alloy III at the different transformation temperatures  
M =  $M_A$  average, r = average correlation factor.

Temp.	M	Intercept	k	r	r <sup>2</sup>
497	2.69	-1.59	0.725	0.93	0.86
423	2.38	-1.39	0.736	0.86	0.74
445	4.15	-1.95	0.557	0.93	0.86
470	4.0	-1.83	0.547	0.99	0.98
487	4.22	-1.99	0.557	0.99	0.98
520	4.72	-2.27	0.557	0.94	0.88
555	4.78	-1.68	0.4271	0.85	0.72
595	3.53	-0.79	0.326	0.8	0.64
640	8.	-1.13	0.186	0.99	0.98

Table XXXIX. ASTM grain size for different austenitizing temperatures.  
(15 min).

Spec. No.	AT (°C)	ASTM (No.)
IV	950	6
IV	1080	4
IV	1210	2
I	955	6-7
I	1085	3-4
I	1200	(1-2)

FIGURE CAPTIONS

Fig. 1. Dimension specifications of the dilatometer specimens.

Fig. 2. Specimen mounting conditions.

Fig. 3. Dilatometer III-R measuring module chamber.

- A. Micrometer adjusting barrel.
- B. Location of calibration shim placement.
- C. Locking screw measuring module travel.
- E. Set screws holding glass rod which centers measuring rods and determines the specimen gap between the rods.
- F. Induction coil furnace where the specimen is placed for heating treatments.
- G. thermocouple attached to specimen (inside the furnace).
- H. Hose that connects the quenching valve to the specimen through which gaseous helium flows for fast quenches.

Fig. 4. Dilatometer III-R. Vacuum system.

Fig. 5. Dilatometer III-R. Pumping station.

- A. On-Off switch, mechanical pump.
- B. On-off switch, diffusion pump.
- C. Switch controlling soft vacuum Gage E (to left--vacuum at fore pump, to right--vacuum in specimen chamber).
- D. Switch controlling ion Gage F.
- E. Soft vacuum gage.
- F. Hand Vacuum ion gage.
- G. Flow valve and meter for quenching gas.

Fig. 6. Typical run for  $M_s$  determination (fast quench).

- Fig. 7. Typical run for the bainite transformation (isothermal run).
- Fig. 8. Effect of austenitizing temperature on  $M_s$ . Alloys I, IV, XXI.
- Fig. 9. Microhardness vs carbon content in martensitic structures. Comparison with Bain and Paxton's plain carbon steels with 15 kg load.
- Fig. 10. Microhardness vs martensite transformation temperature.
- Fig. 11. Reproducibility of average quenching rate for 6 martensitic transformation runs of alloy XIV.
- Fig. 12. Effect of quenching rate on  $M_s$  after Ansell.<sup>31</sup> Showing the quenching rate working range.
- Fig. 13 TTT diagram of the austenite to bainite transformation for through  
Fig. 32. the various alloys studied (I-XX).
- Fig. 33. Diagrams for the starting time (curve) of the austenite to bainite transformation for the three Si steels.
- Fig. 34. Upper-lower bainite range vs carbon content.
- Fig. 35. Effect of quenching rate on the bainite kinetics IV, I.
- Fig. 36. Effect of quenching rate on the bainite kinetics XVI.
- Fig. 37. Effect of slight variations in quenching rate on reproducibility IV, I.
- Fig. 38. Reproducibility of bainite reaction kinetic data for the same alloy V at different temperatures 560, 415°C.
- Fig. 39. Effect of austenitizing temperature on the bainite kinetics for alloys IV, I.

Fig. 40. Reaction times for progressive stages of the transformation vs the austenitizing temperature (IV, I).

Fig. 41. Microhardness vs bainite transformation temperature for seven alloys (Mo II, Ni V, Cr VI, Mn XII, Al XIV, Si XVII, and Co XX).

Fig. 42. A. Typical percent transformed curves vs time (e.g., alloy I).  
B. Typical percent transformed curves vs  $\ln$  (time) (e.g., alloy I).

Fig. 43. Times for transformation at different temperatures for some alloys plotted according to the Johnson Mehl-Zenner equation

- a. Mo alloy No. I
- b. Ni alloy No. V
- c. Si alloy No. XVII
- d. Al alloy No. XIV.

Fig. 44. Times for transformation at different temperatures for some alloys plotted according to Austin-Rickett equation.

- a. Mo alloy No. I
- b. Ni alloy No. V
- c. Si alloy No. XVII
- d. Al alloy Mo. XIV.

Fig. 45.  $N_A$  index as a function of temperature at various stages of (%) transformation for some alloys

- a. Mo alloy No. I
- b. Mo alloy No. III
- c. Ni alloy No. IV
- d. Cr alloy No. VI
- e. Mn alloy No. XII
- f. Ni-Mo alloy No. IX.



Fig. 46.  $N_A$  index as a function of time elapsed at the different isothermal holds for some alloys

- a. Mn alloy No. XII
- b. Mo alloy No. III
- c. Cr-Mo alloy No. X
- d. Cr-Ni alloy No. VIII.

Fig. 47.  $-\ln(\text{time})$  vs  $1/T$  for different stages (%) of transformation in order to observe the variations of activation energies (it was not a constant slope over the bainitic regions).

Results for some alloys shown

- a. Mo III
- b. Ni IV
- c. Cr VIII
- d. Mn XIII
- e. Al XIV
- f. Si XVI
- g. Co XIX.

Fig. 48. Effect of austenitizing temperature on grain size  $d$ -diameter of an equivalent spherically shaped grain.

Fig. 49 Show the martensitic structures of seven of the alloys studied through

Fig. 55. (Mo II, Ni V, Cr VII, Mn XII, Al XIV, Si XVIII, Co XX).

Fig. 56. Alloy V at 660°C isothermal hold. Degenerate pearlite.

Fig. 57. Alloy V at 512°C. Degenerate structure.

Fig. 58. Alloy V at 489°C. Upper bainite.

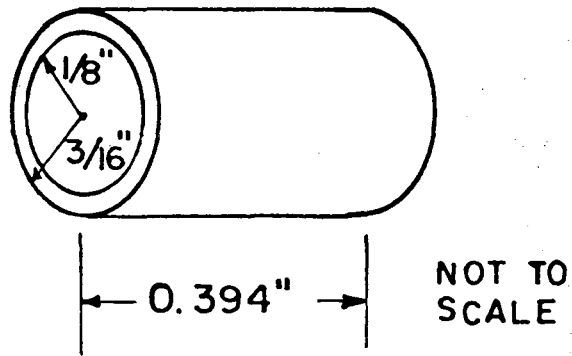
Fig. 59. Alloy V at 460°C. Upper-lower bainite.

Fig. 60. Alloy V at 400°C. Lower bainite.

- Fig. 61. Alloy II at 620°C. Degenerate pearlite.
- Fig. 62. Alloy II at 512°C. Upper bainite.
- Fig. 63. Alloy II at 435°C. Upper-lower bainite.
- Fig. 64. Alloy VI at 660°C. Preeutectoid ferrite and eutectic matrix.
- Fig. 65. Alloy VI at 555°C. Degenerate pearlite.
- Fig. 66. Alloy VI at 460°C. Upper-lower bainite.
- Fig. 67. Alloy VI at 460°C. Upper-lower bainite.
- Fig. 68. Alloy XII at 610°C. Preeutectoid ferrite and eutectic matrix.
- Fig. 69. Alloy XII at 560°C. Partly transformed upper bainite.
- Fig. 70. Alloy XII at 400°C. Upper-lower bainite.
- Fig. 71. Alloy XII at 350°C. Lower-upper bainite.
- Fig. 72. Alloy XIV at 400°C. Lower bainite.
- Fig. 73. Alloy XIV at 440°C. Lower-upper bainite.
- Fig. 74. Alloy XIV at 460°C. Upper bainite.
- Fig. 75. Alloy XIV at 500°C. Upper bainite. Notice Windmastaten ferrite present.
- Fig. 76. Alloy XIV at 450°C. Upper bainite.
- Fig. 77. Alloy XIV at 620°C. Degenerate pearlite.
- Fig. 78. Alloy XVIII at 400°C. Lower bainite.
- Fig. 79. Alloy XVIII at 440°C. Lower bainite.
- Fig. 80. Alloy XVIII at 460°C. Upper bainite.
- Fig. 81. Alloy XVIII at 540°C. Upper bainite and pearlite eutectic matrix.
- Fig. 82. Alloy XX at 400°C. Lower bainite.
- Fig. 83. Alloy XX at 440°C. Lower bainite.

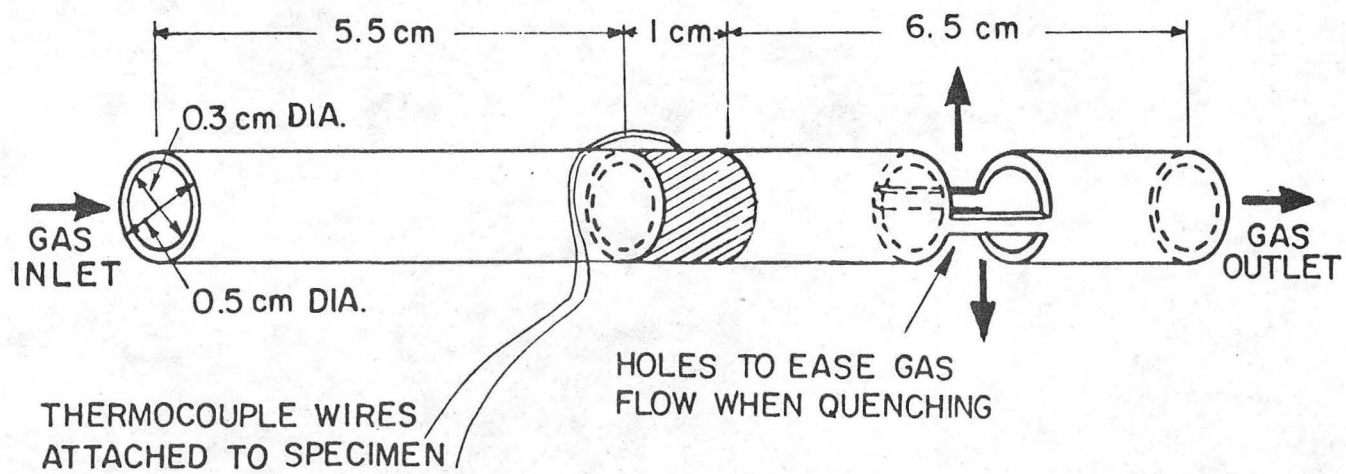
Fig. 84. Alloy XX at 460°C. Upper bainite.

Fig. 85. Alloy XX at 540°C. Degenerate pearlitic and bainite structures.



XBL 75 12-9273

Fig. 1

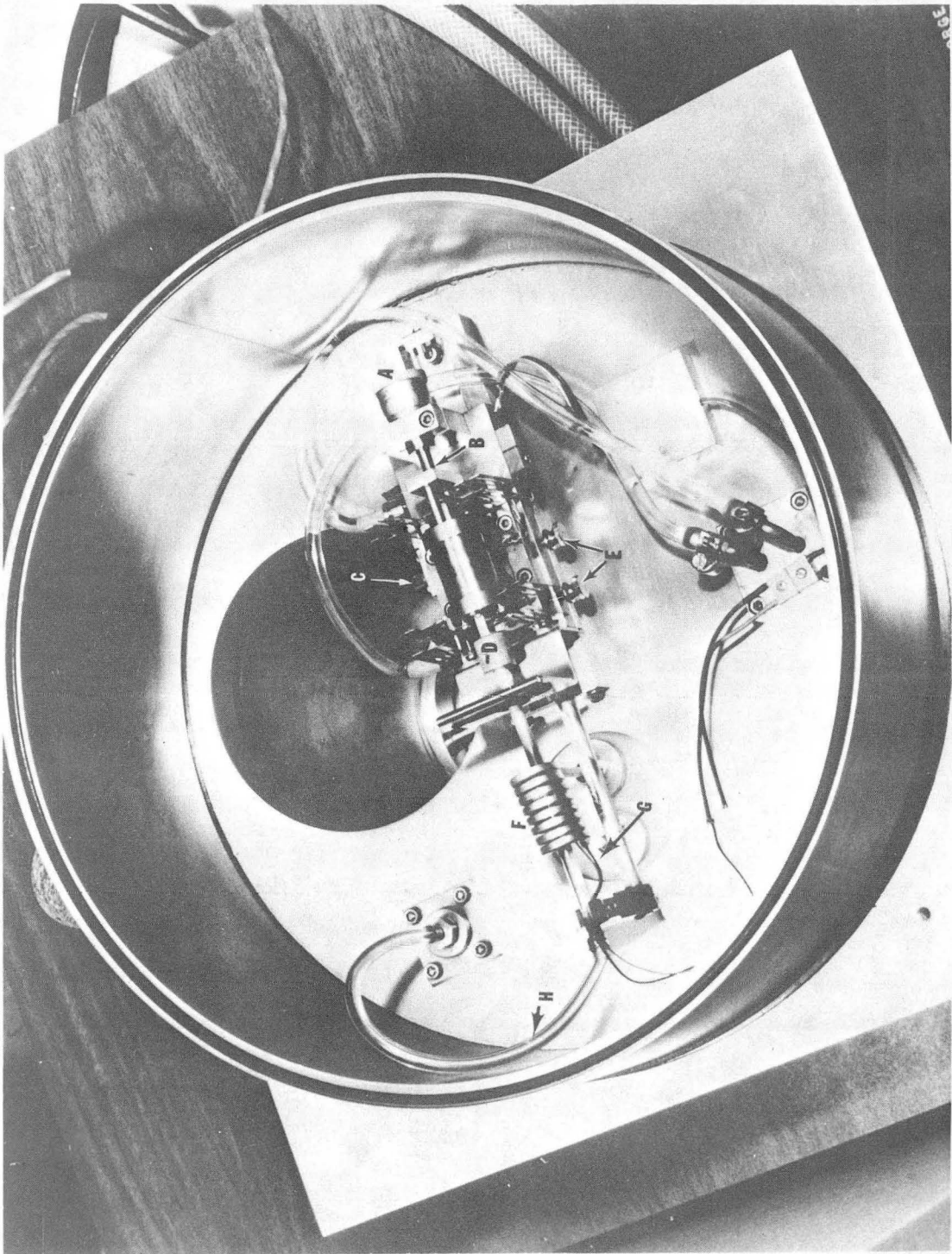


NOT TO SCALE

XBL 7512-9274

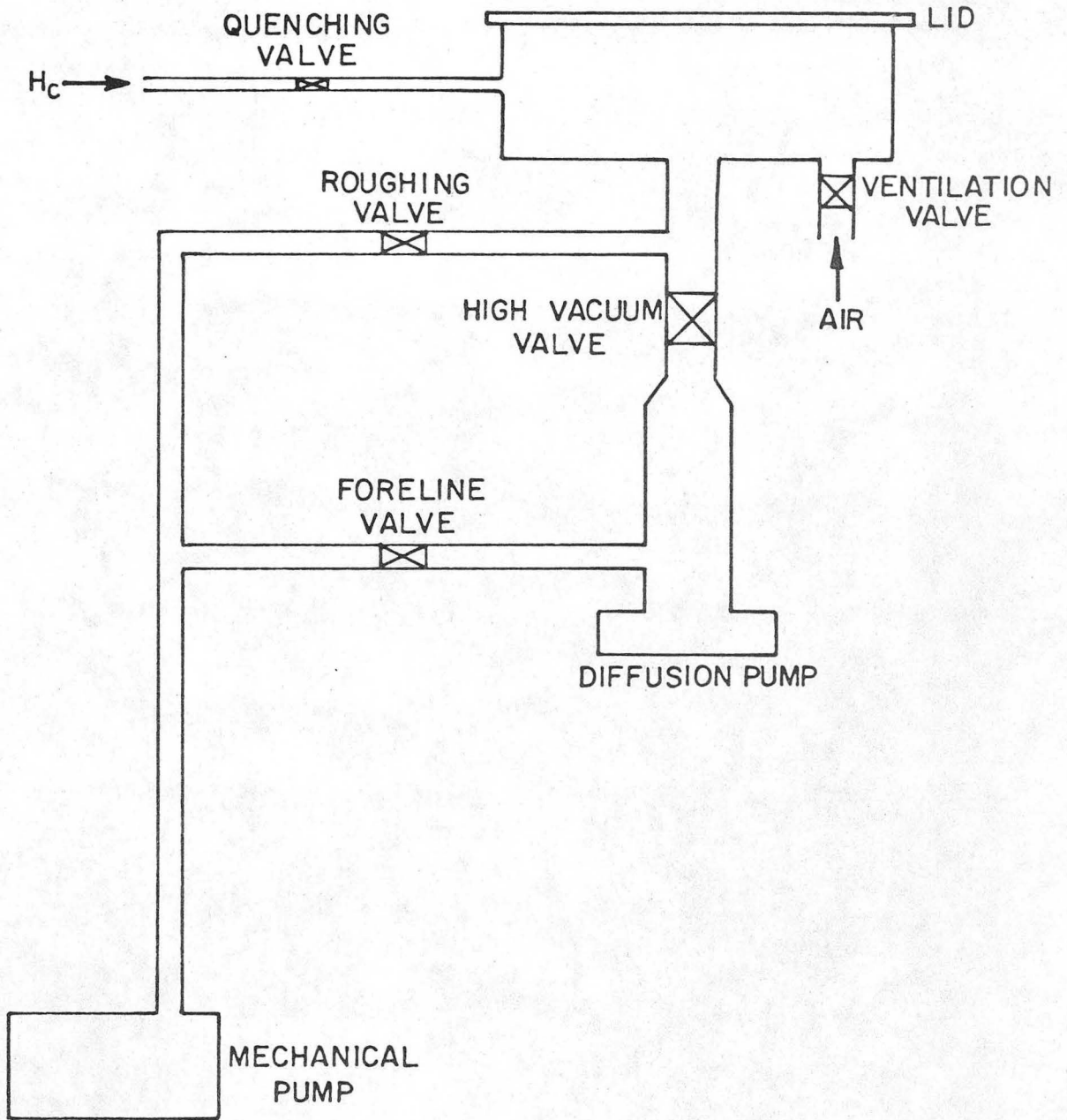
Fig. 2

00004708660



XBB7512-2369B

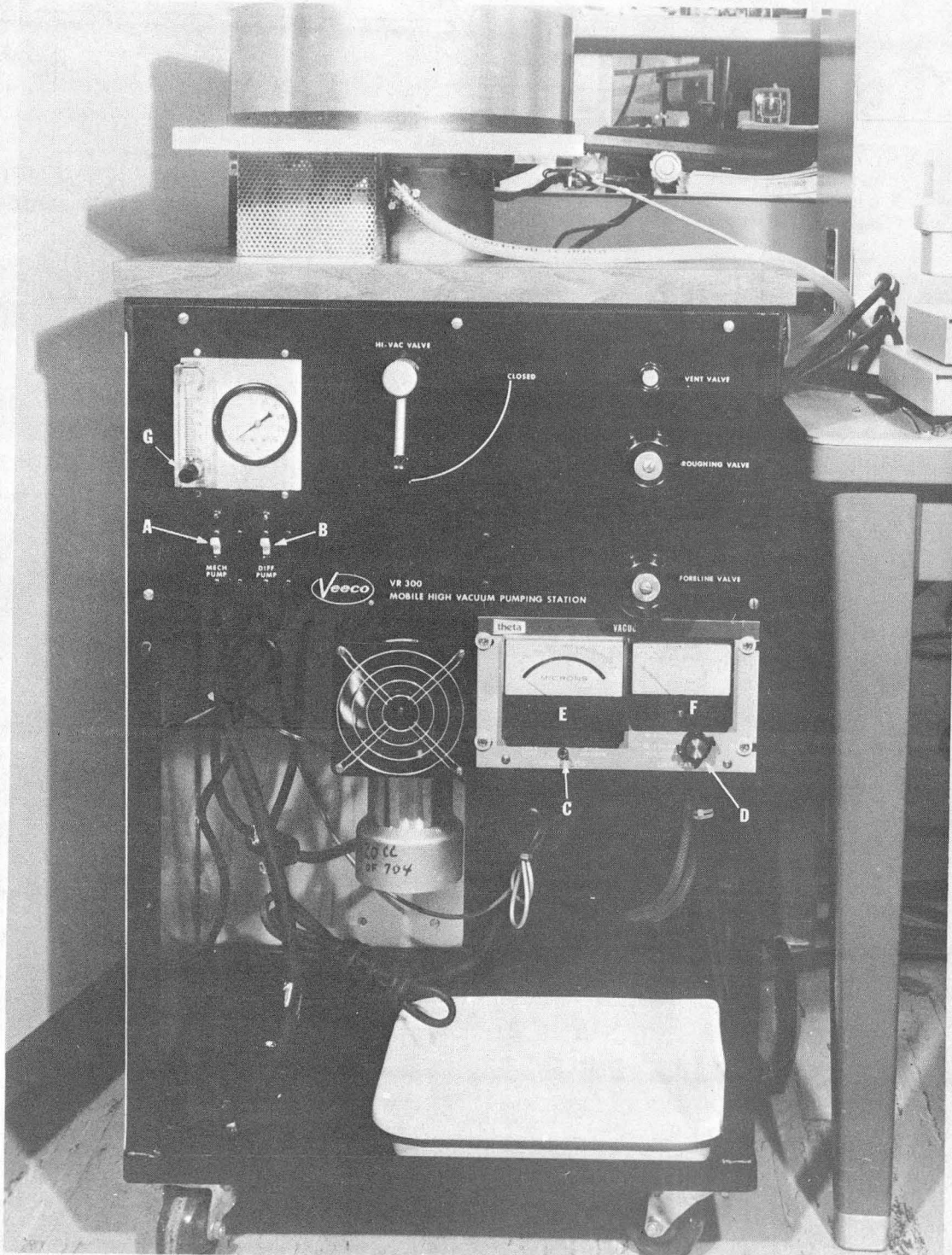
Fig. 3



XBL 7512-9275

Fig. 4





XBB 753-2368A

Fig. 5



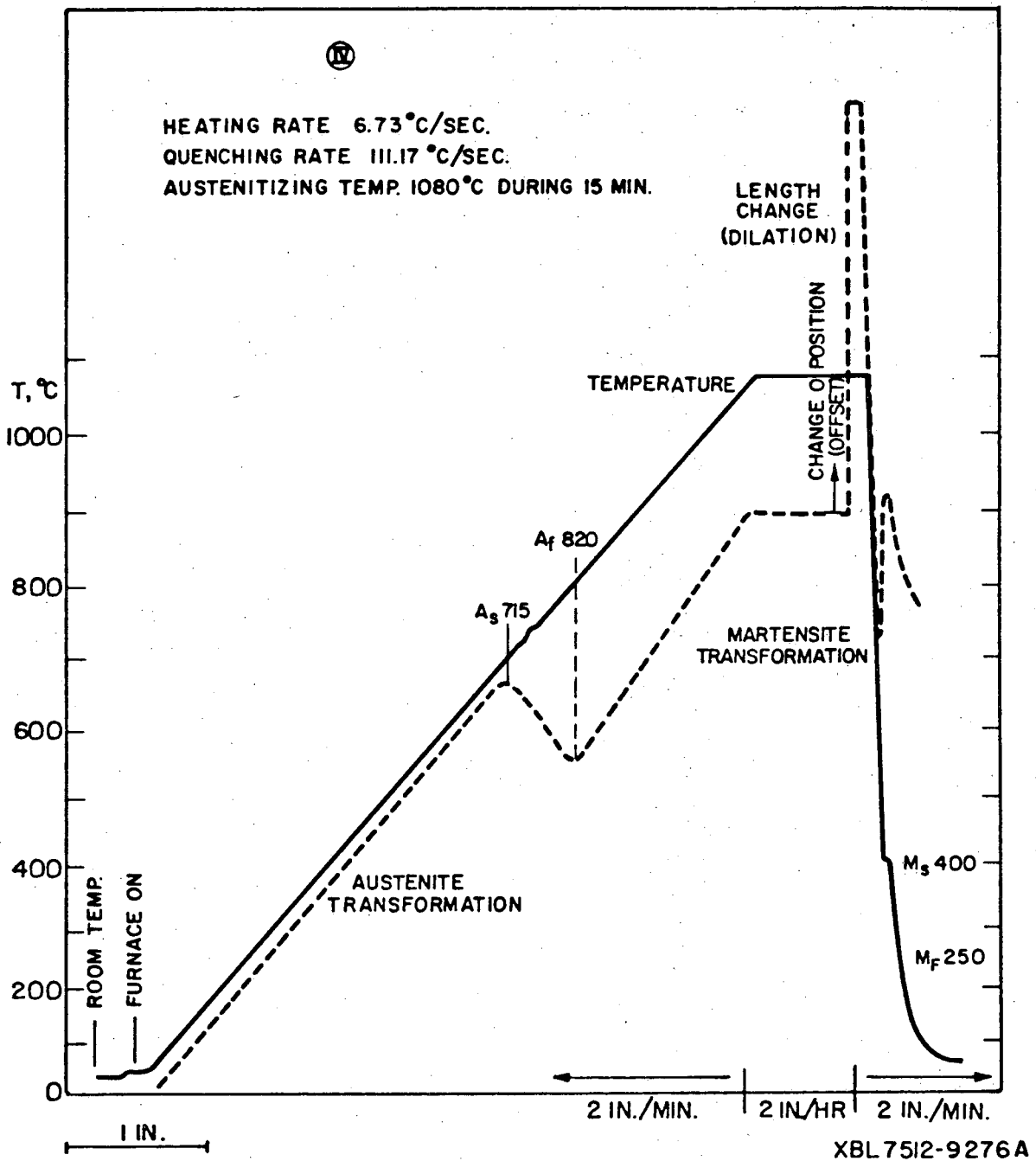
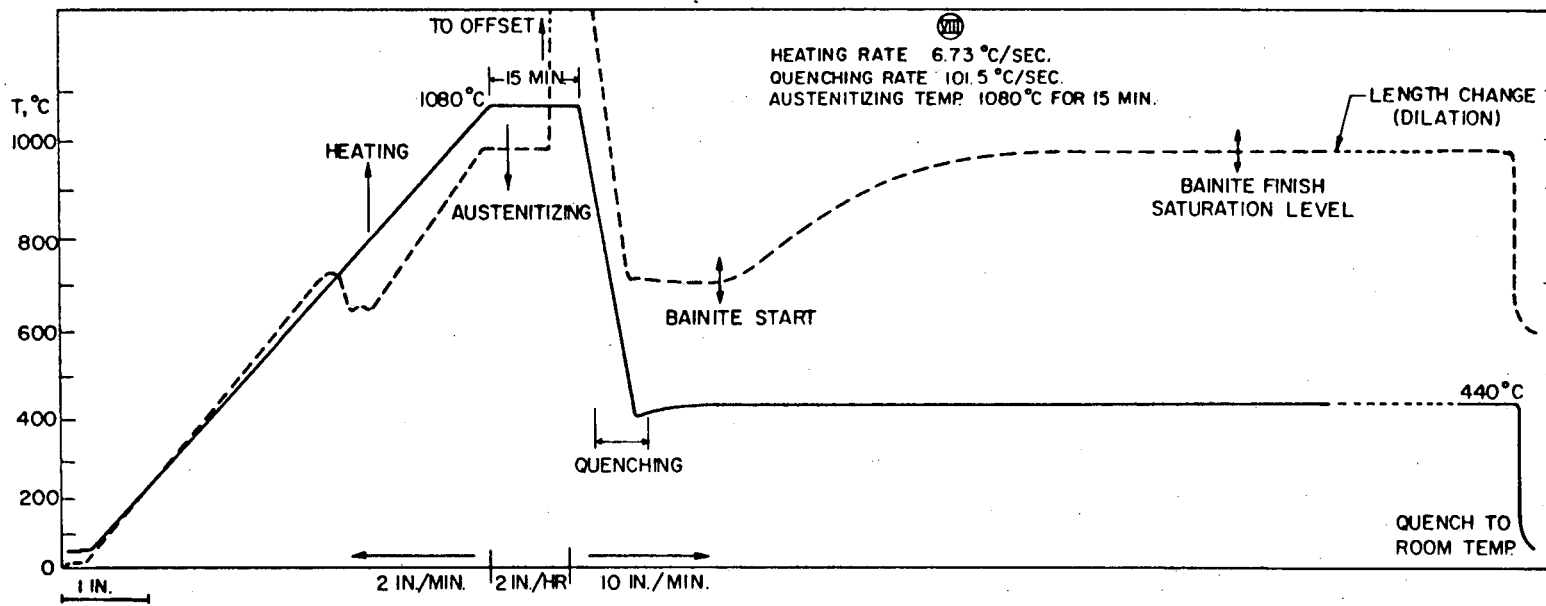
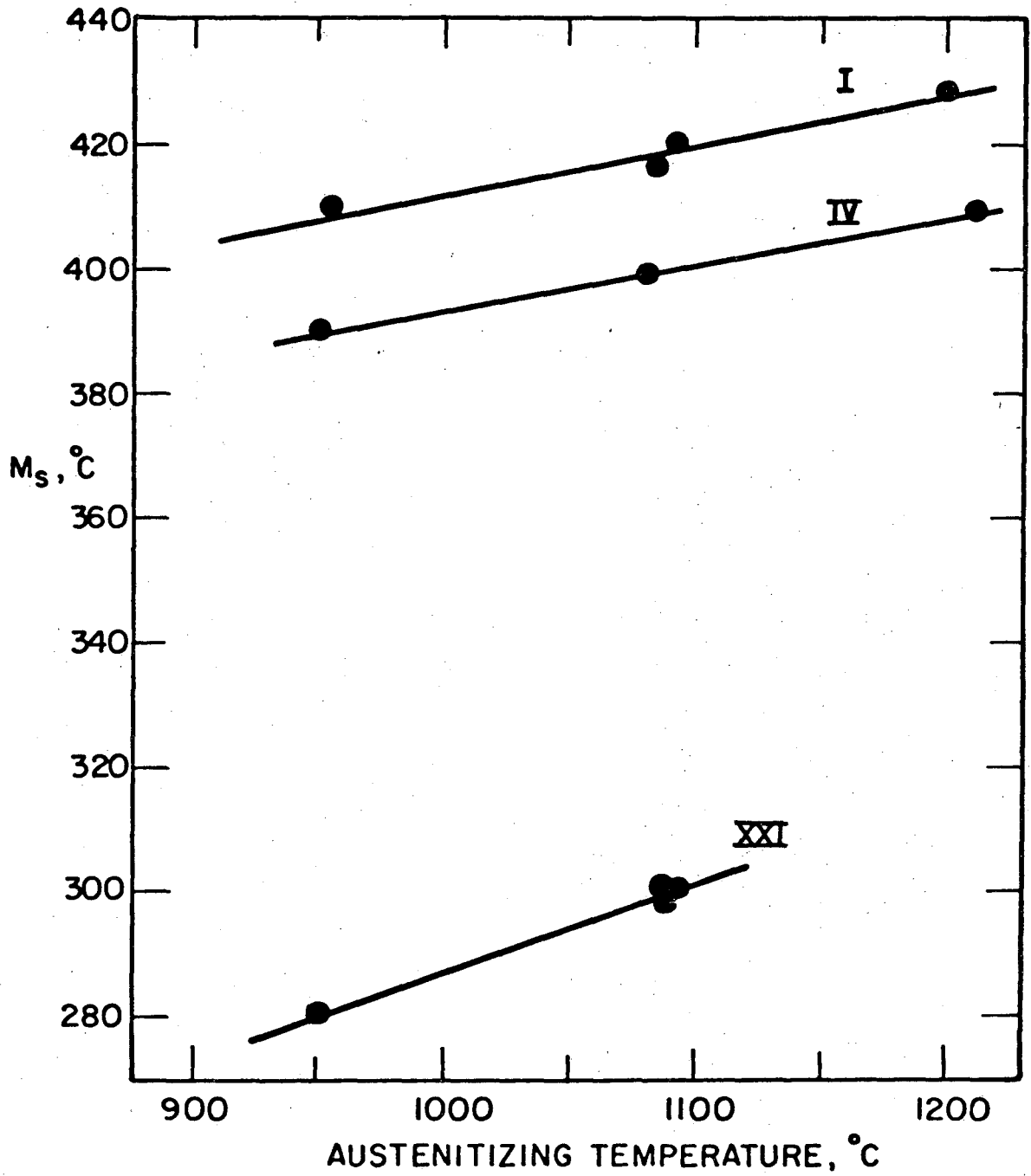


Fig. 6



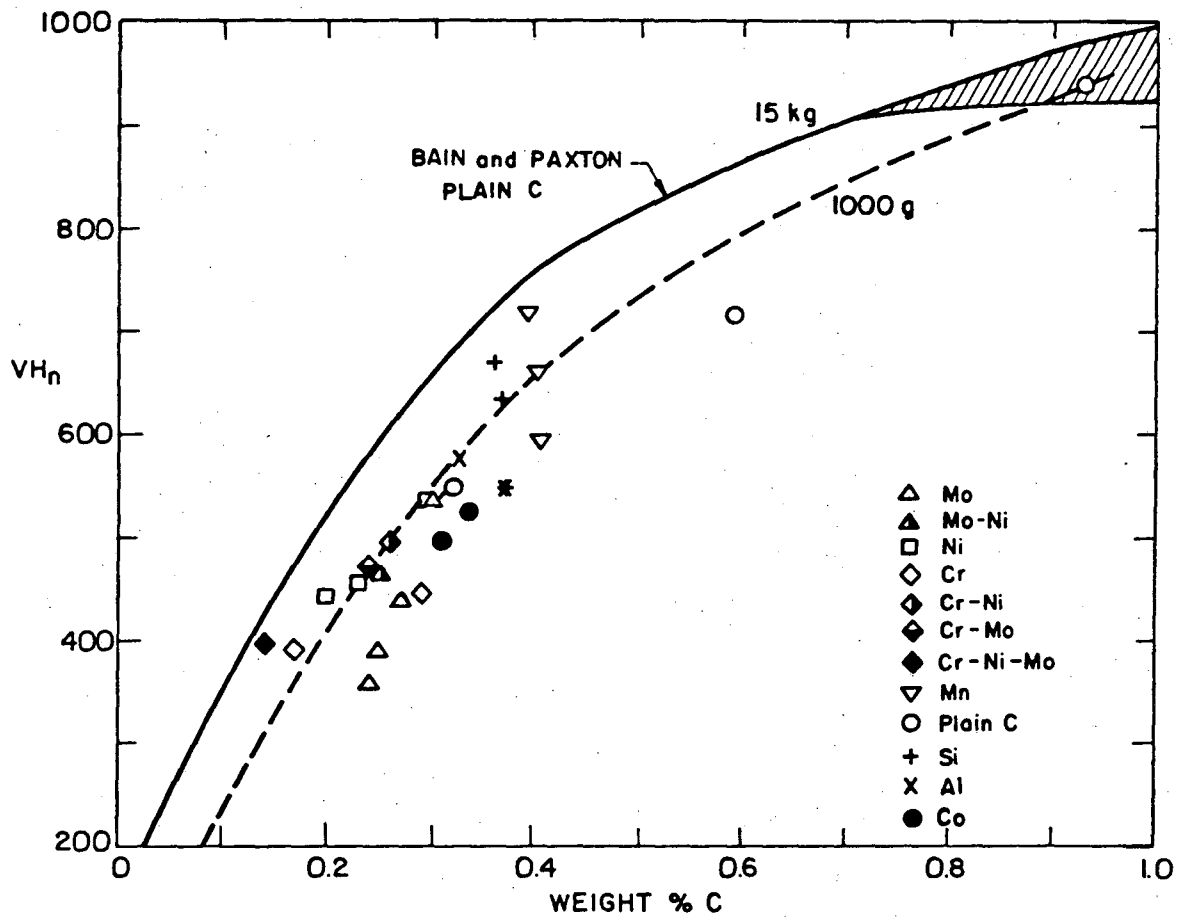
XBL 7512-9277 A

Fig. 7



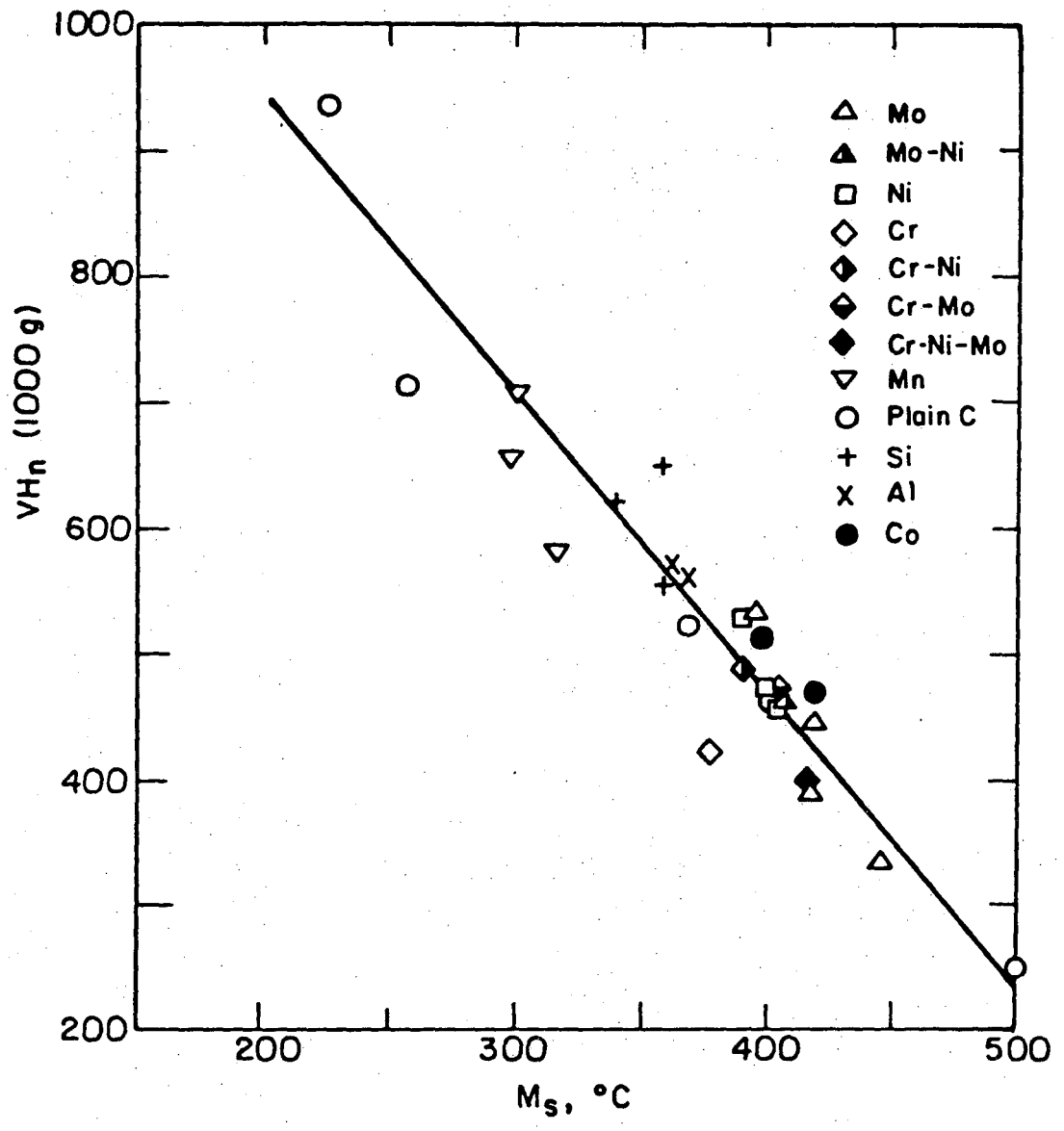
XBL 7612-7972

Fig. 8



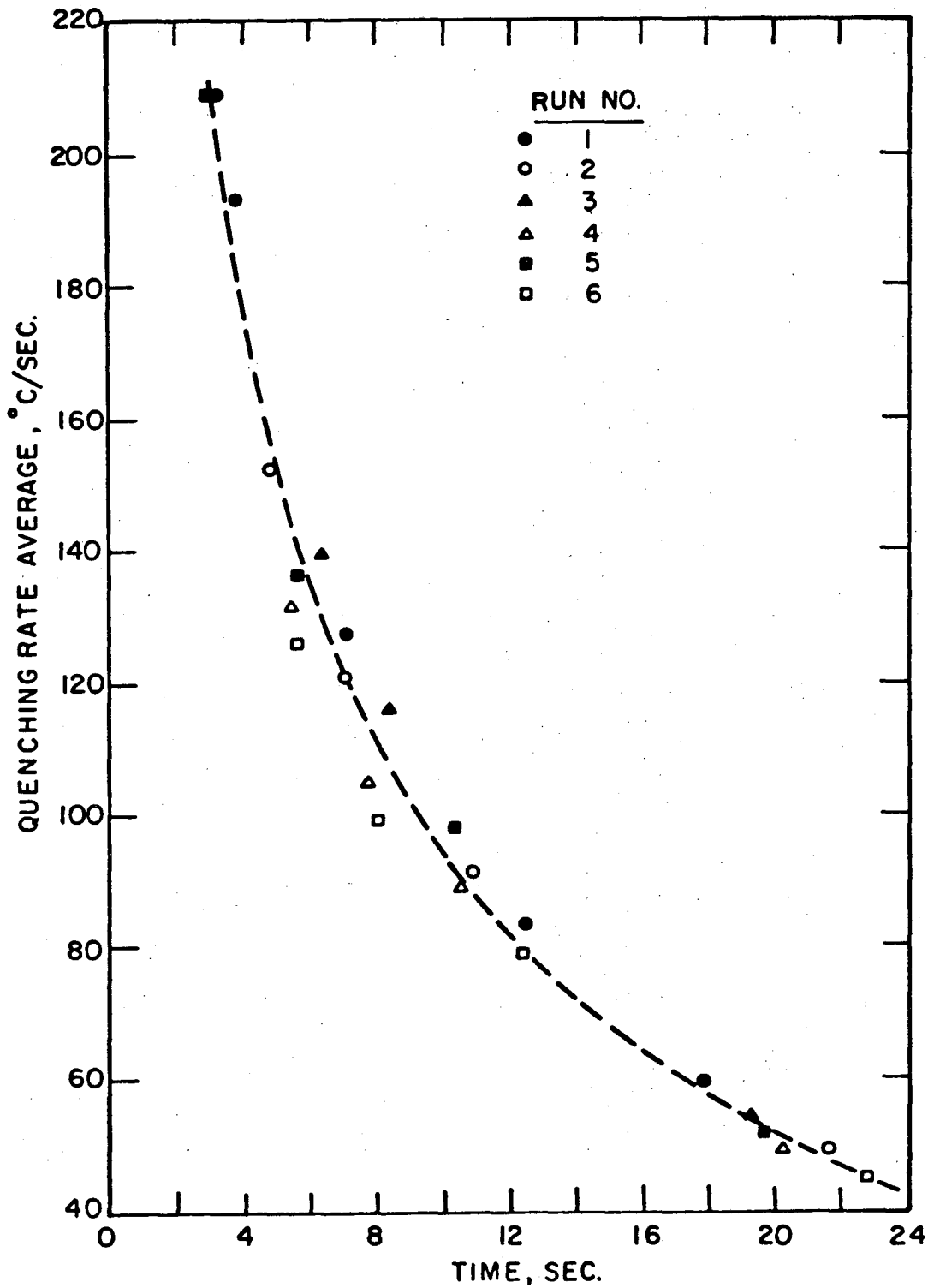
XBL 7512-10,004A

Fig. 9



XBL 7512-9288

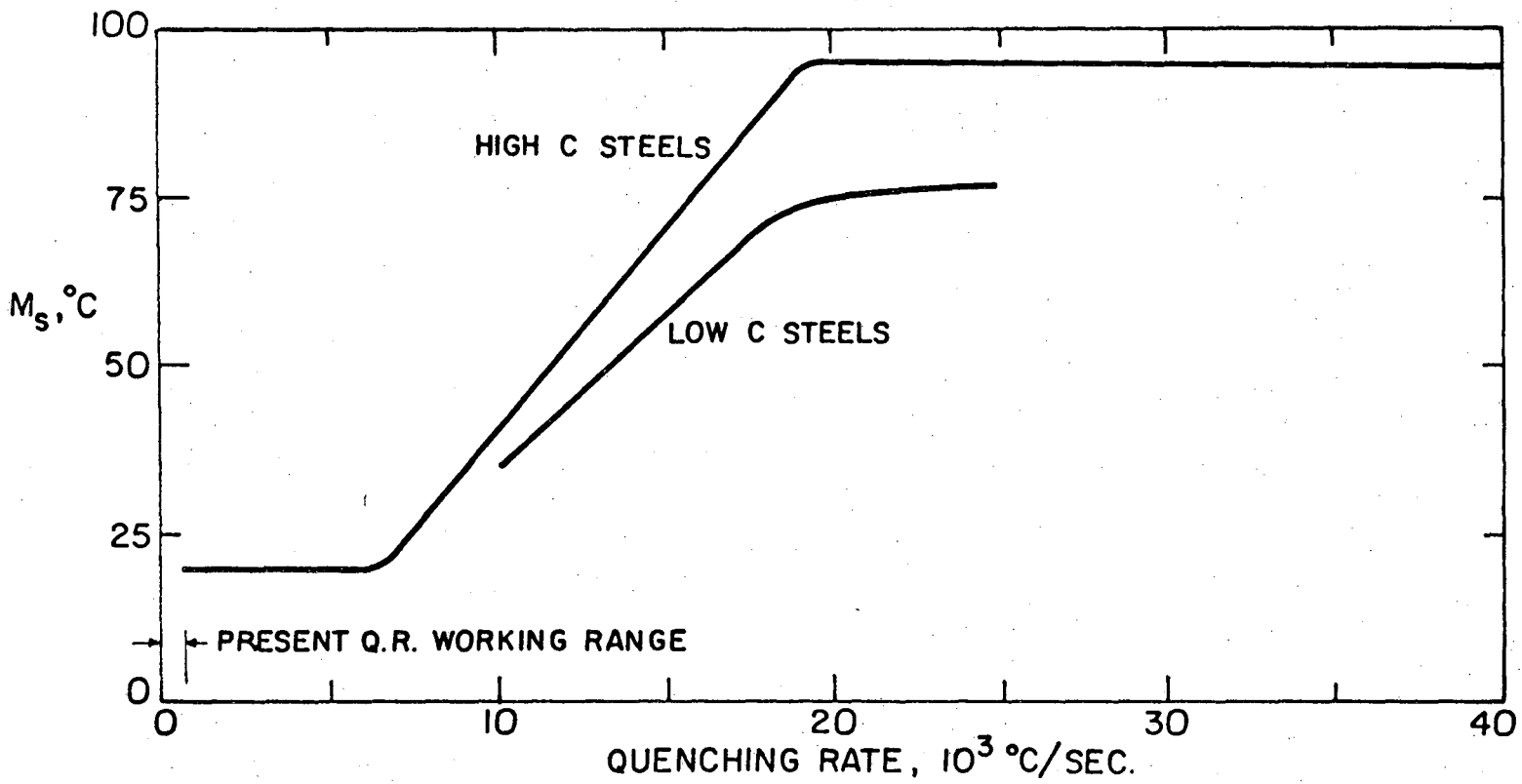
Fig. 10



XBL7612-7973

Fig. 11

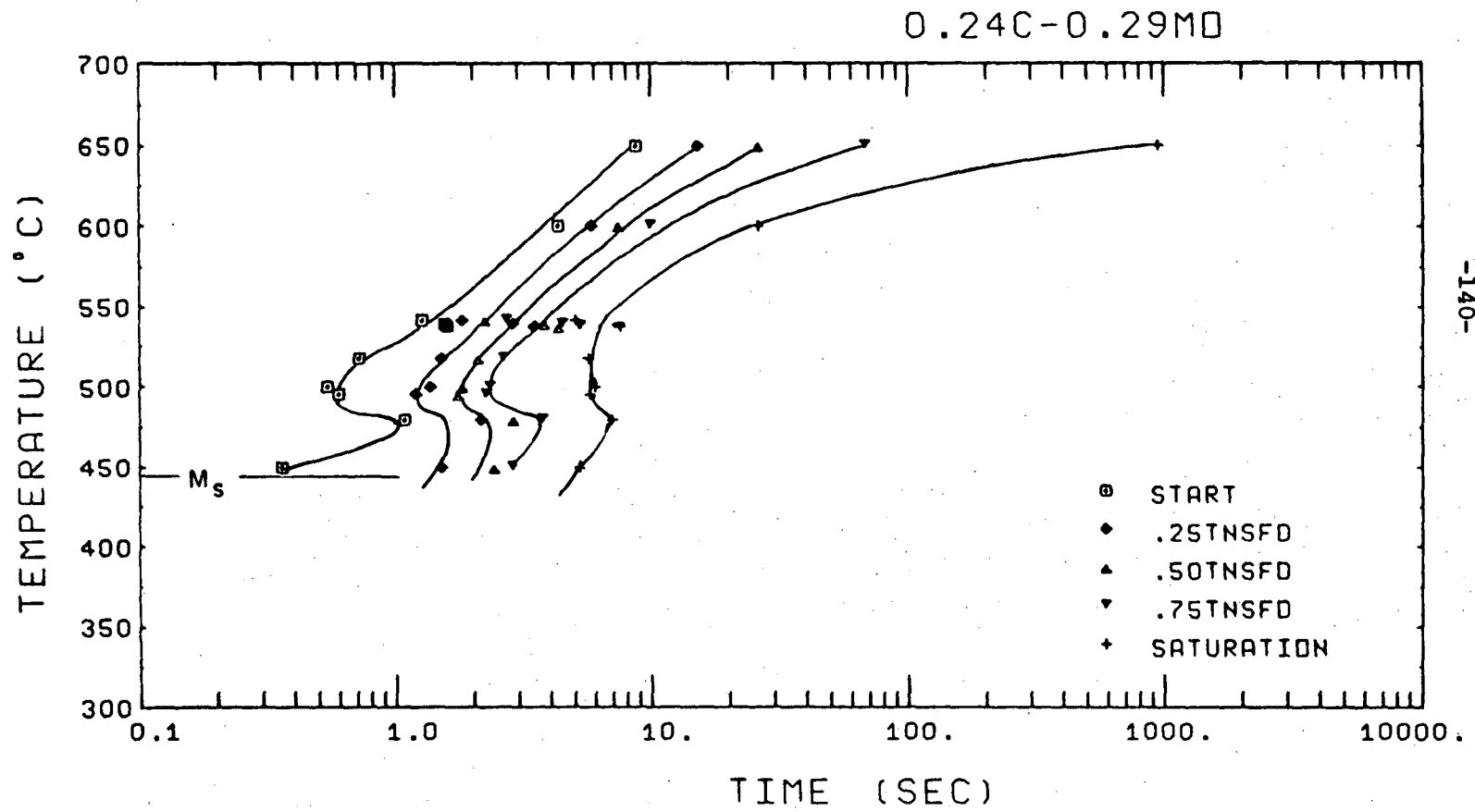
00004708664



-139-

XBL 7512-9285

Fig. 12

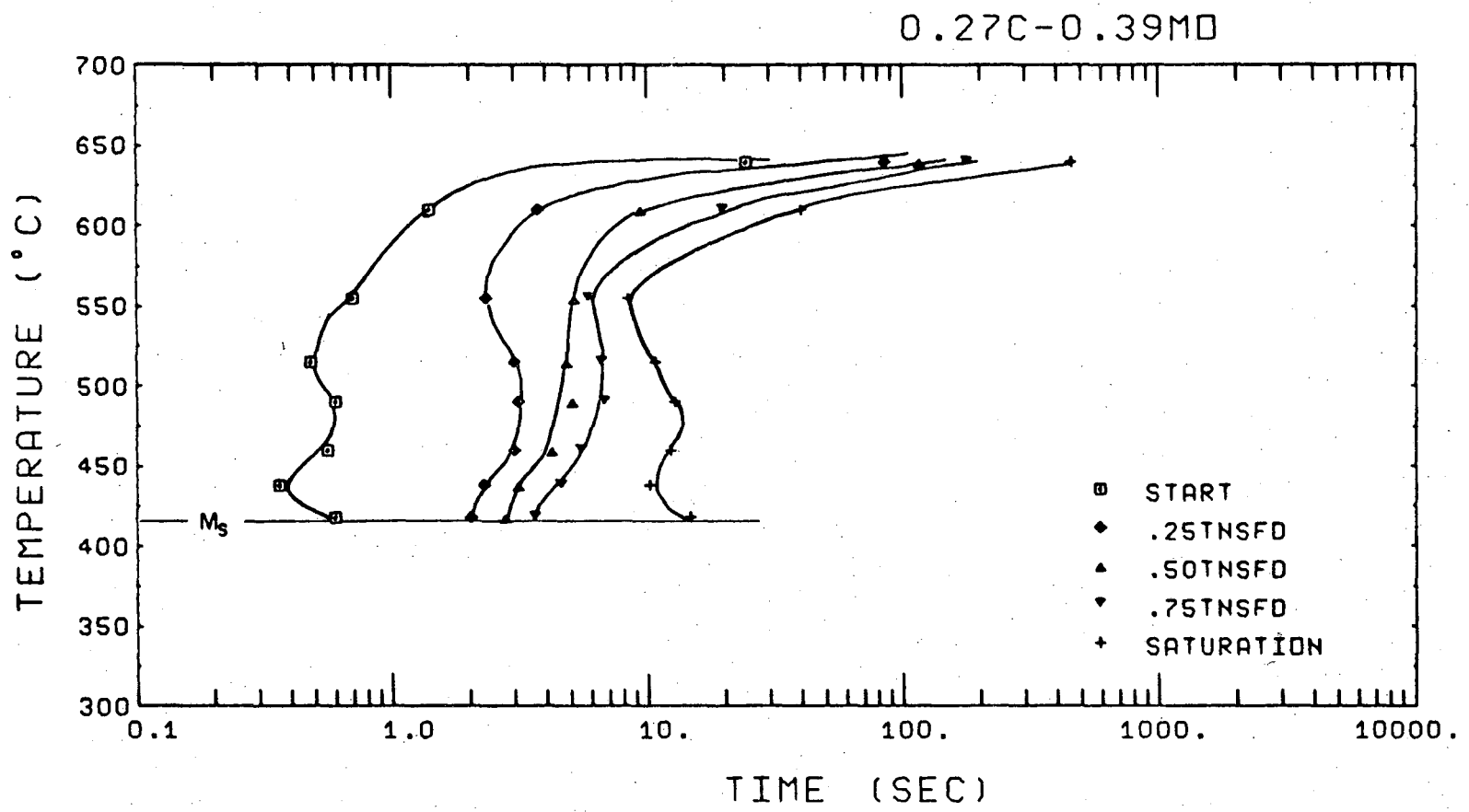


XBL 769-10423

Fig. 13



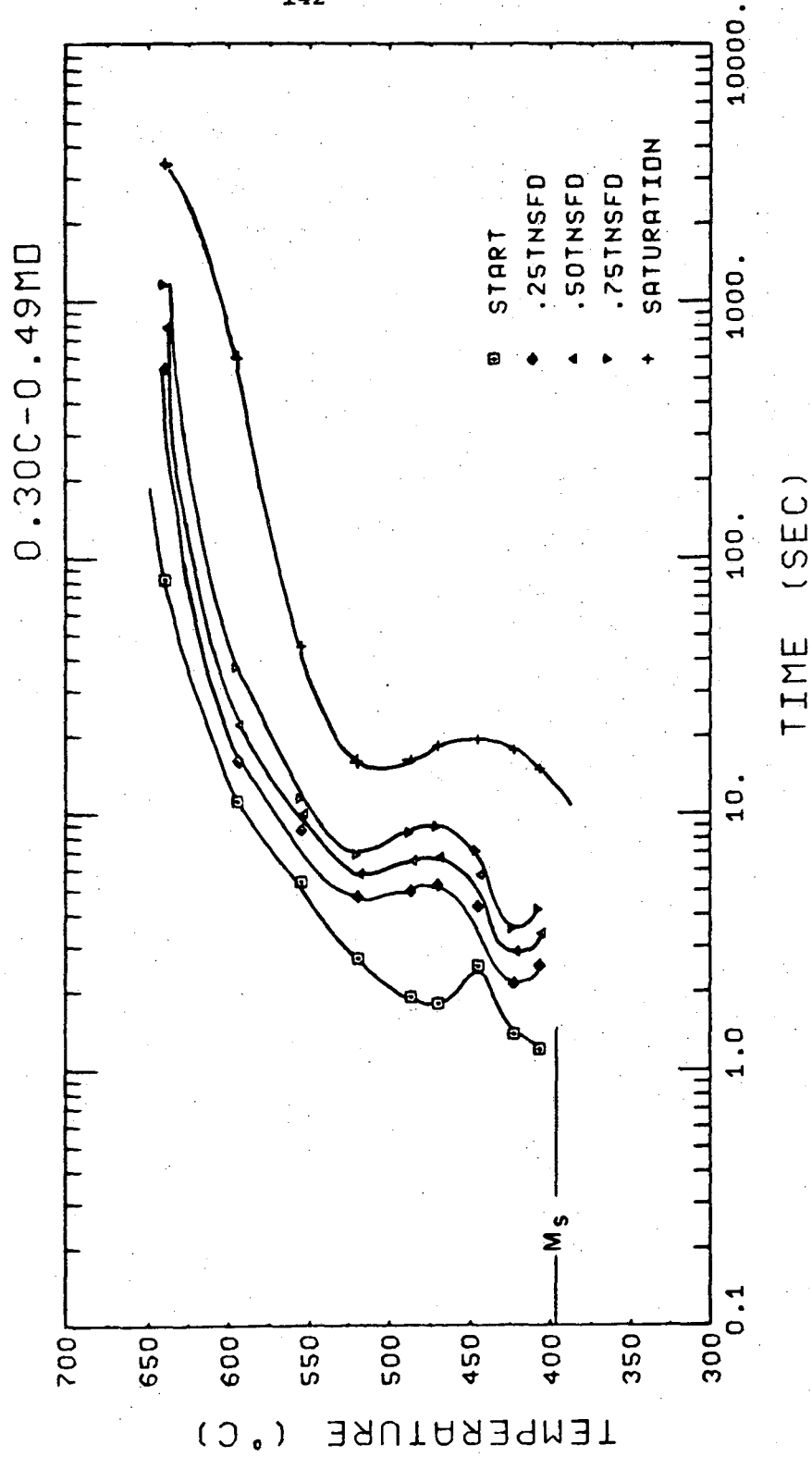
00004708665



-141-

XBL 769-10422

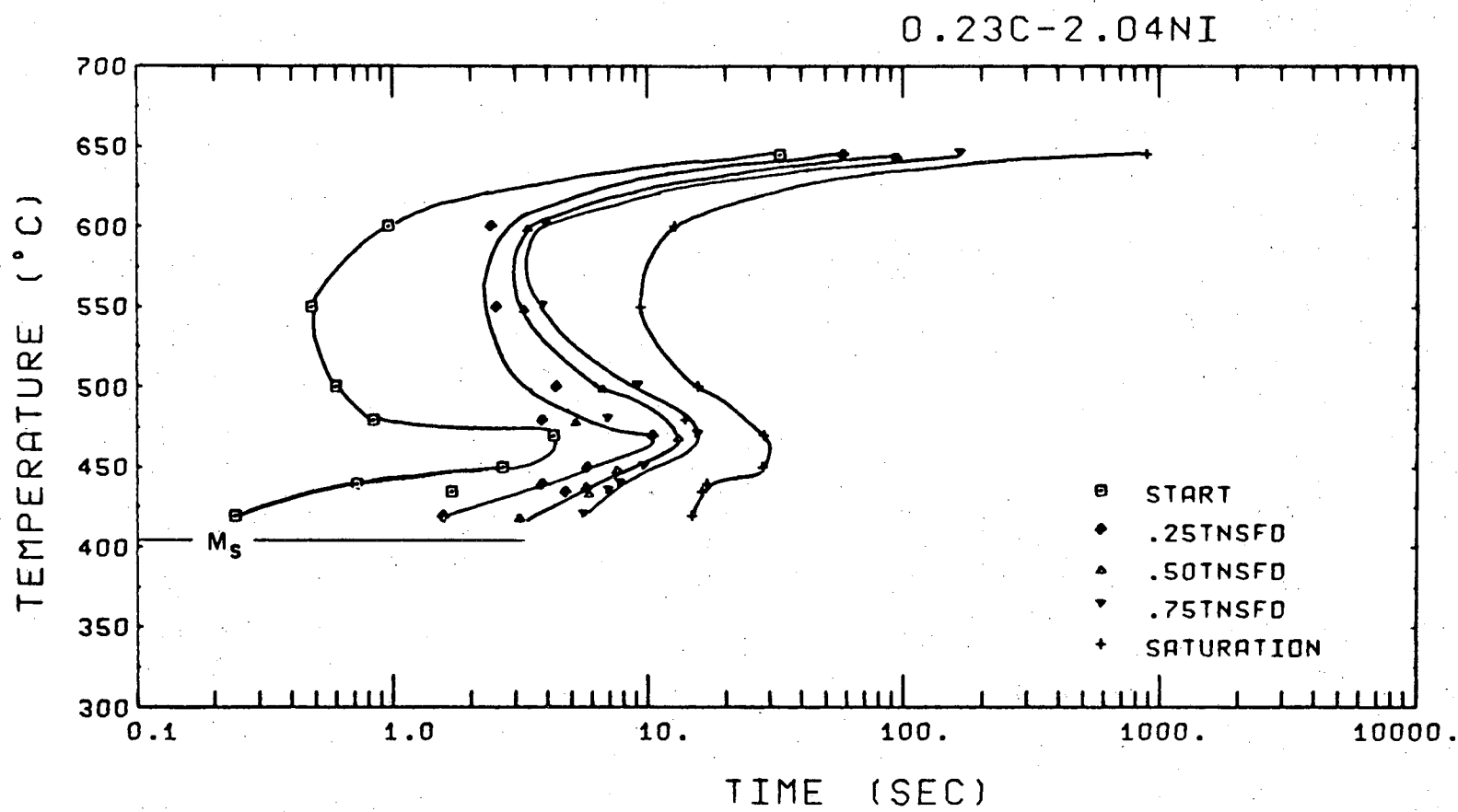
Fig. 14



XBL 769-10420

Fig. 15

00004708666

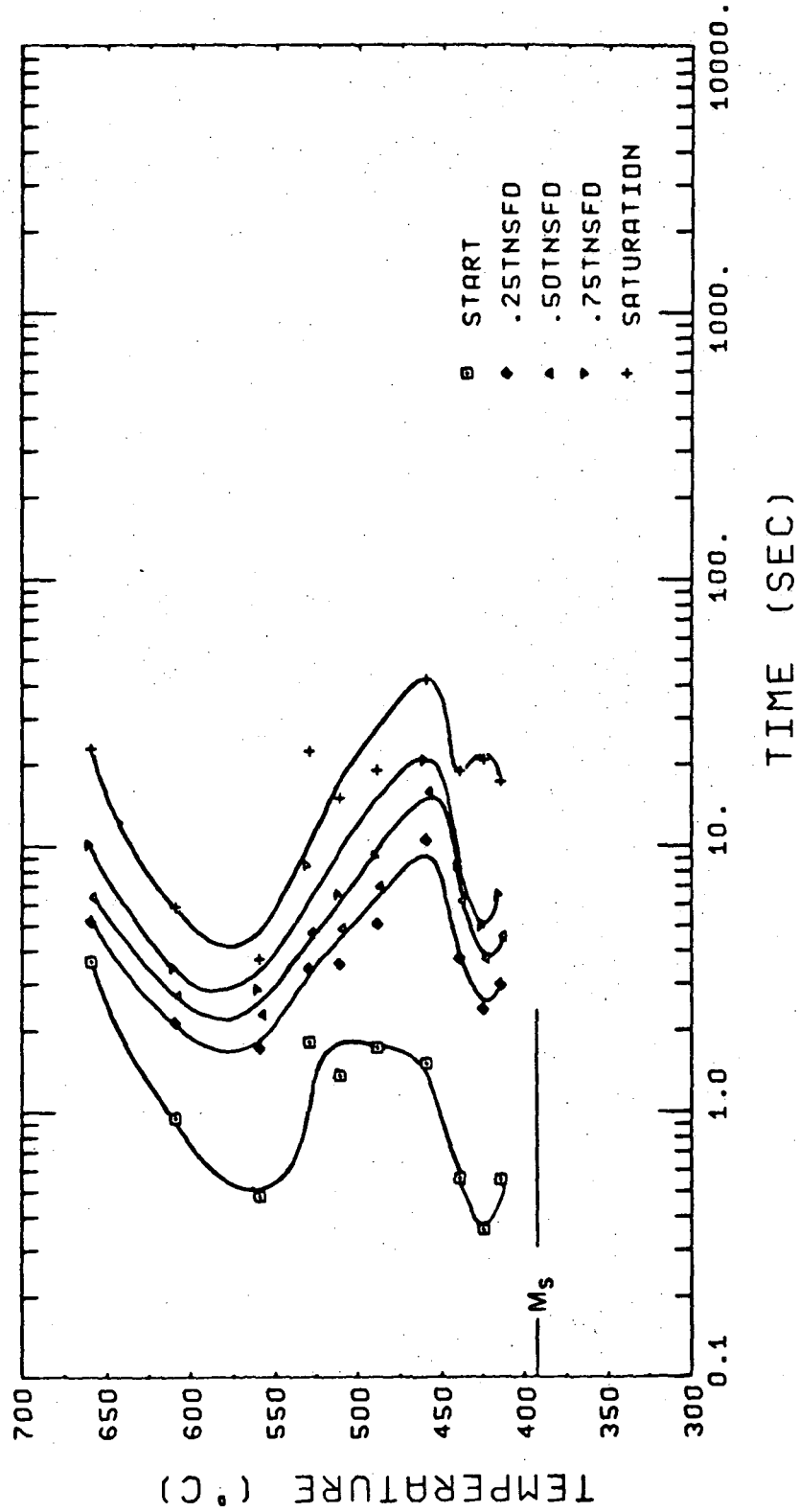


-143-

Fig. 16

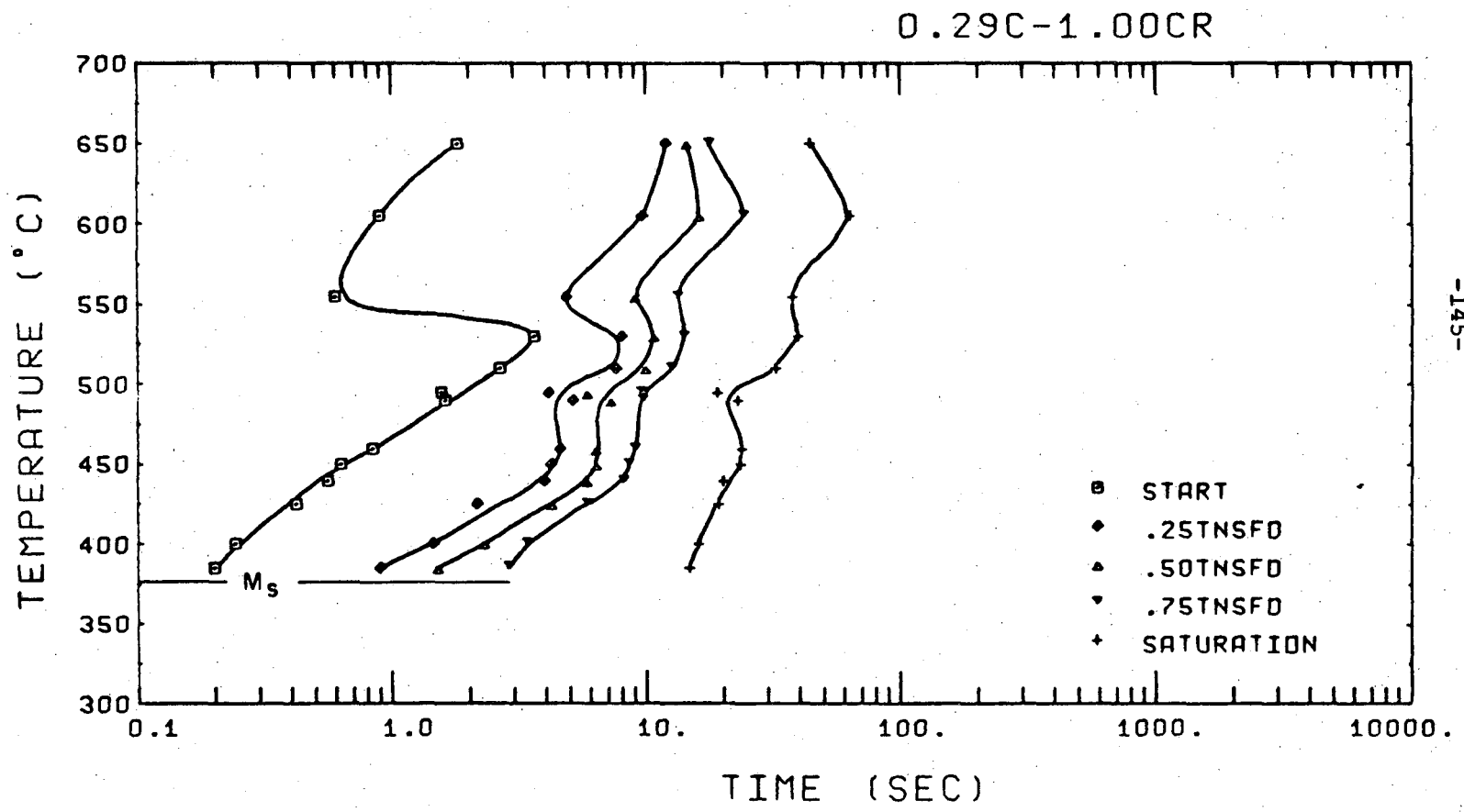
XBL 769-10417

0.29C-1.01NI



XBL 769-10419

Fig. 17

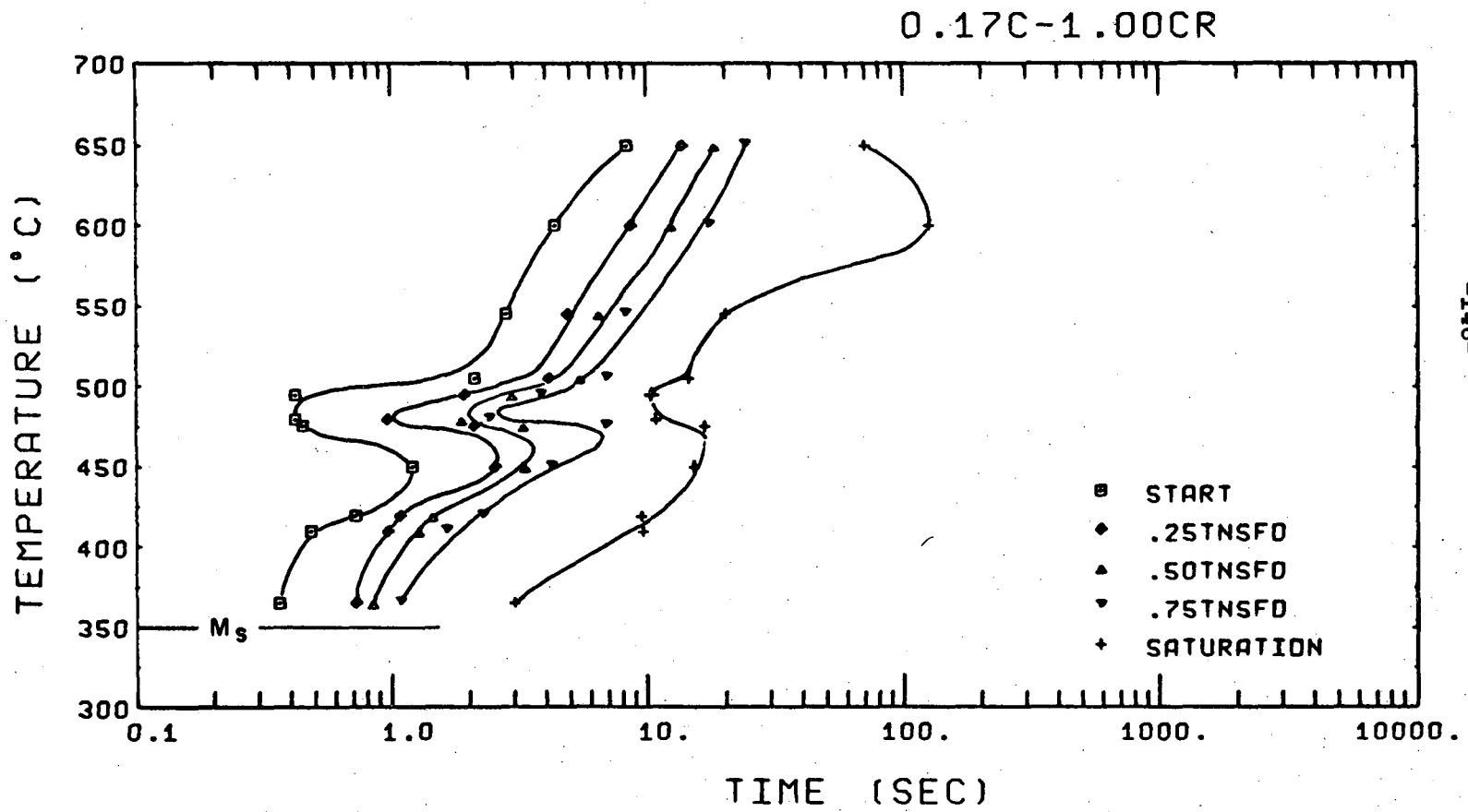


-145-

00004708667

XBL 769-10424

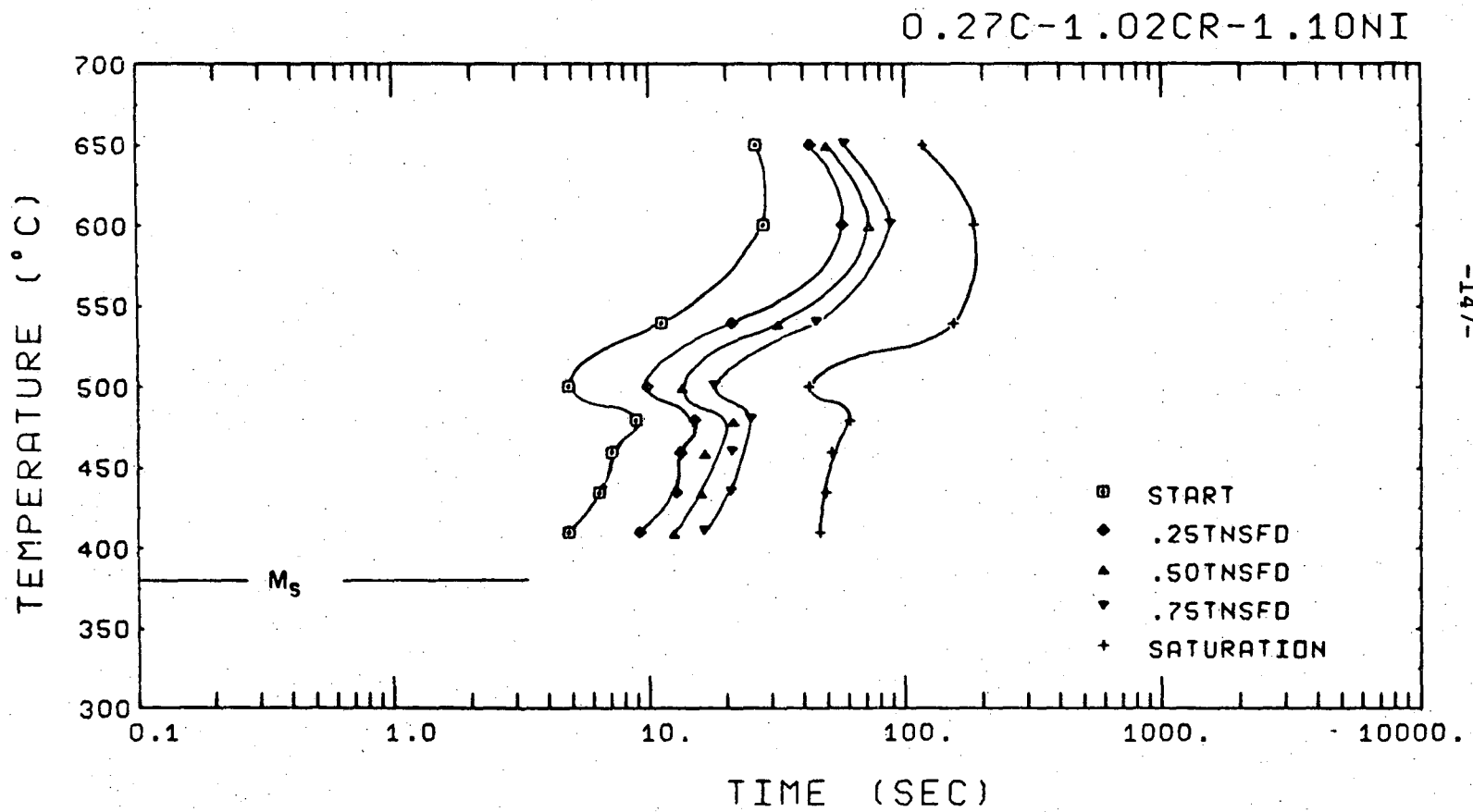
Fig. 18



XBL 769-10421

Fig. 19

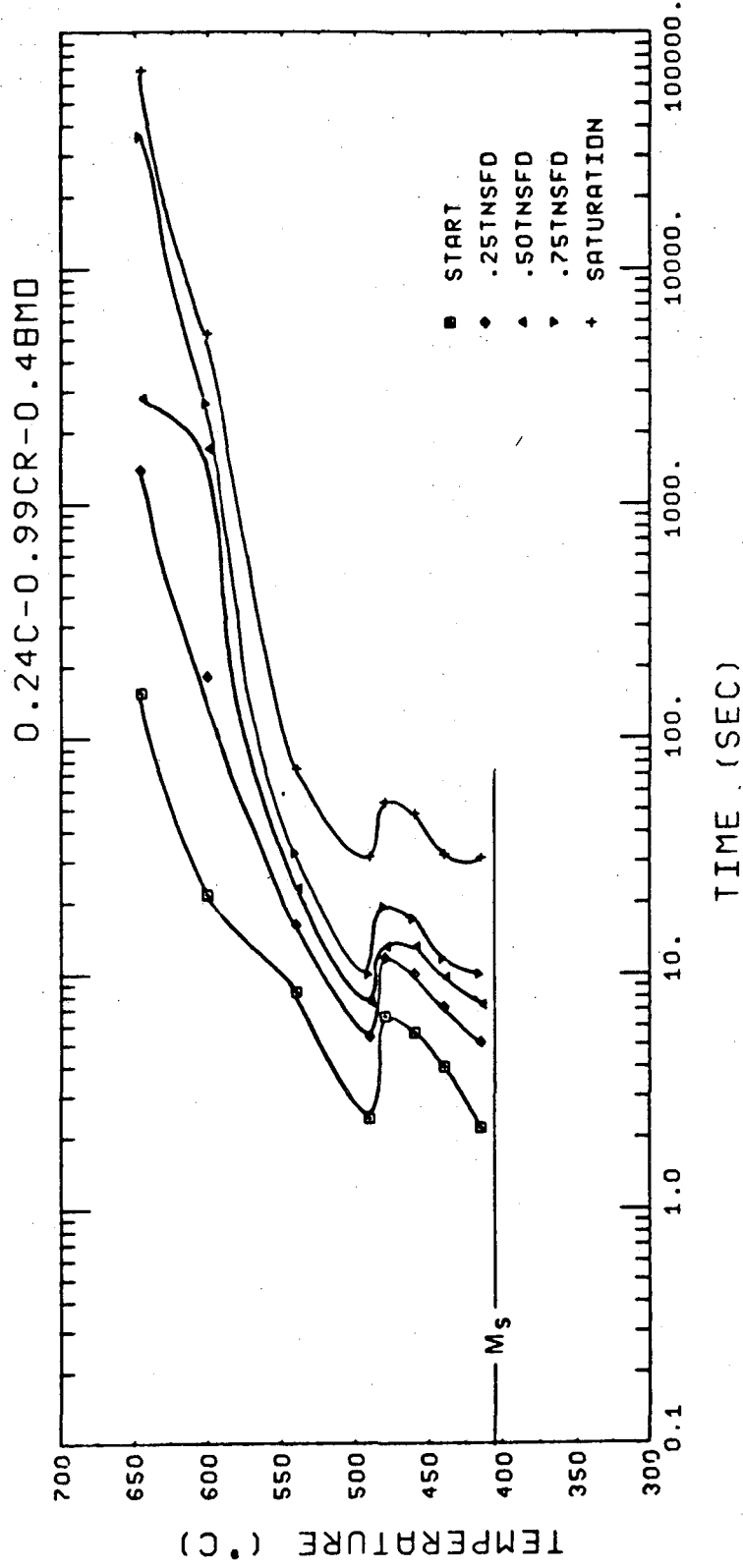
00104708668



-147-

Fig. 20

XBL 769-10412

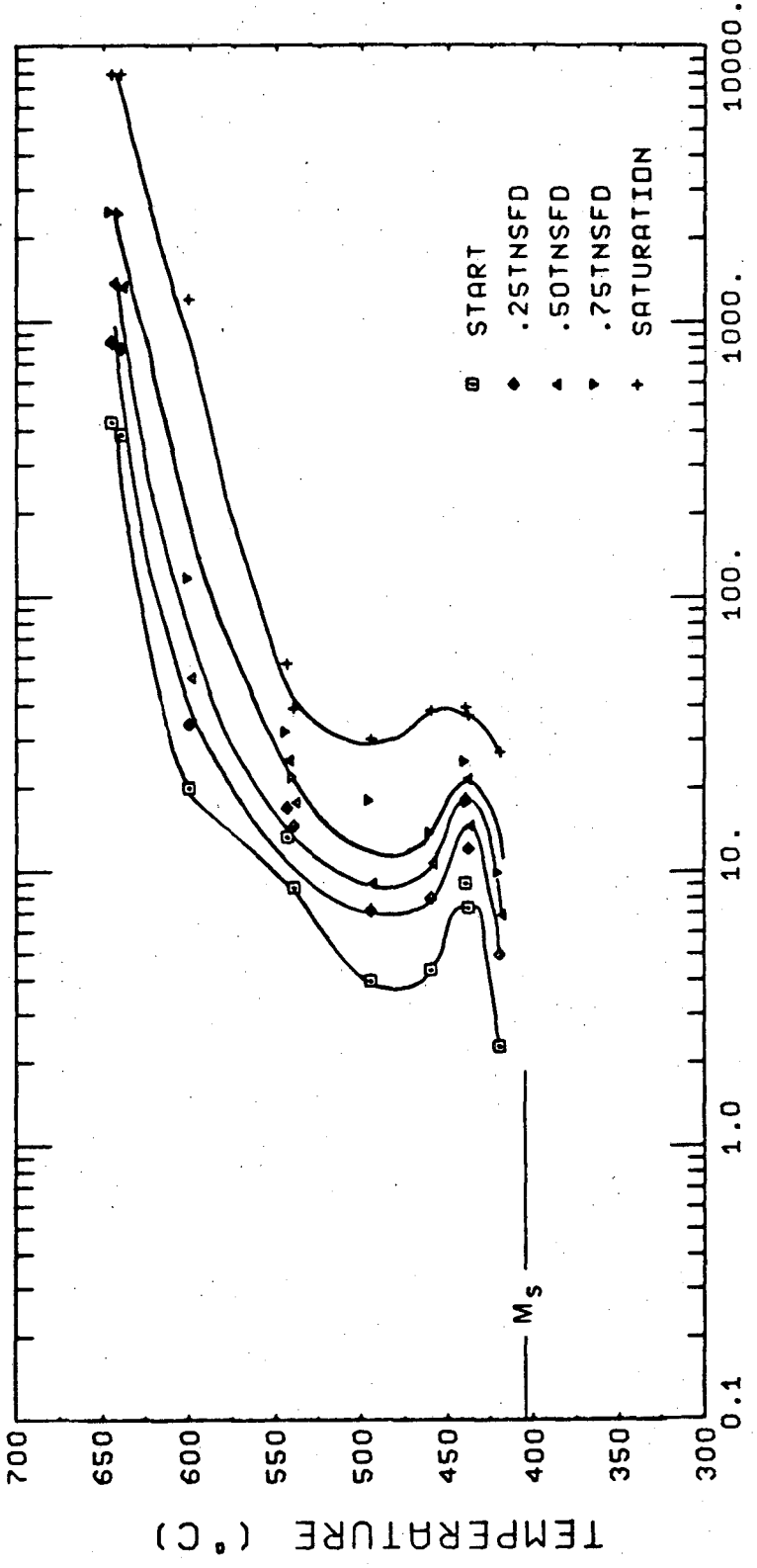


XBL 769-10414

Fig. 21



0.25C-1.00NI-0.48MD

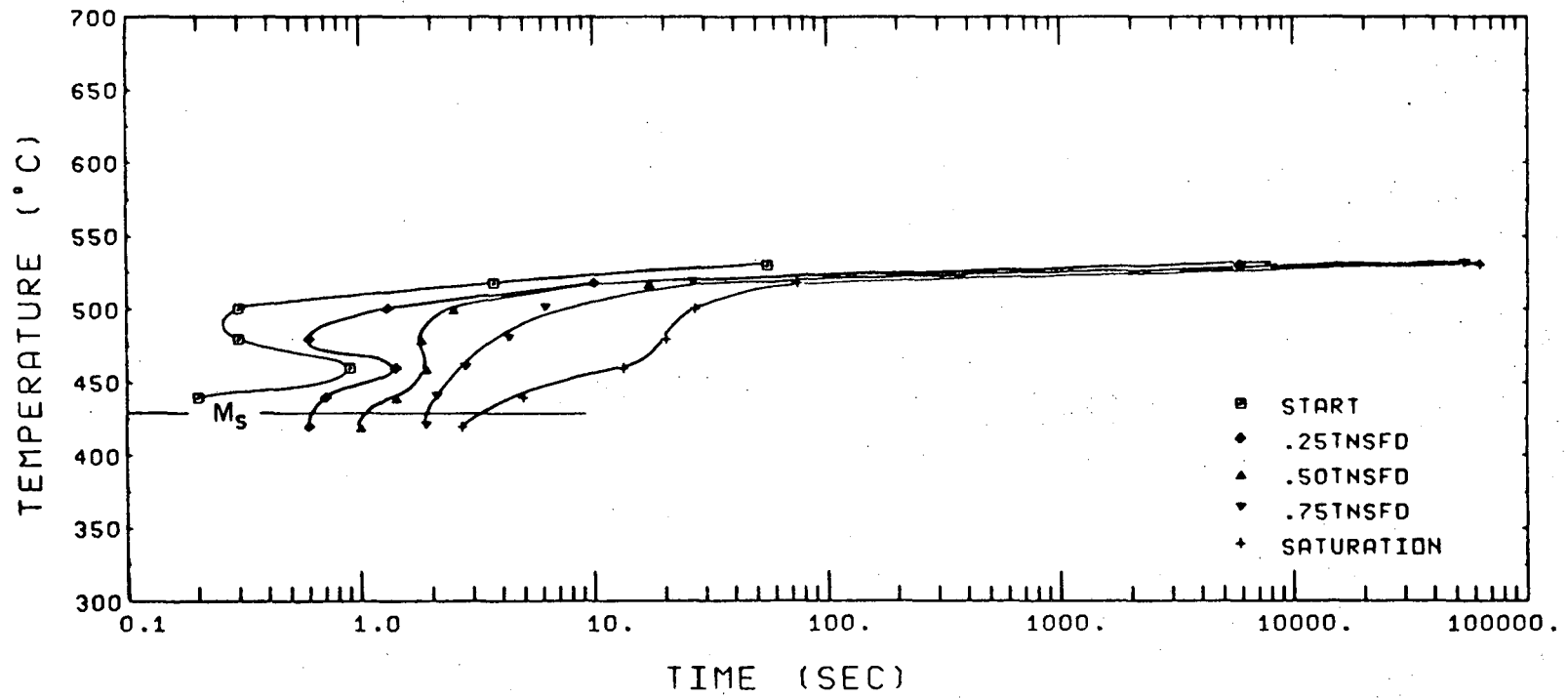


TIME (SEC)

XBL 769-10415

Fig. 22

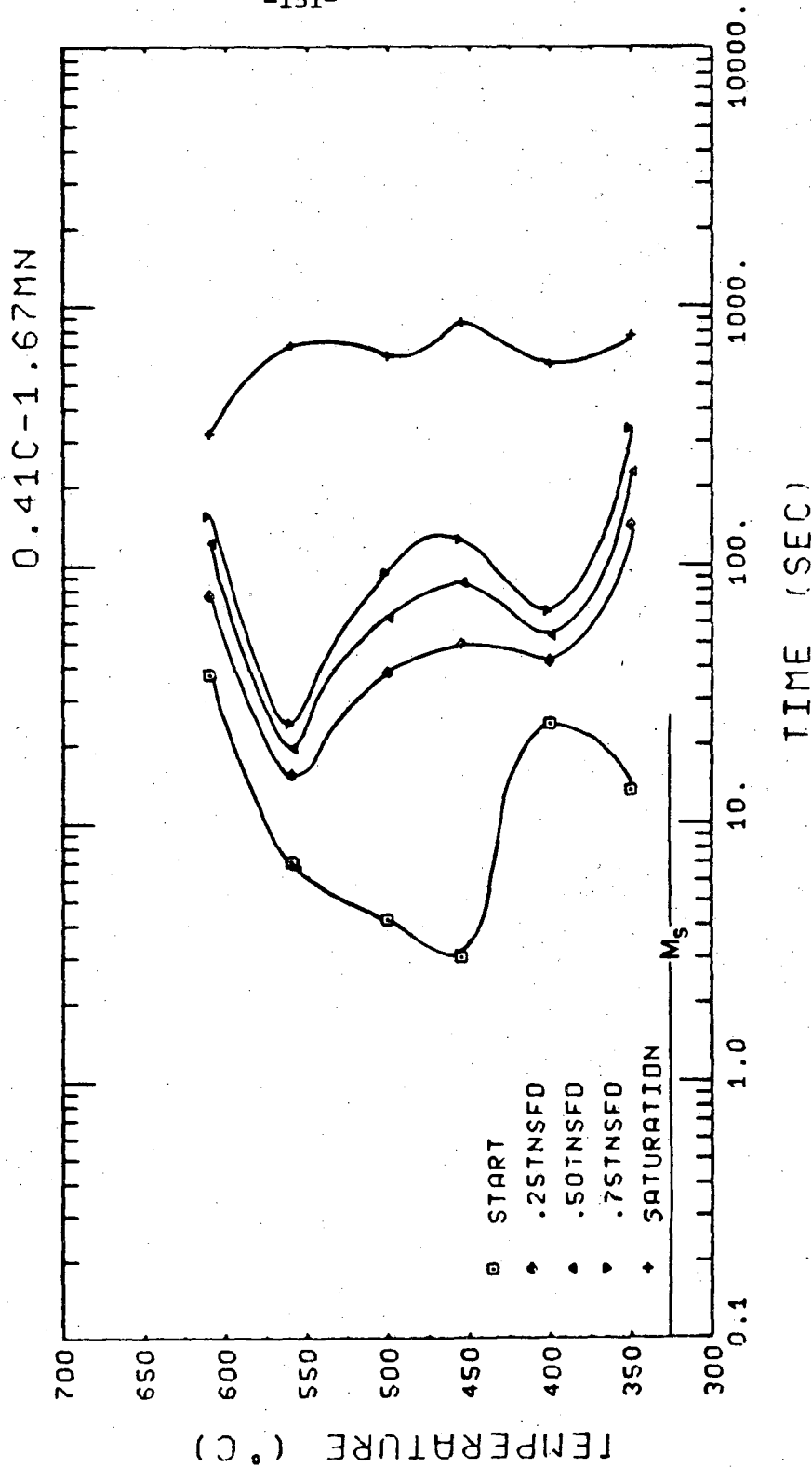
0.14C-0.97CR-1.01NI-0.47MO



-150-

Fig. 23

XBL 769-10413



XBL 769-10416

Fig. 24

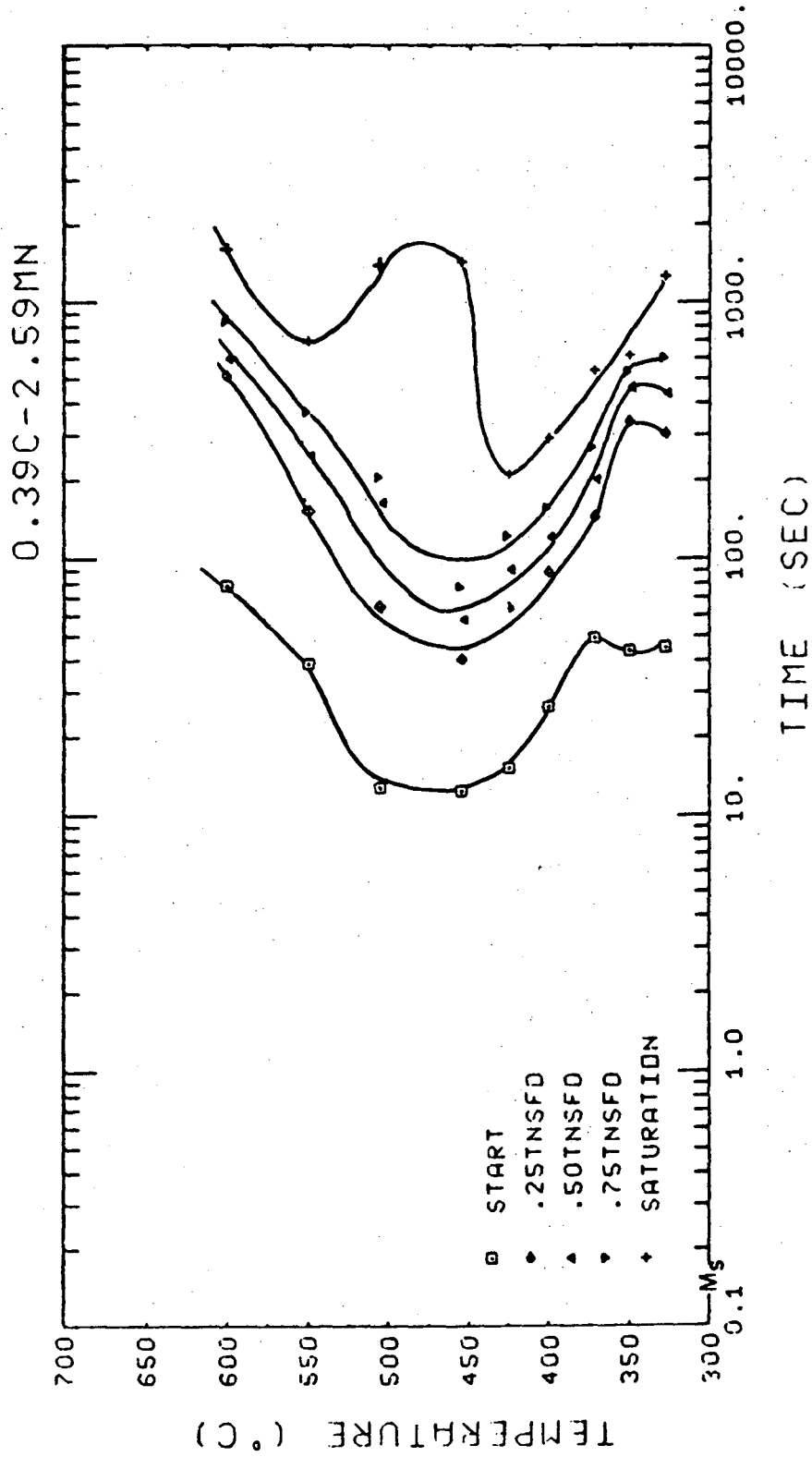
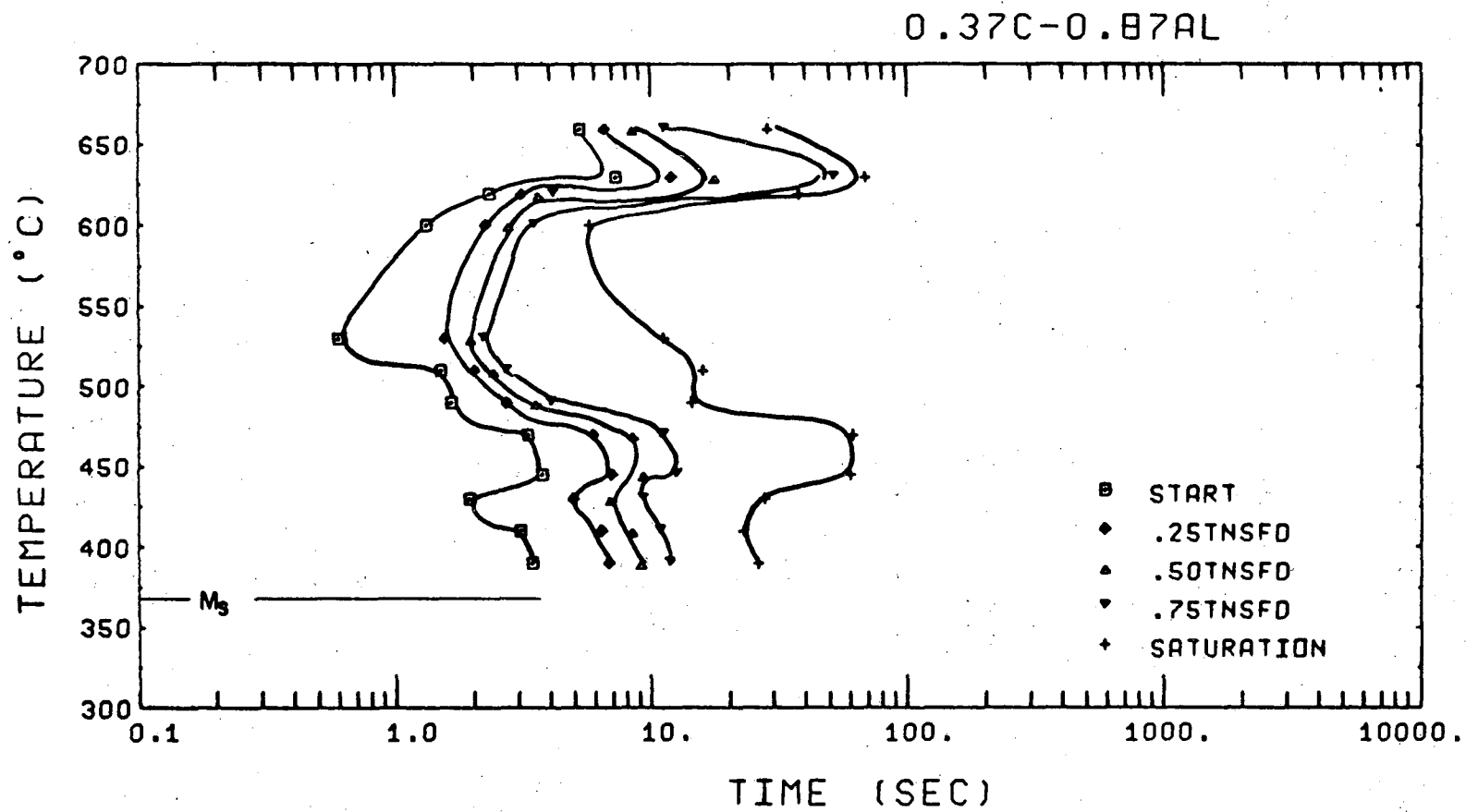


Fig. 25

XBL 769-10418

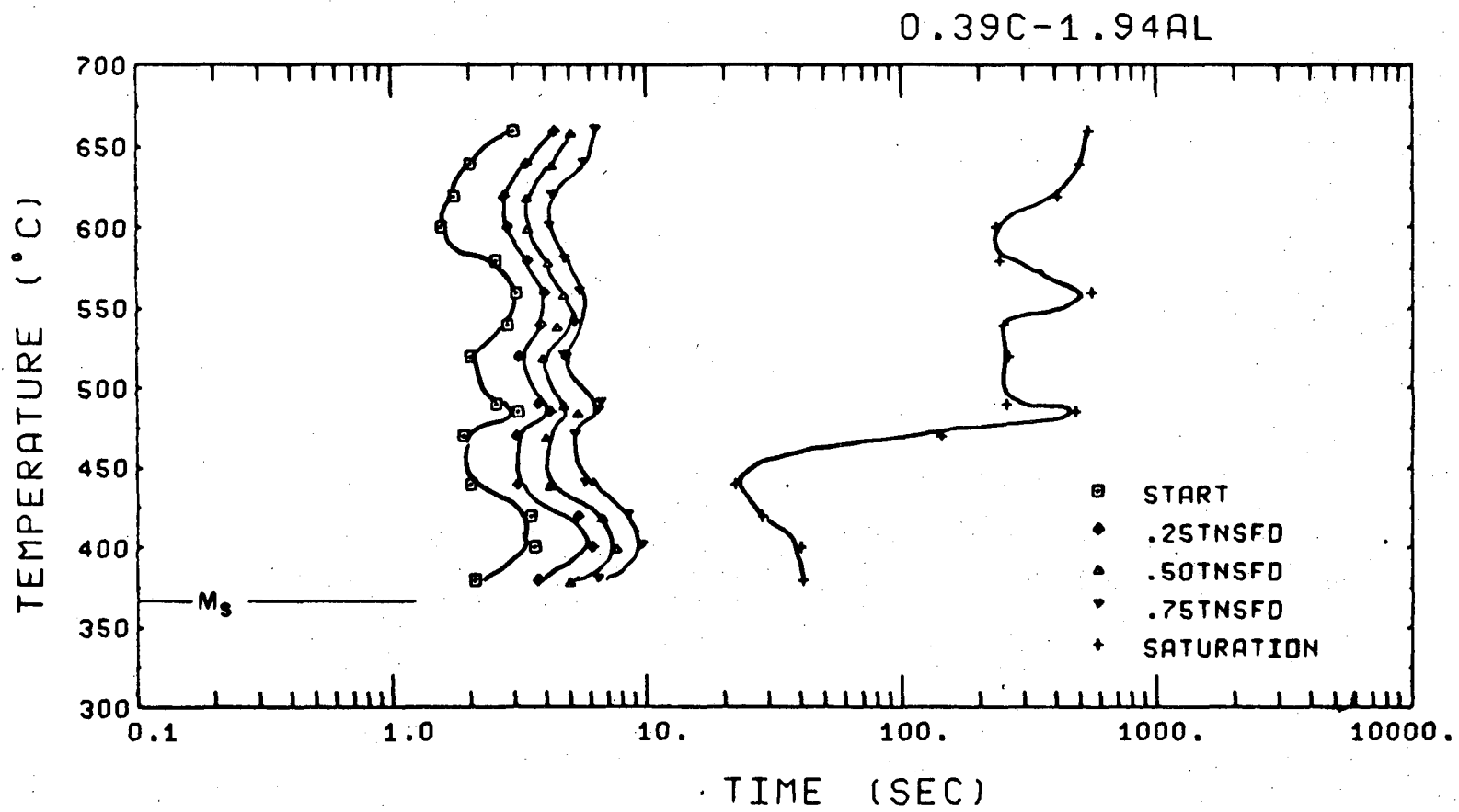
00004708671



-153-

XBL7612-7981

Fig. 26

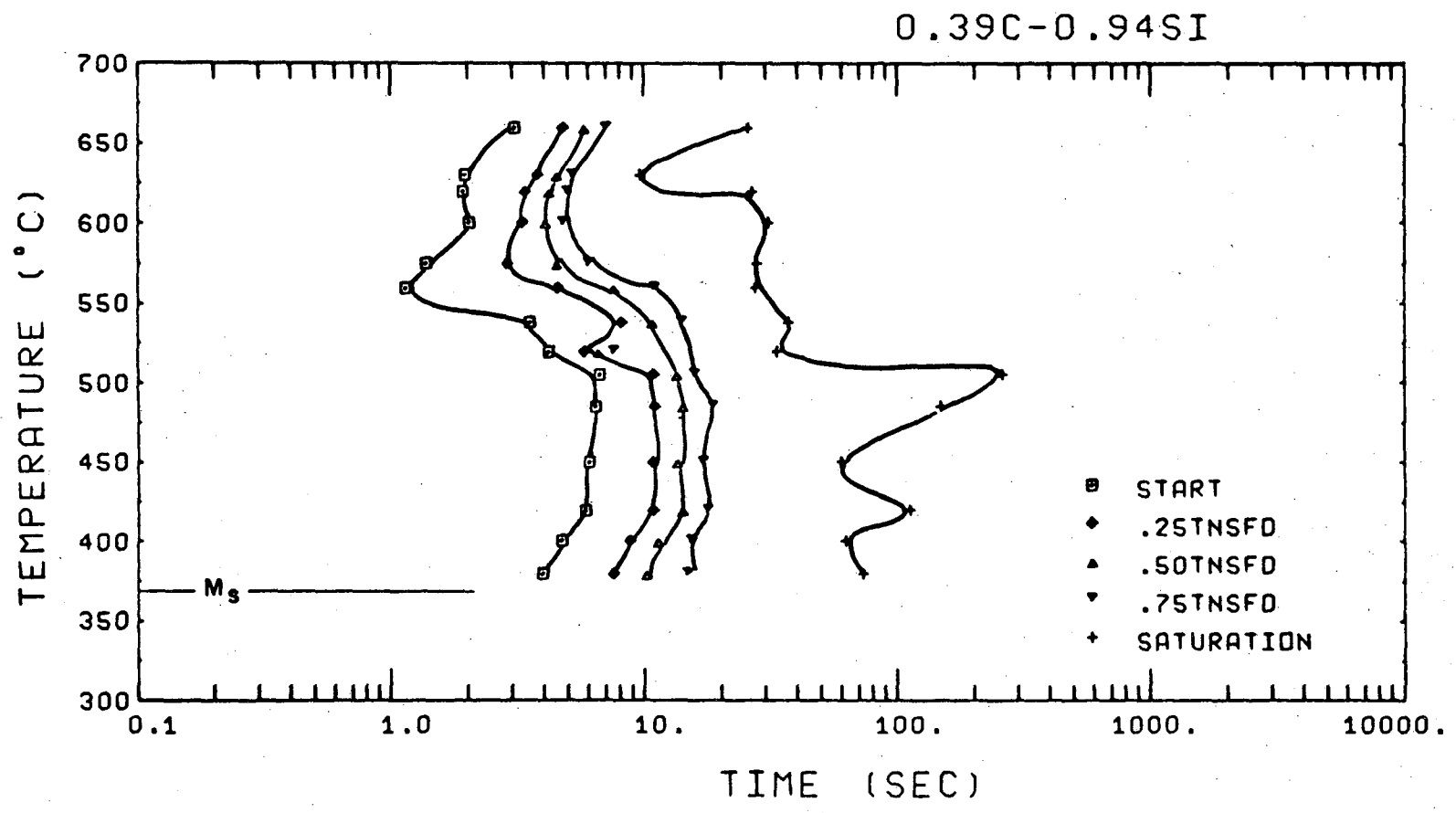


-154-

Fig. 27

XBL7612-7980

00004708672



-155-

Fig. 28

XBL 7 612-7977

0.3BC-1.91SI

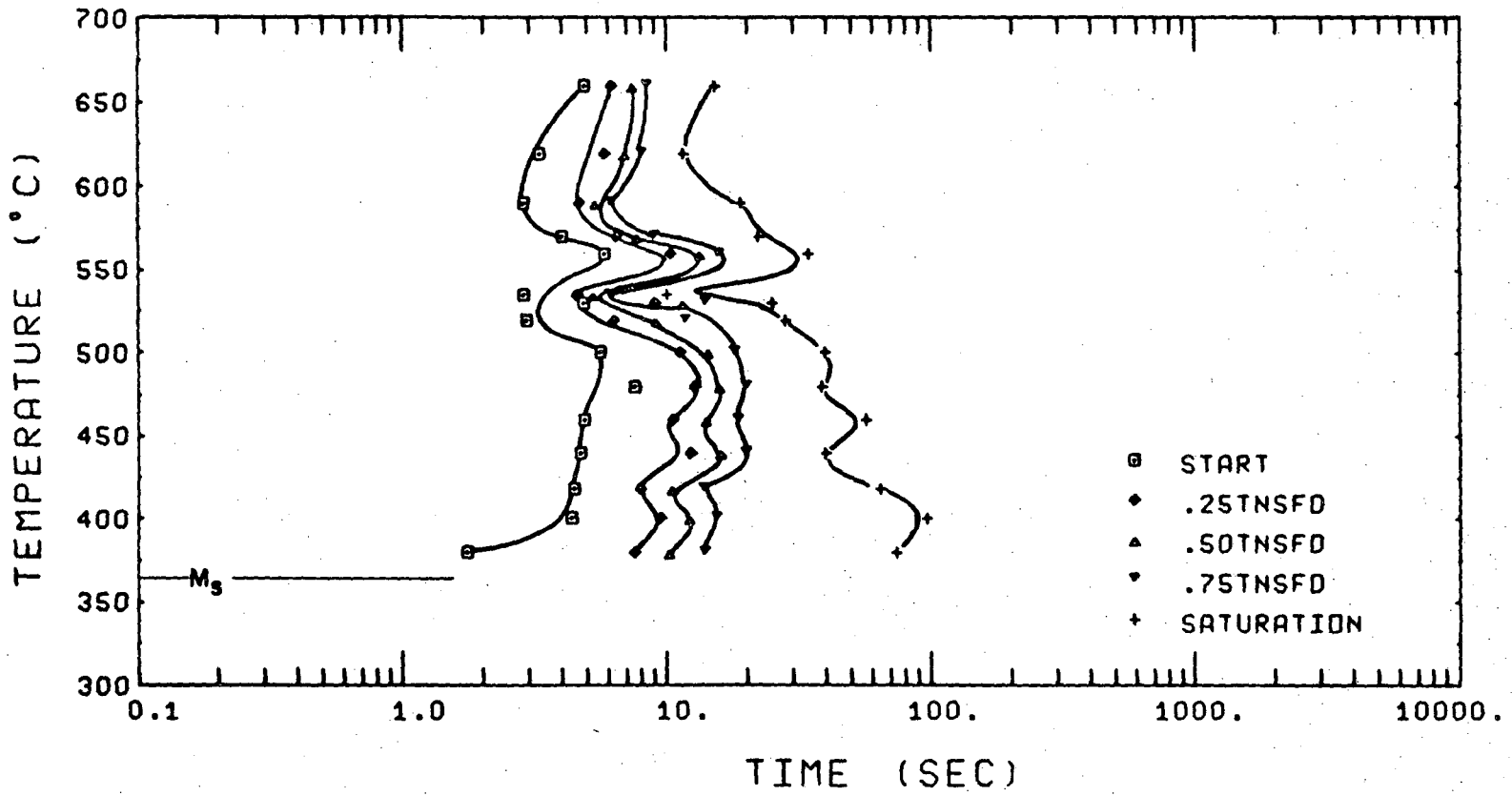
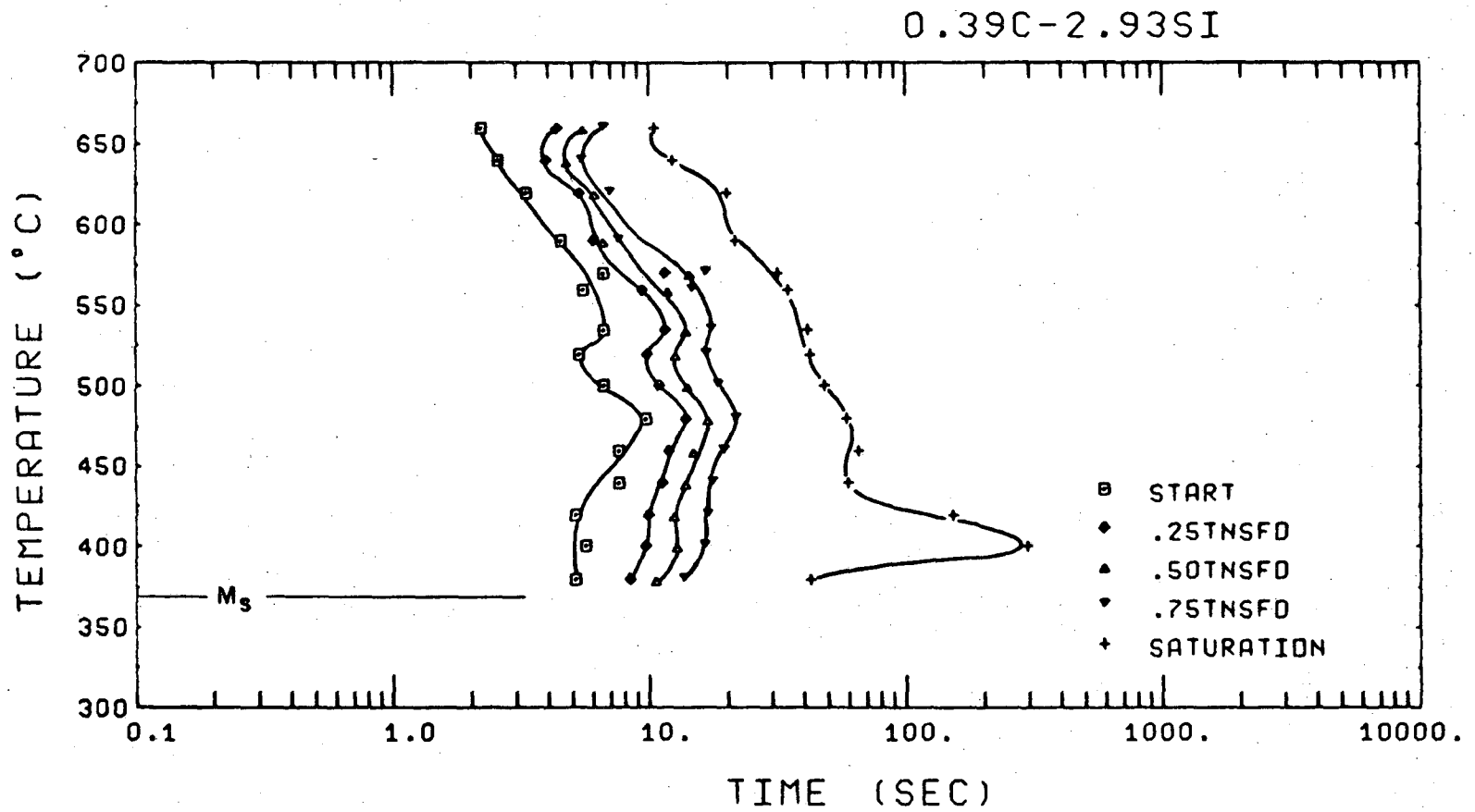


Fig. 29

XBL 7612-7978





-157-

00004708673

XBL7612-7979

Fig. 30

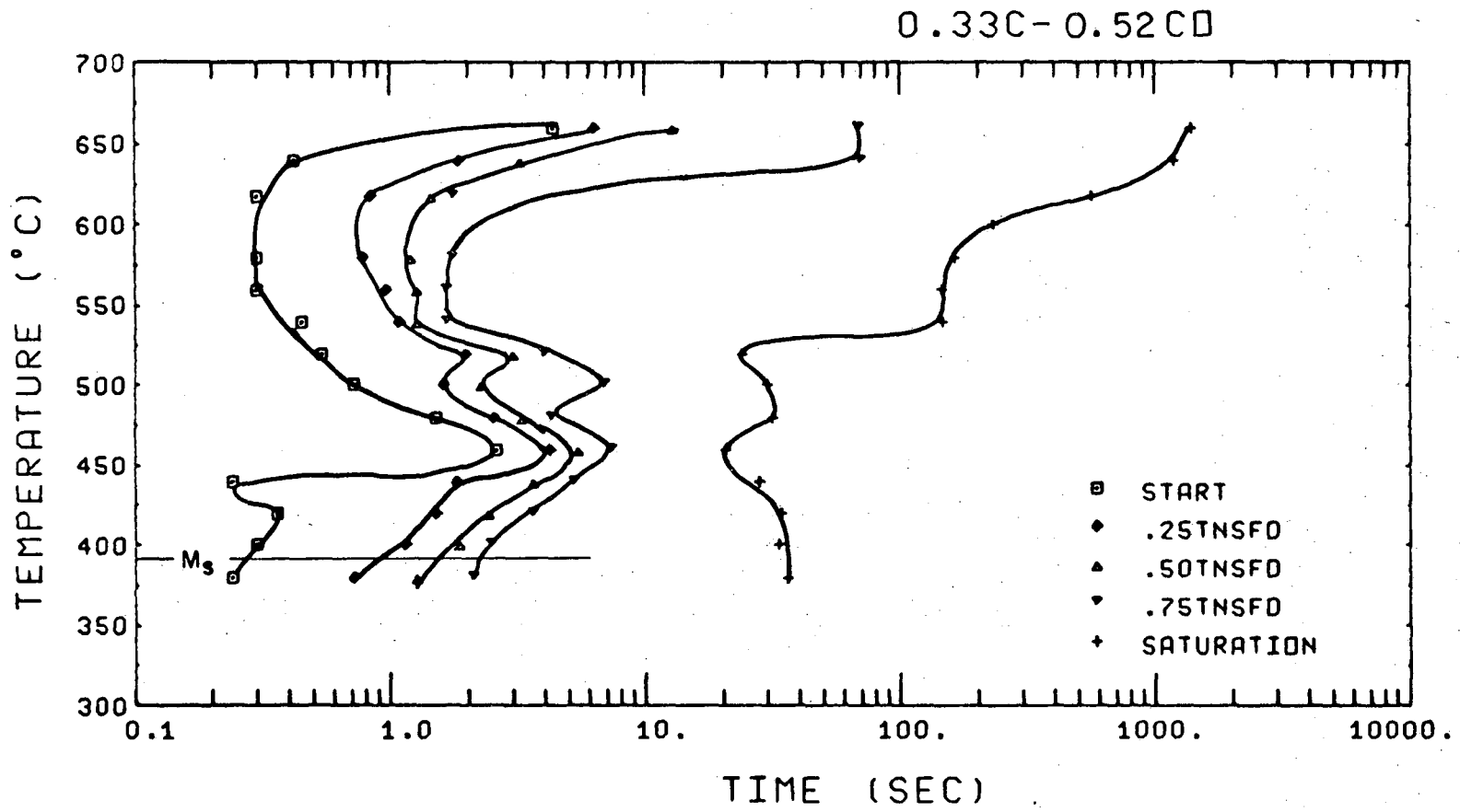


Fig. 31

XBL 7612-7976

00004708674

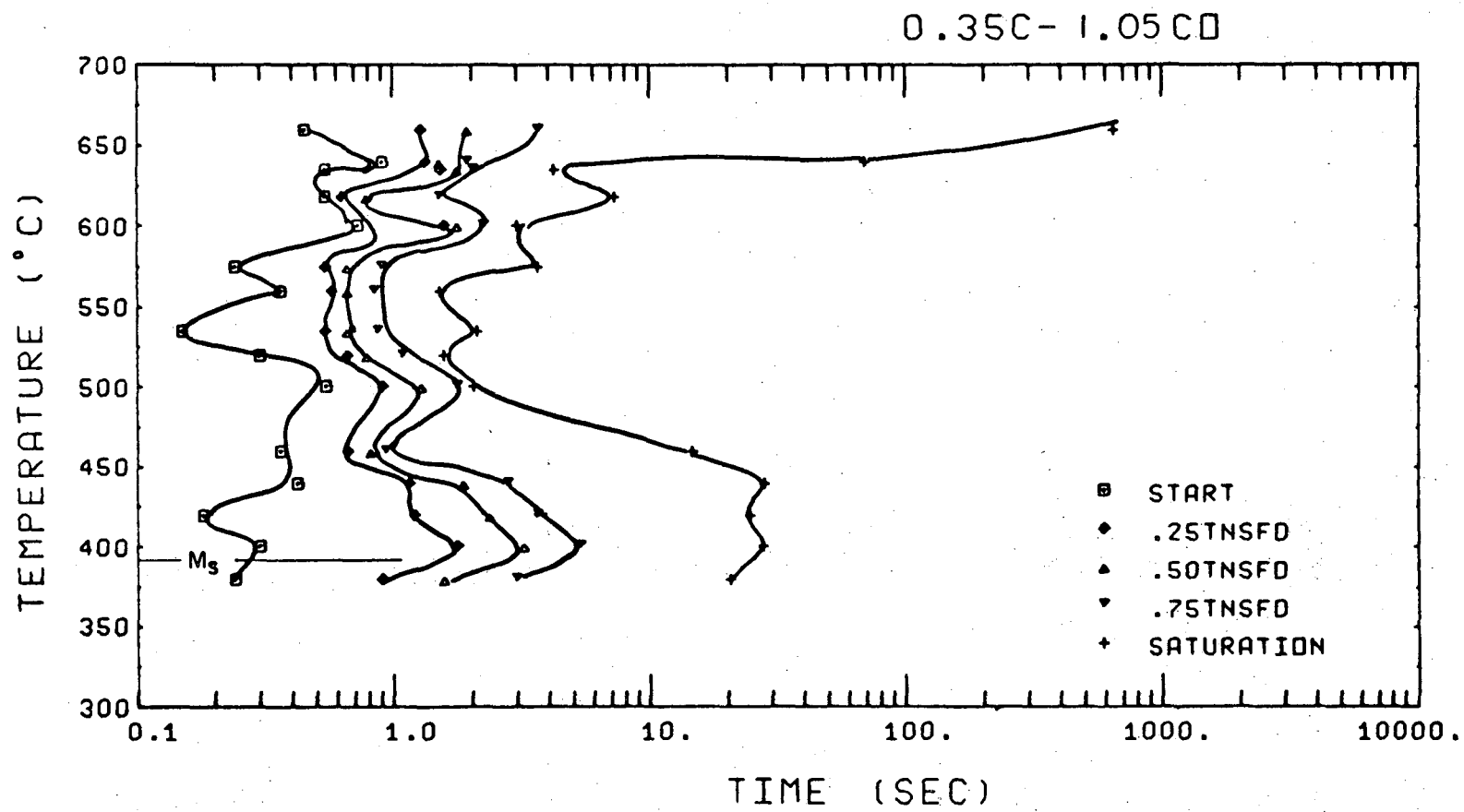
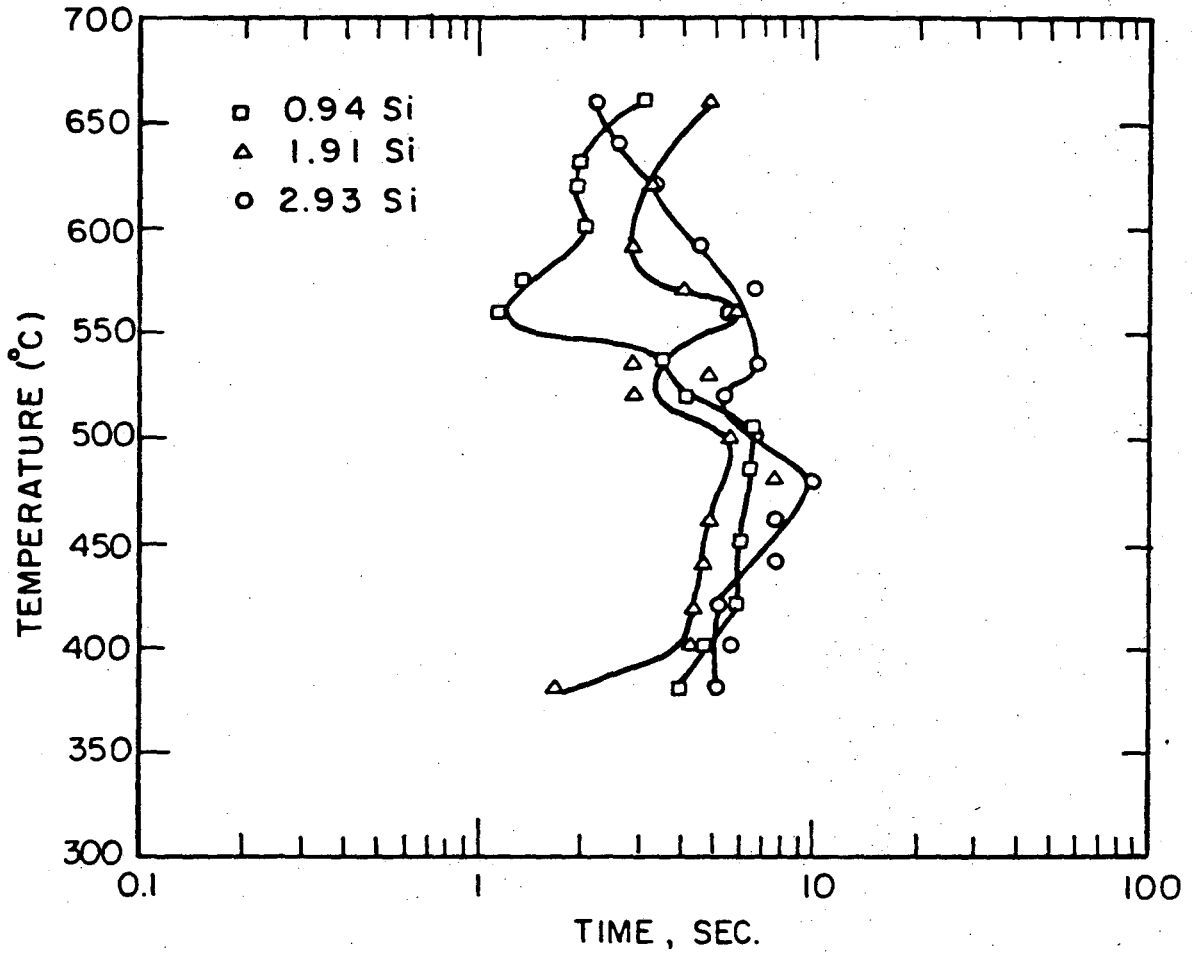


Fig. 32

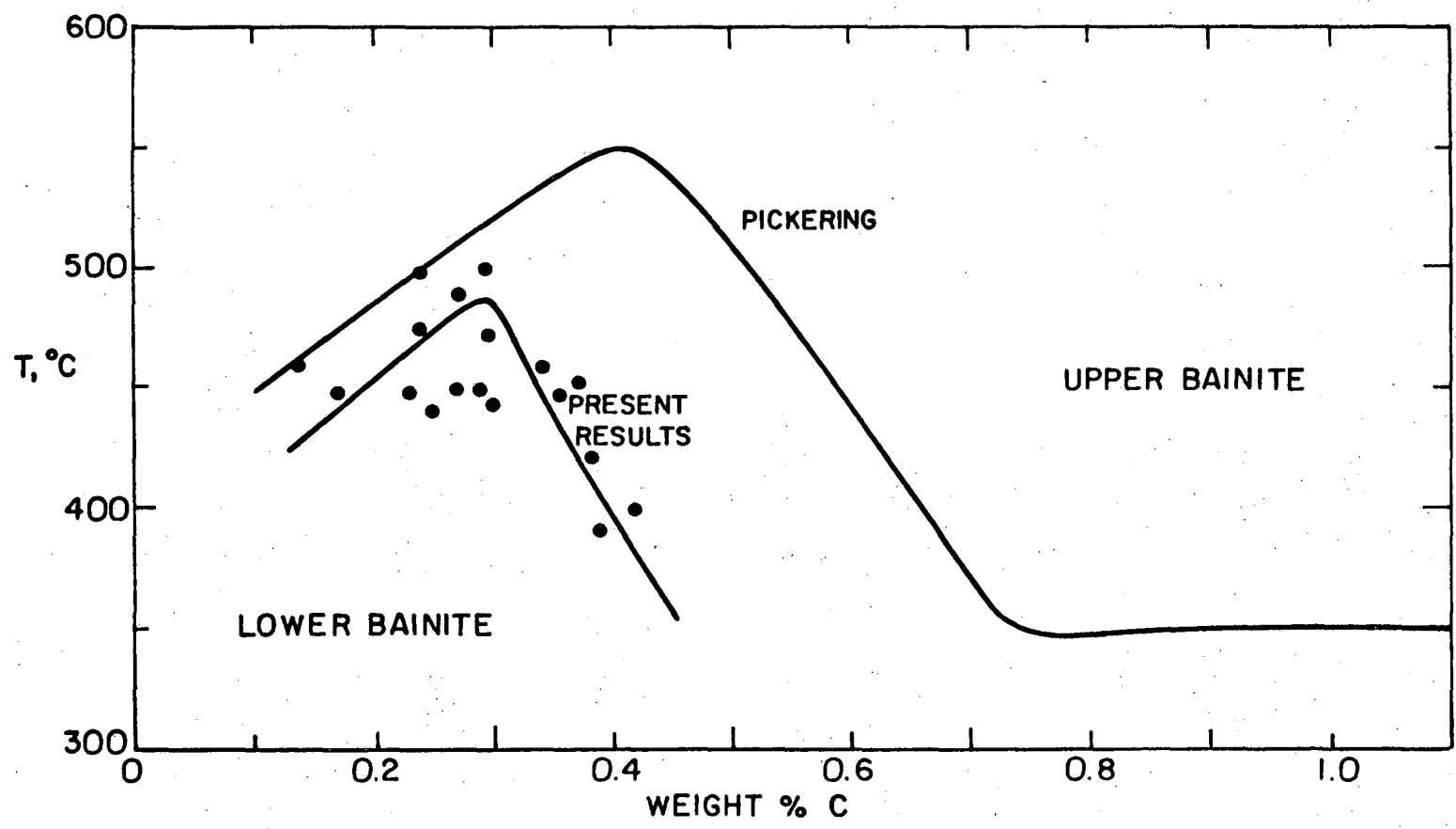
XBL 7.612-7975



XBL7612-11,025

Fig. 33

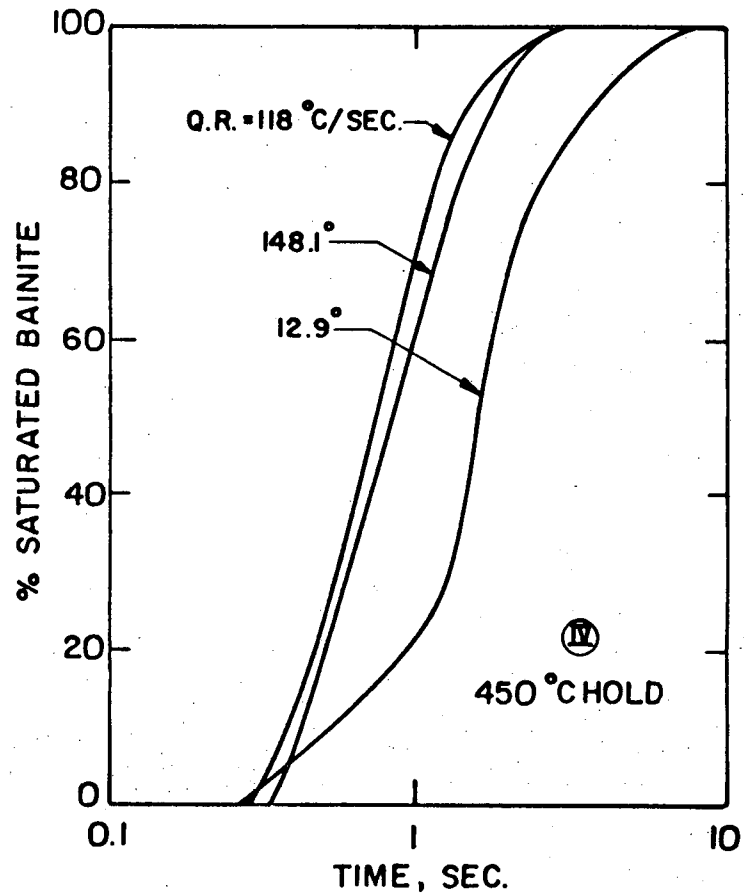
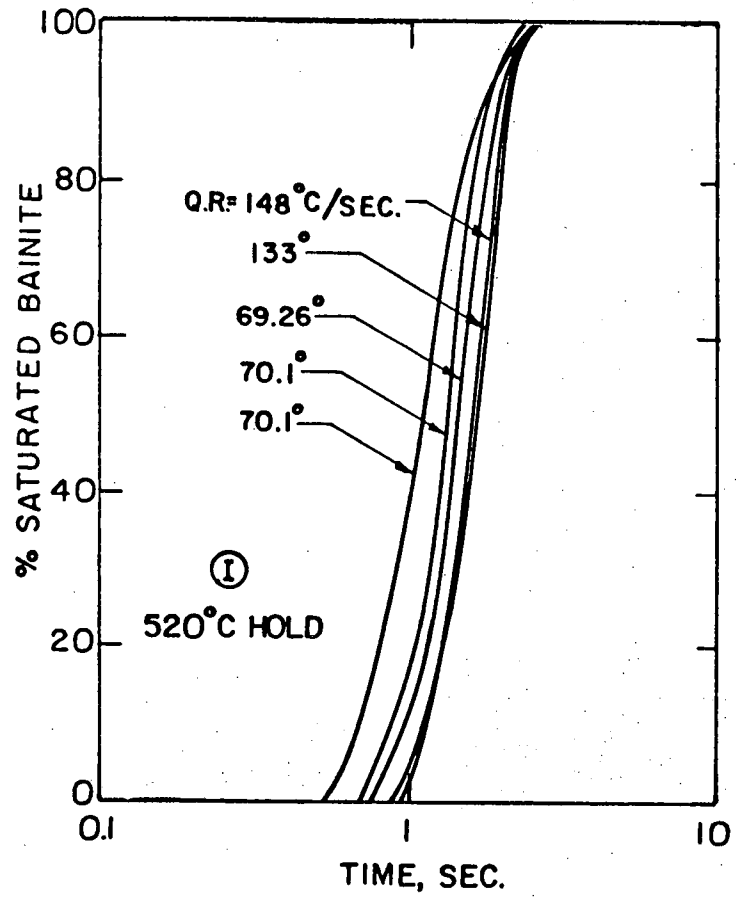
00004708675



-161-

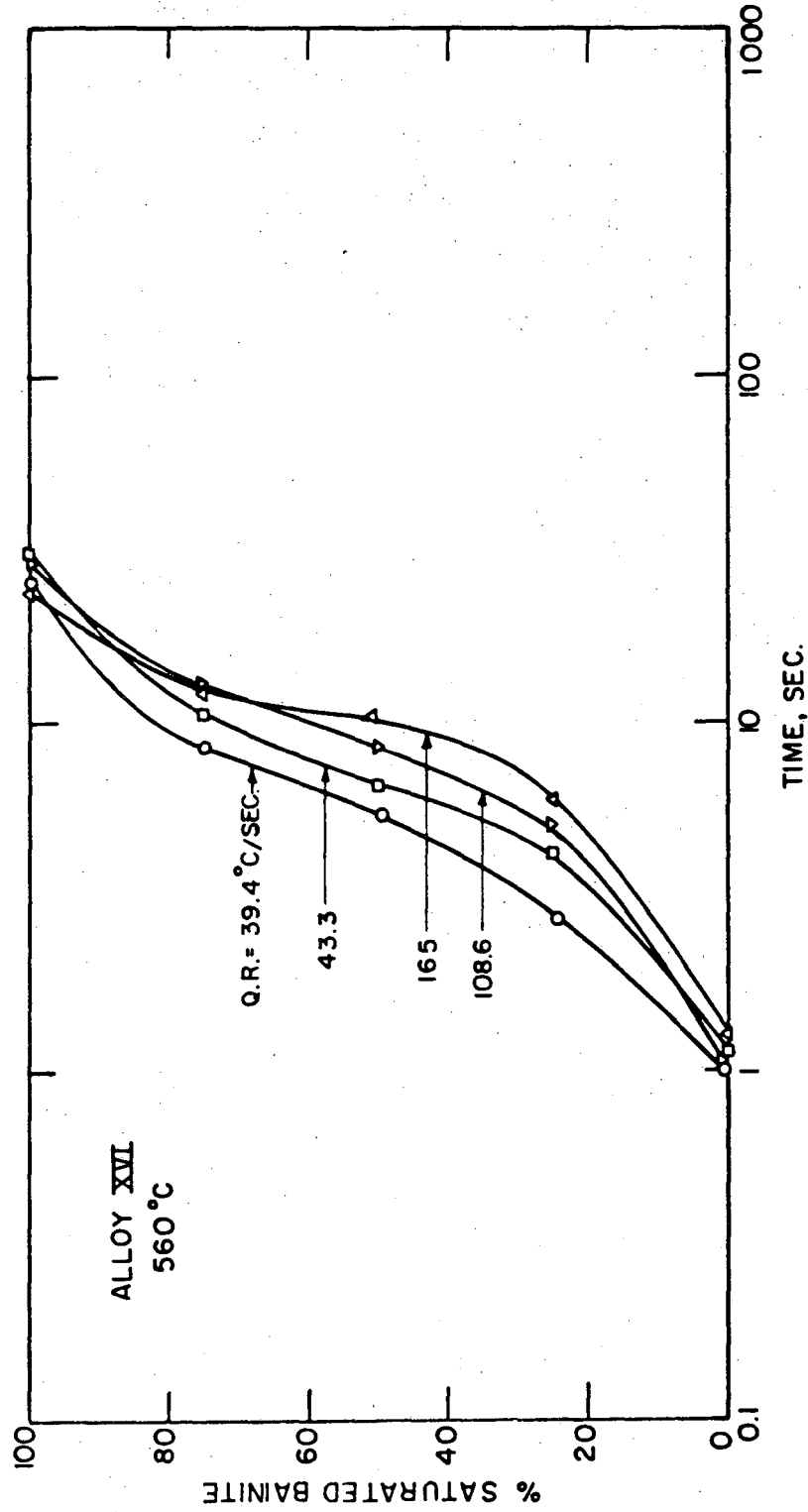
XBL7512-9286

Fig. 34



XBL7512-9283A

Fig. 35



XBL 7612-II, 006

Fig. 36

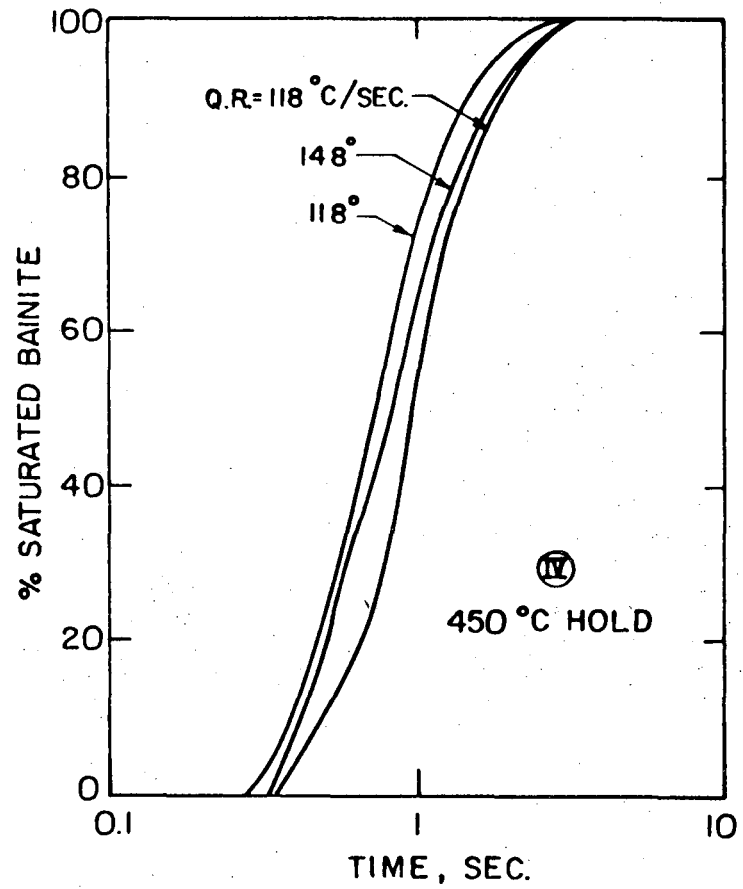
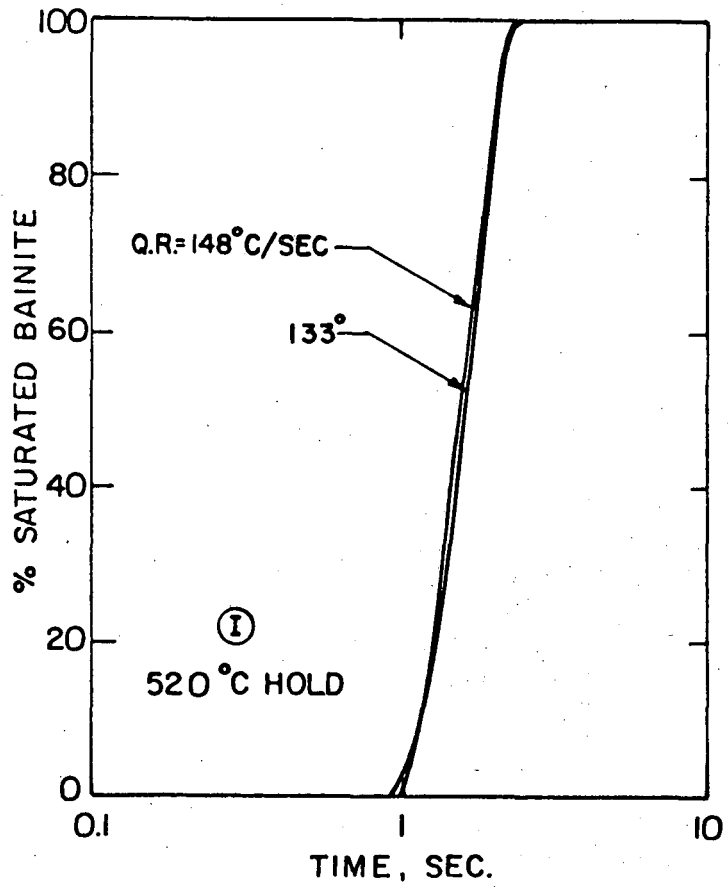
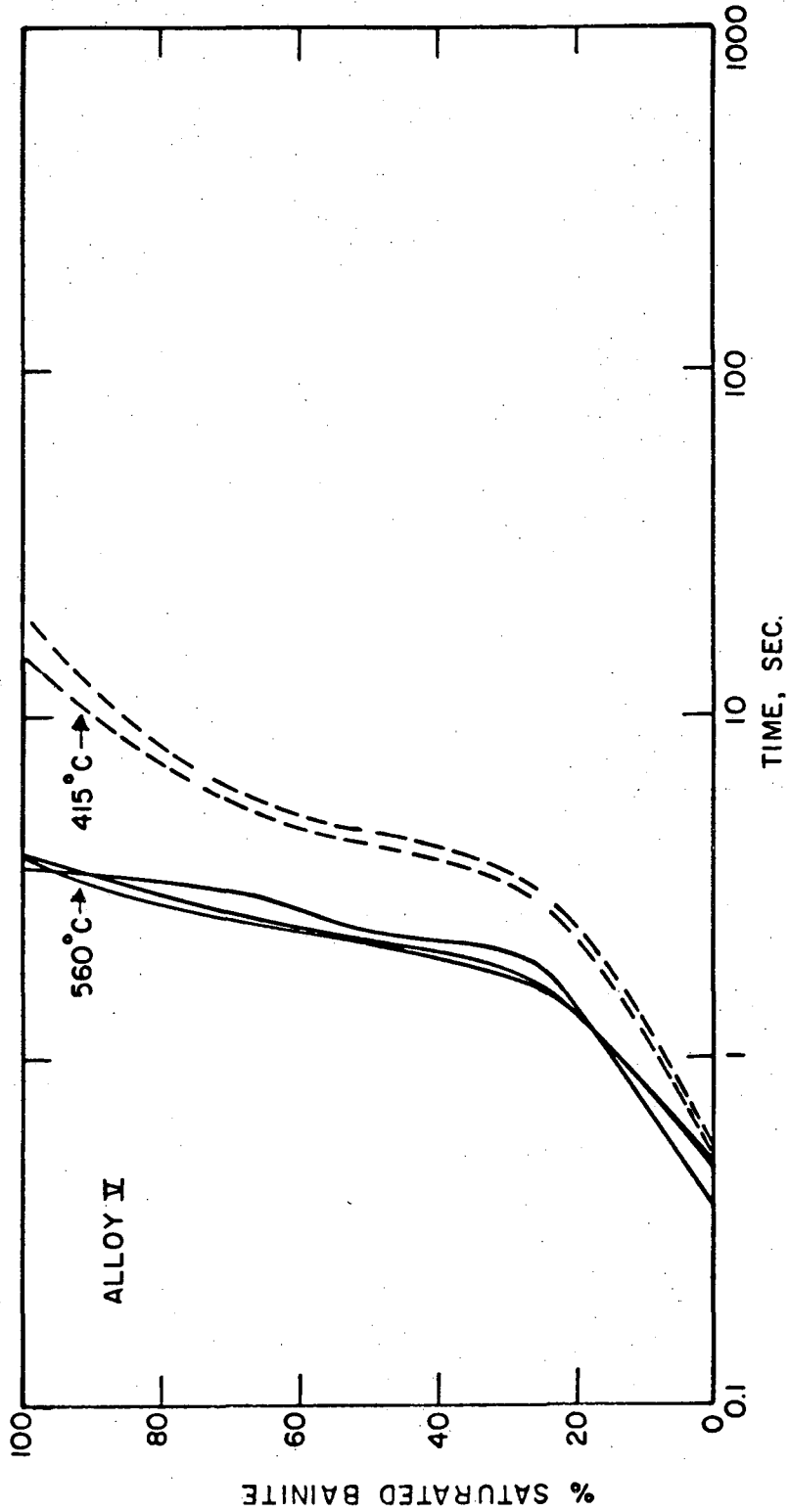


Fig. 37

XBL 7512-9282A





XBL7612-11,005

Fig. 38

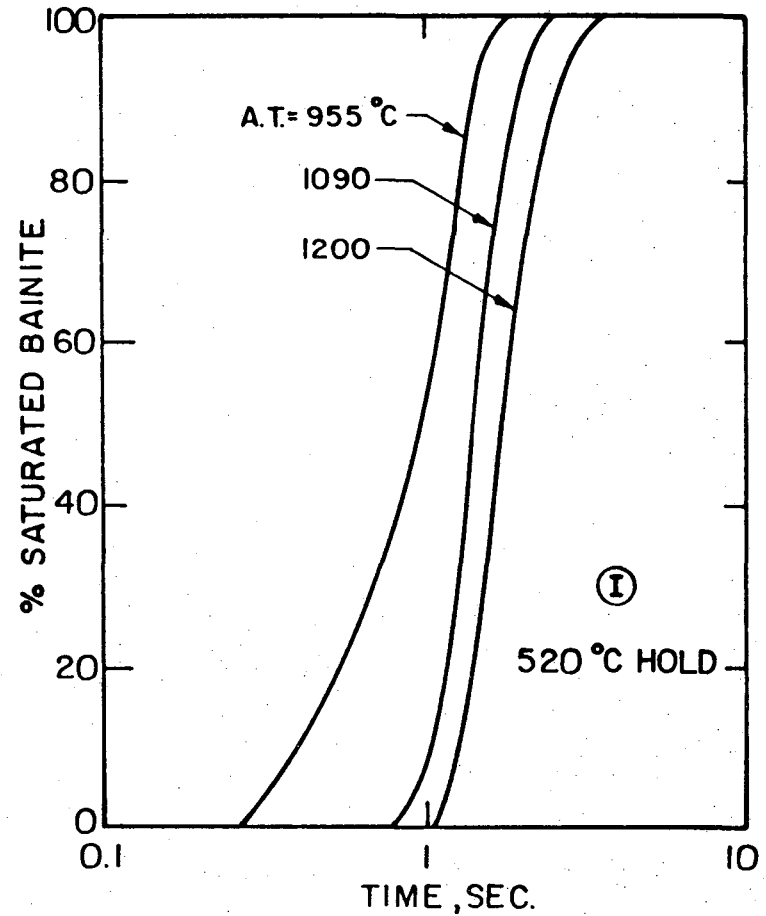
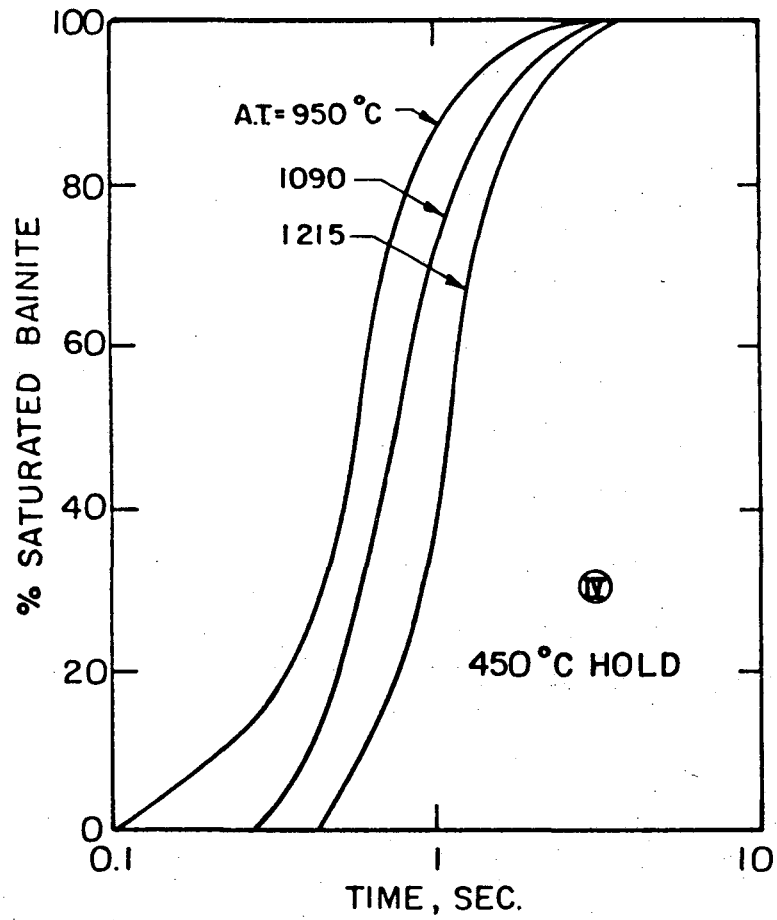
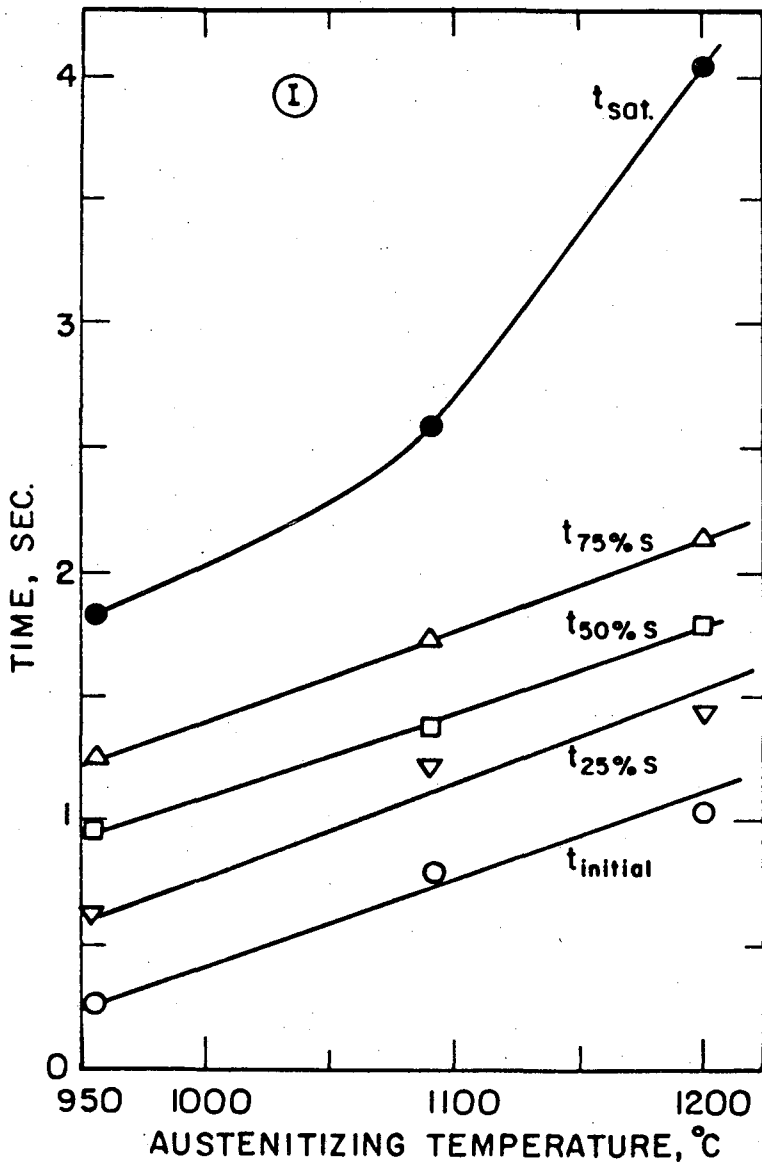
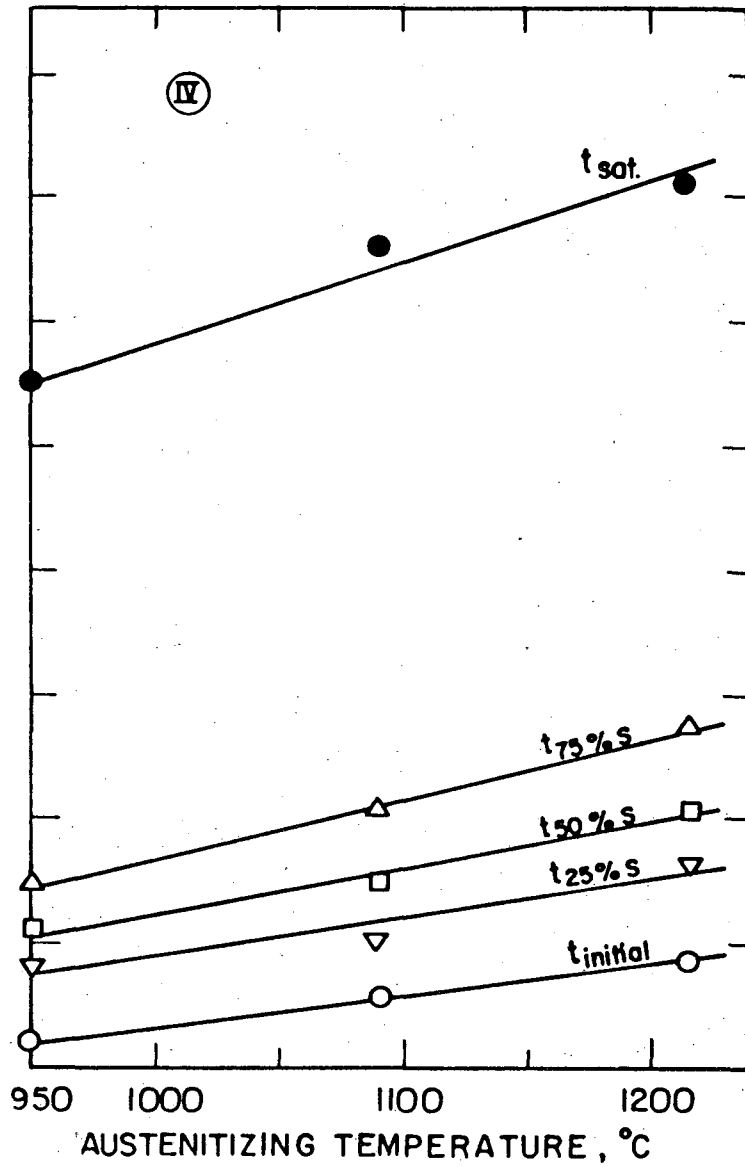


Fig. 39

XBL7512-9281A



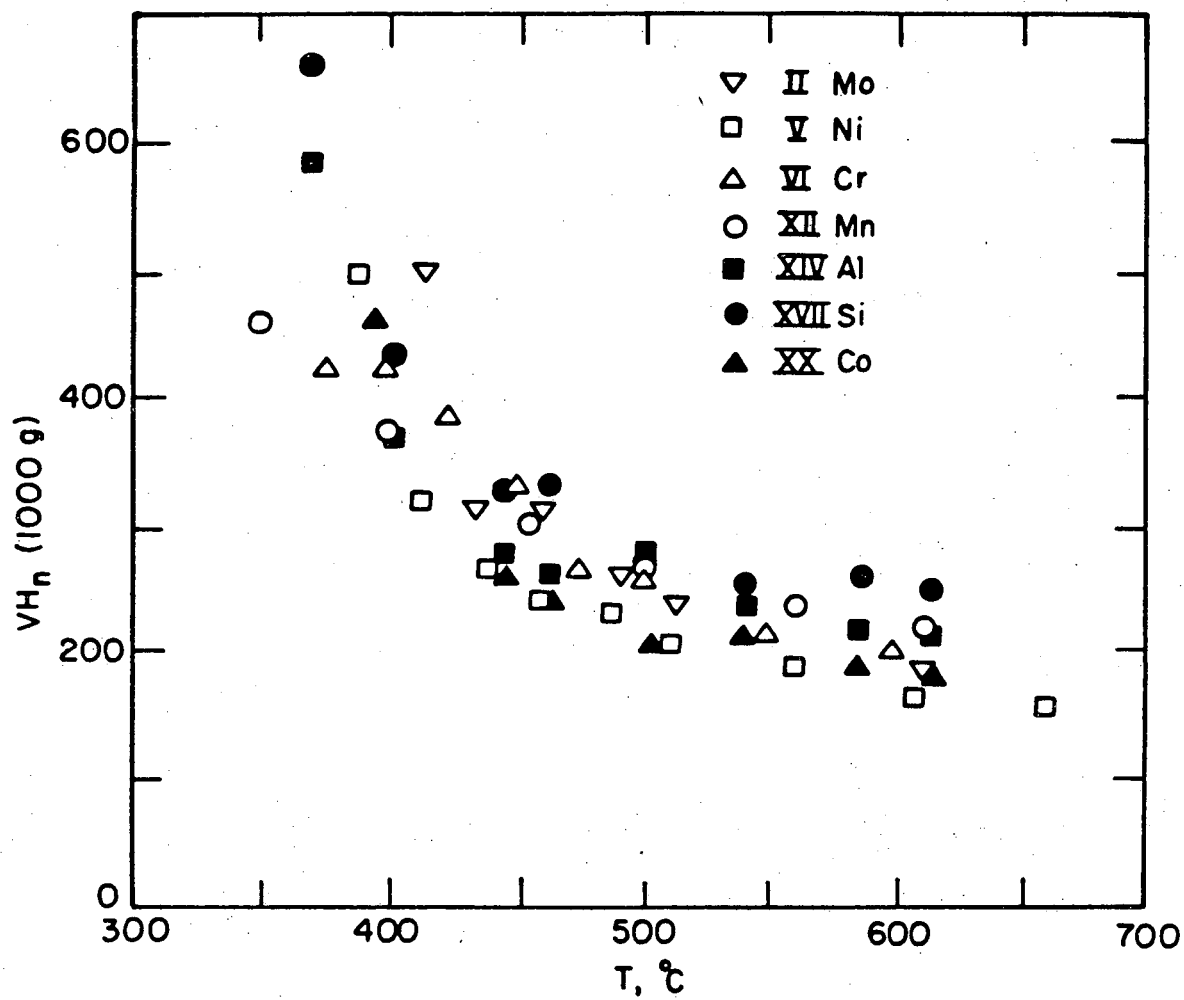
(a)



(b)

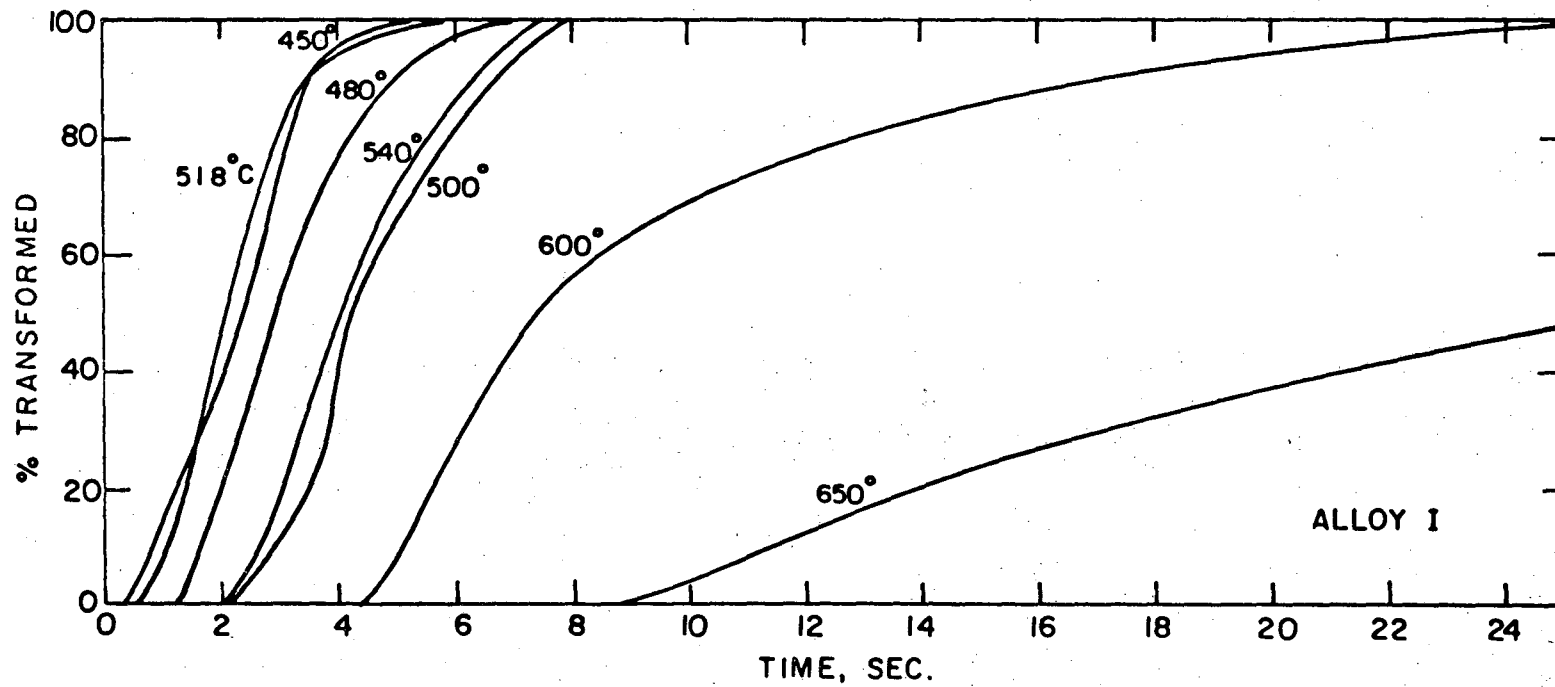
XBL7512-9284A

Fig. 40



XBL 7612-9280A

Fig. 41

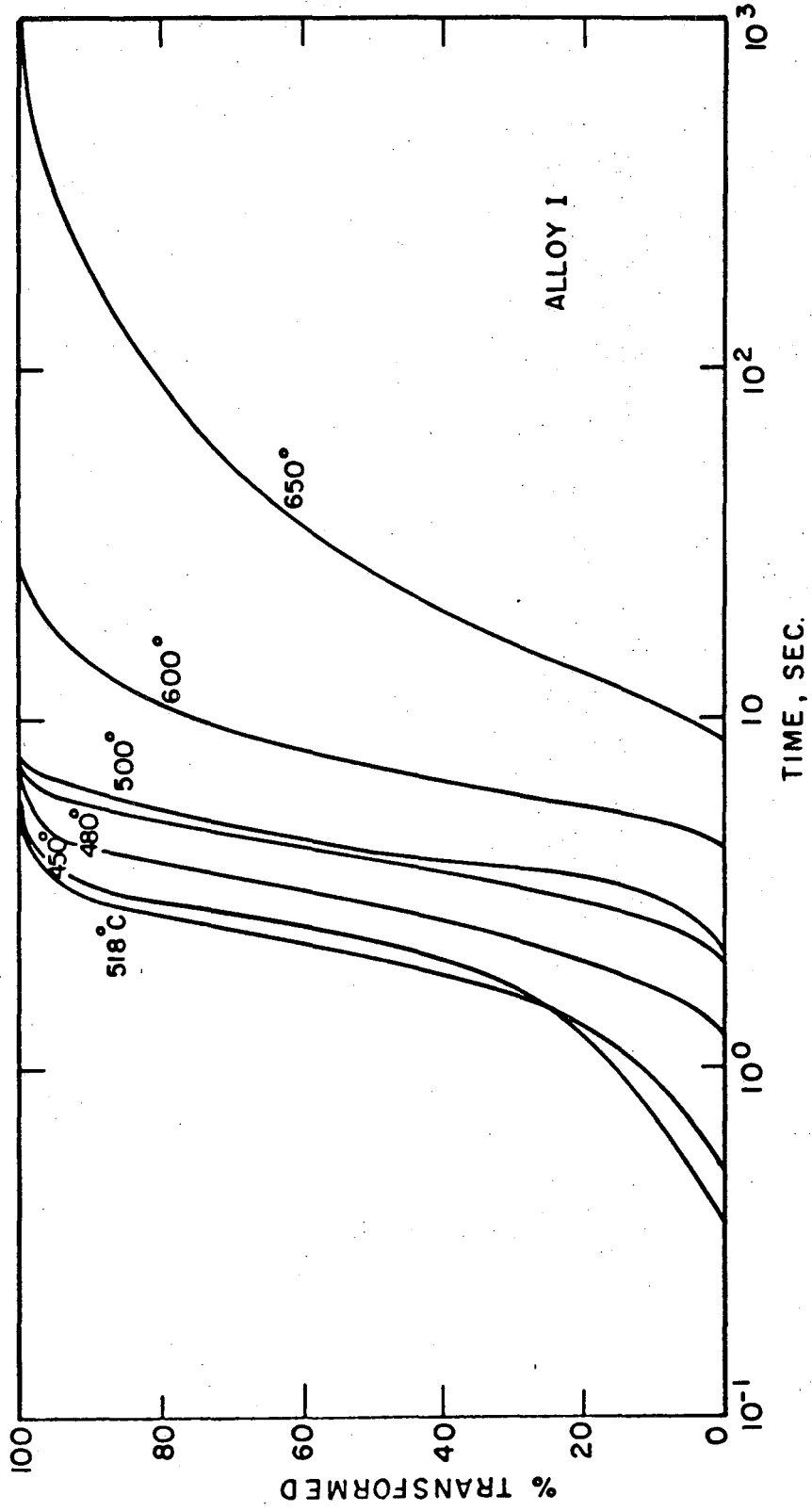


ALLOY I

XBL7612-7974

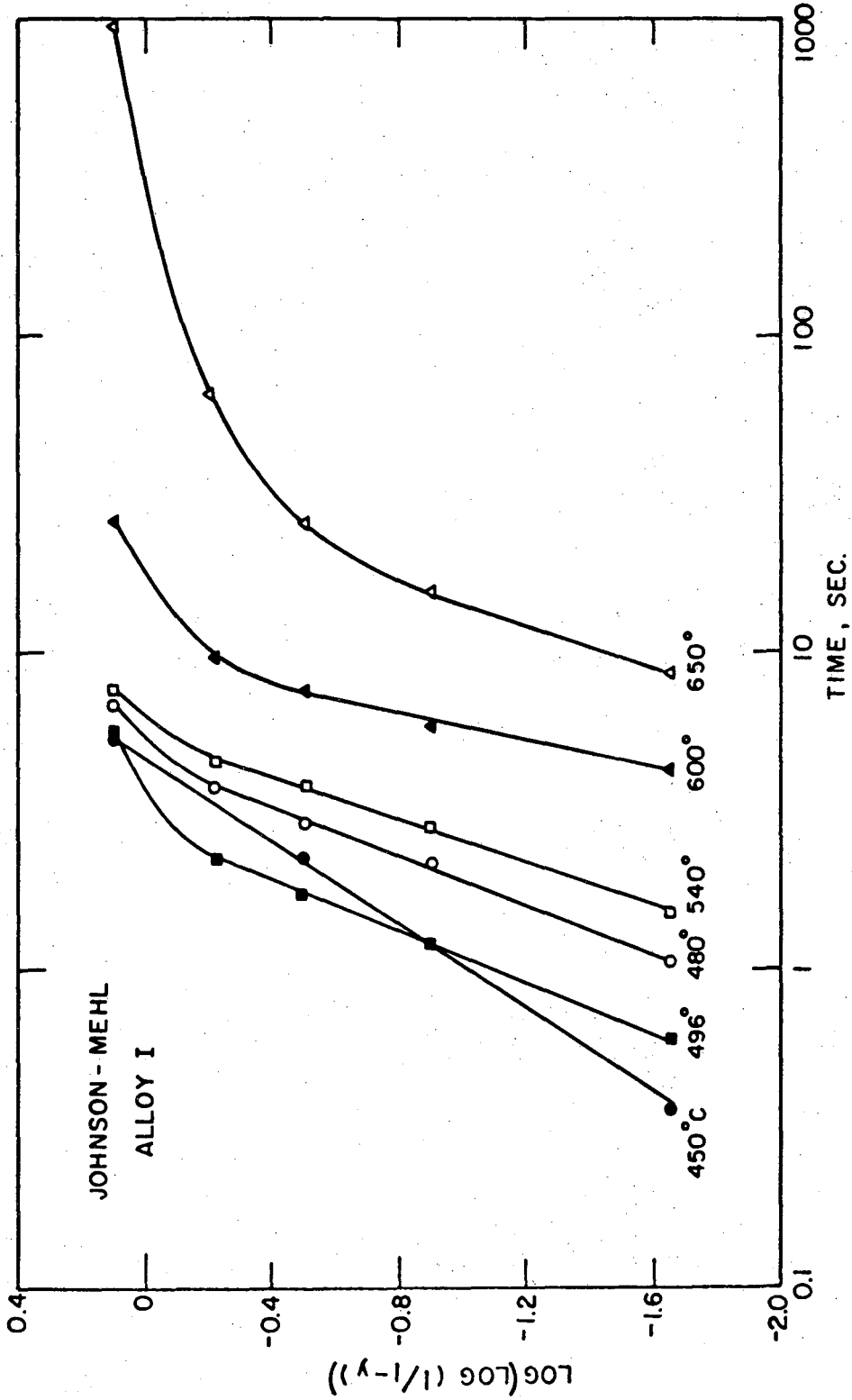
Fig. 42A

00004708679



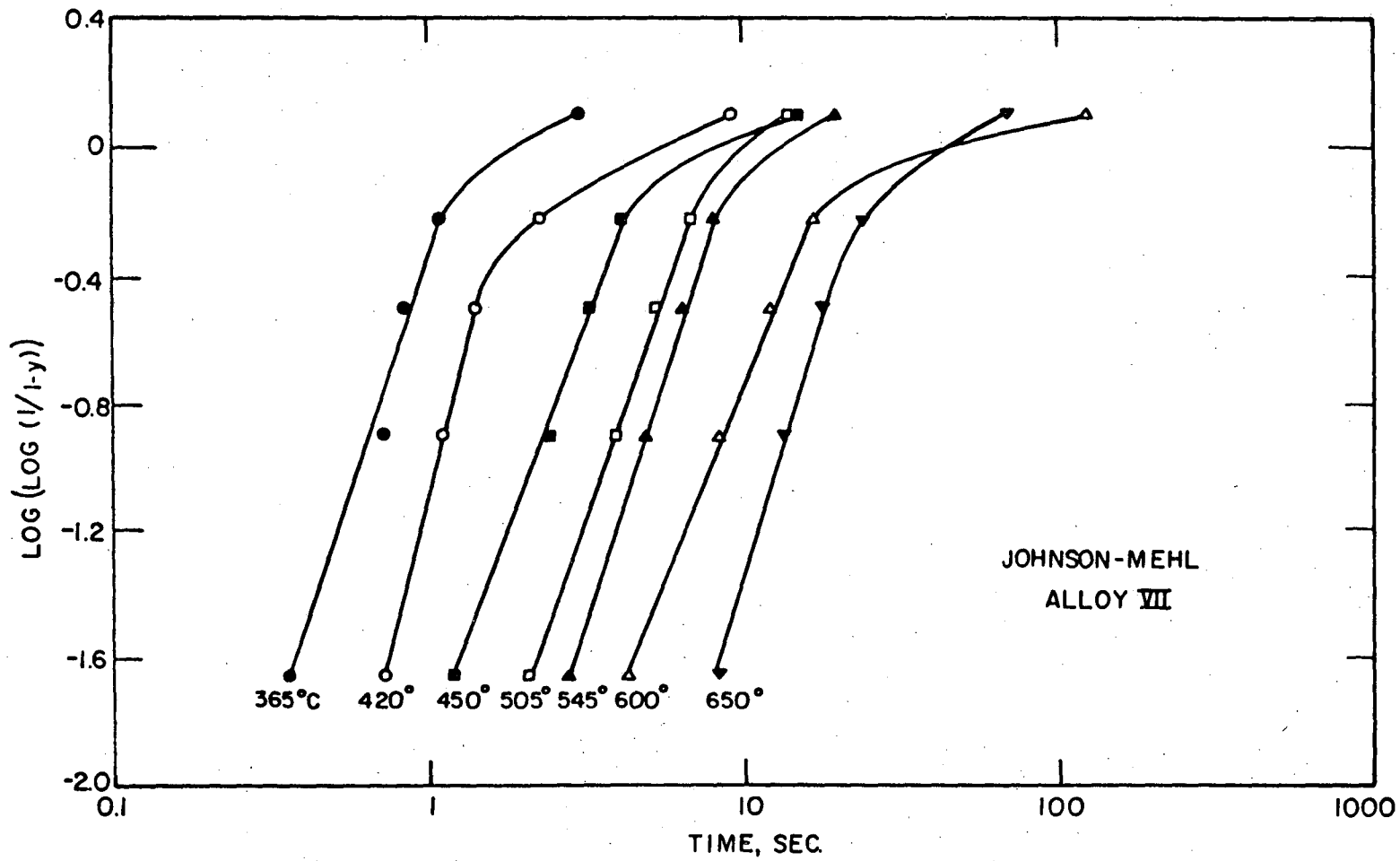
XBL 7612-7999

Fig. 42B



XBL 7612-10,997

Fig. 43A



XBL 76 12-11,001

Fig. 43B



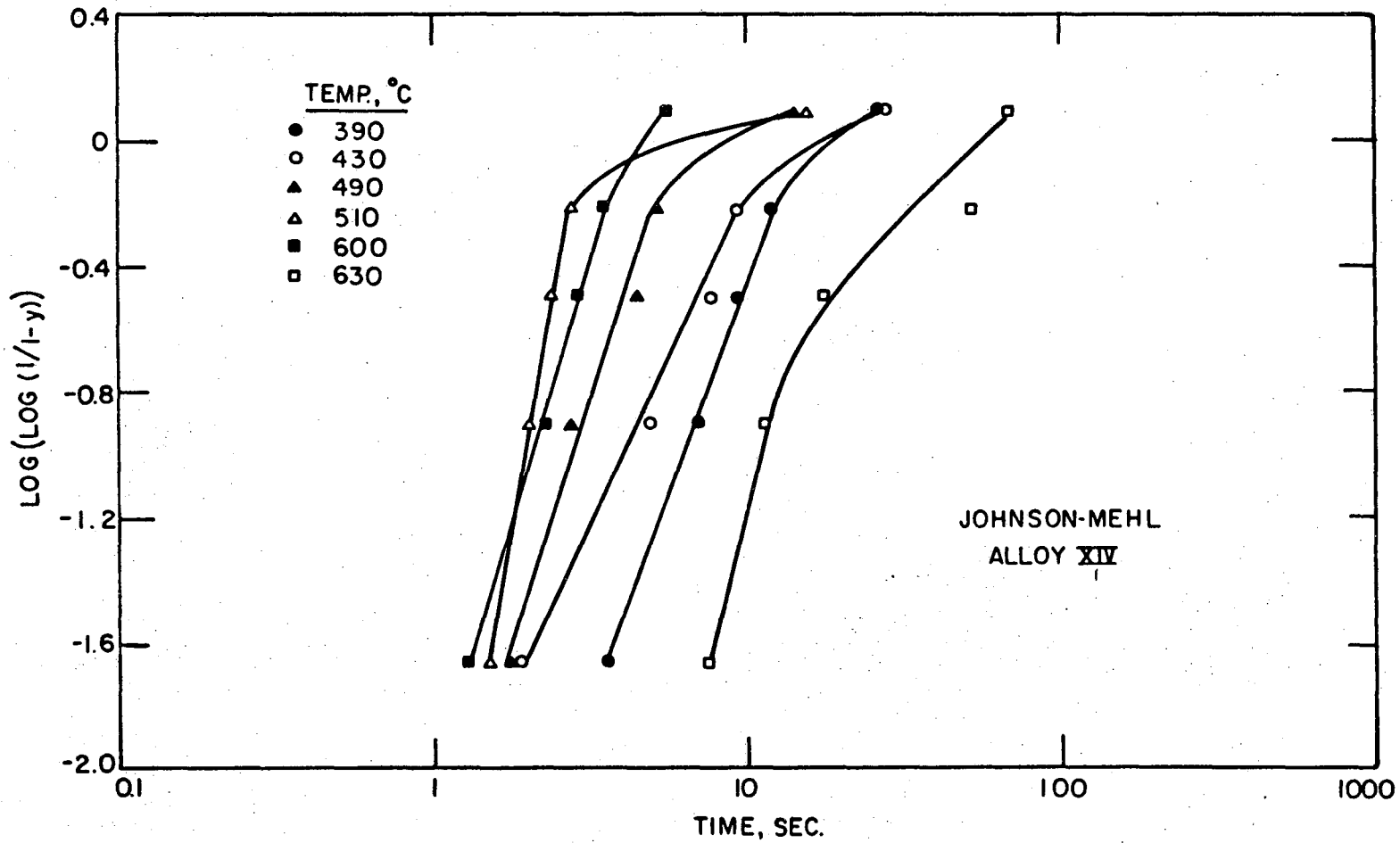


Fig. 43C

XBL 7612-11,003

0010470881

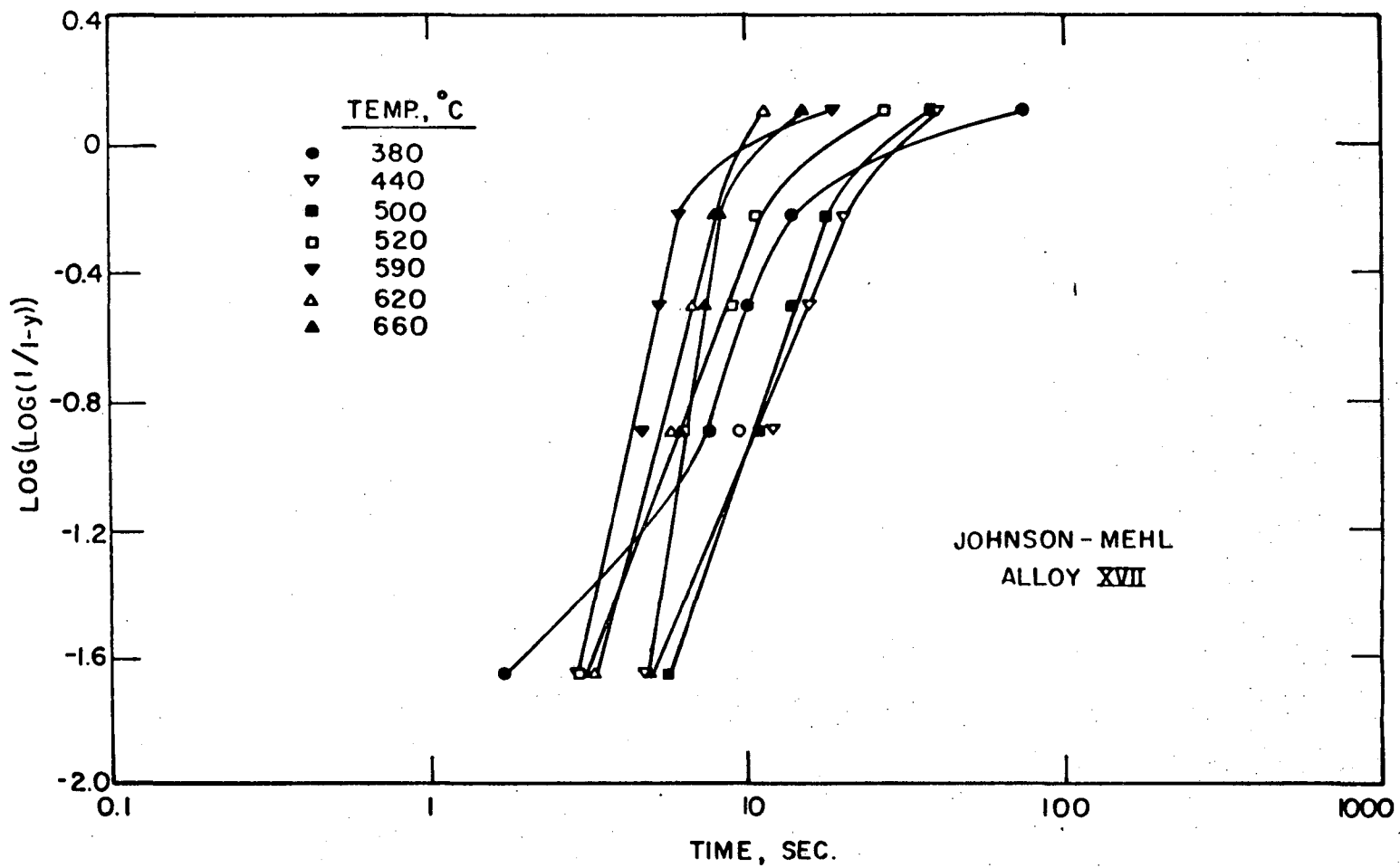


Fig. 43D

XBL 7612-10,999

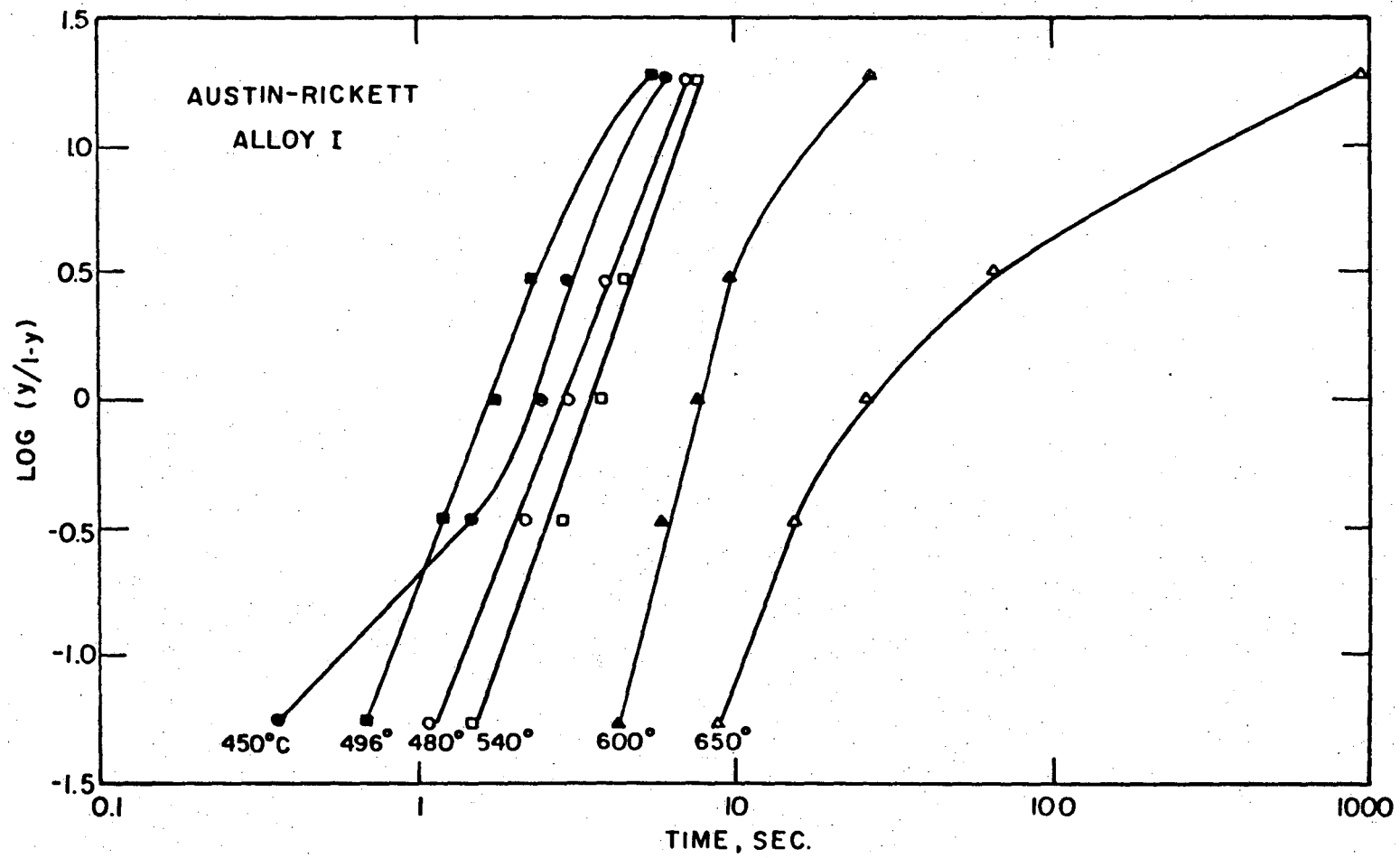


Fig. 44A

XBL7612-10,998

00004708682

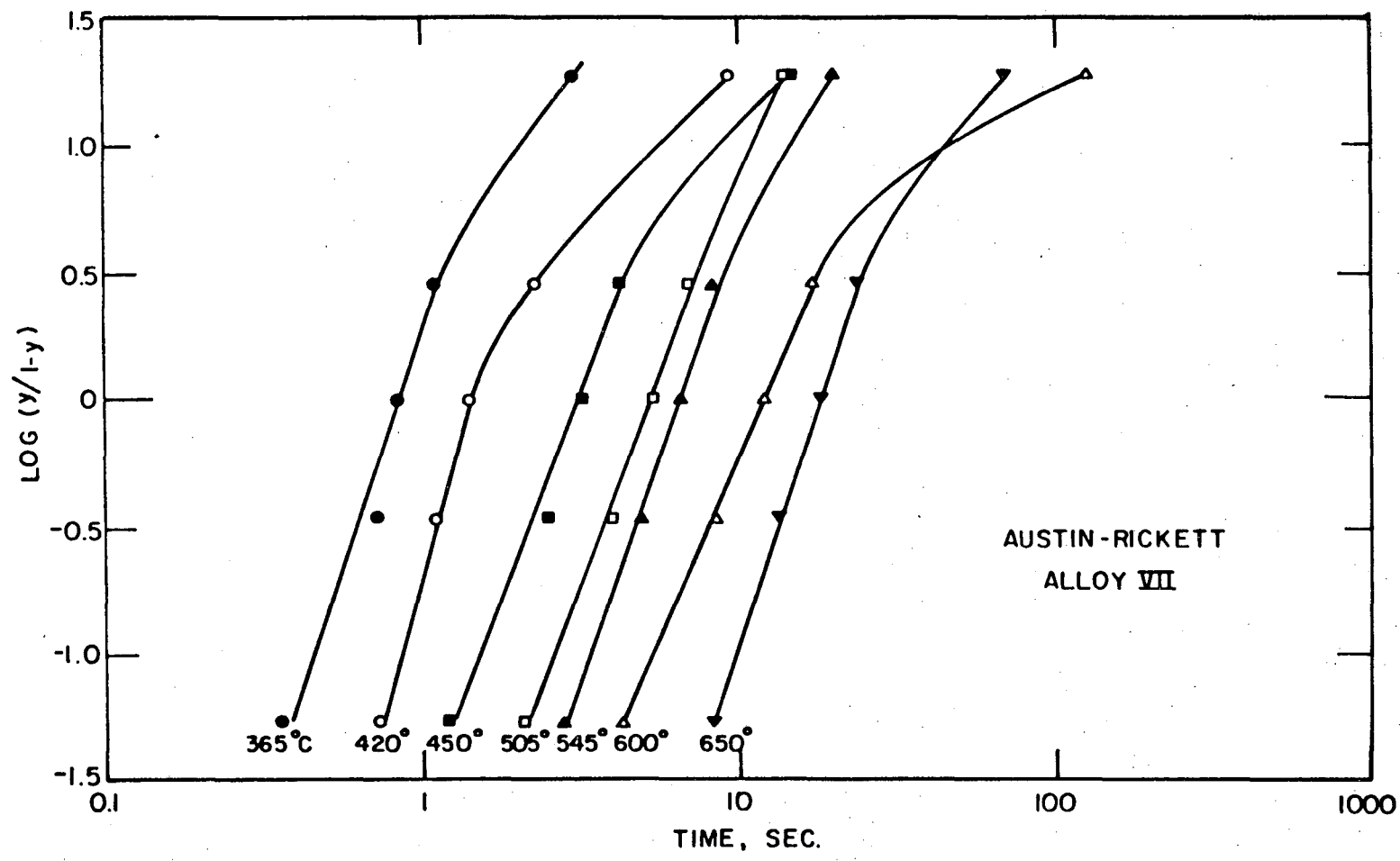


Fig. 44B

XBL 7612-11,002

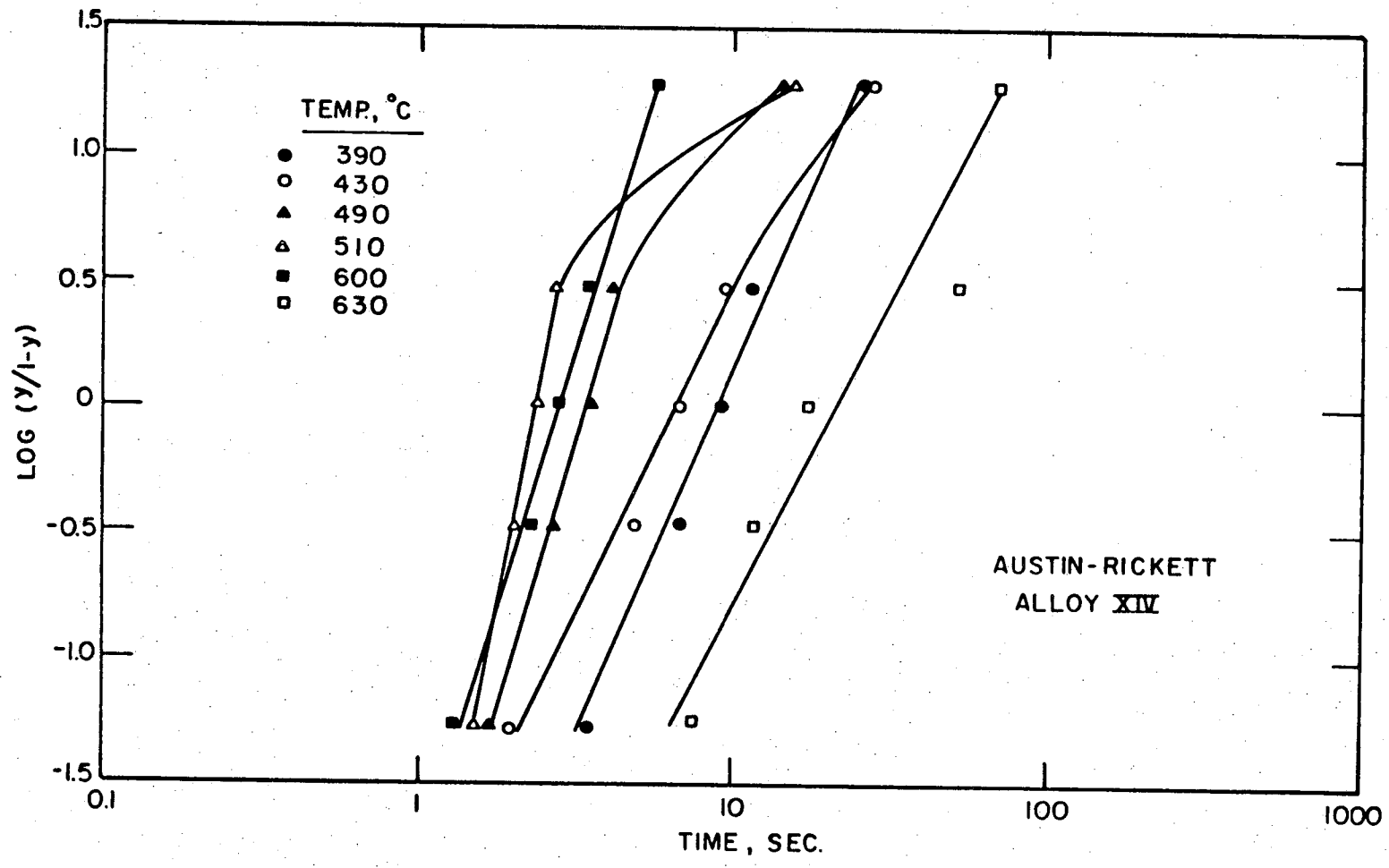


Fig. 44C

XBL 7612-11,004

00004708683

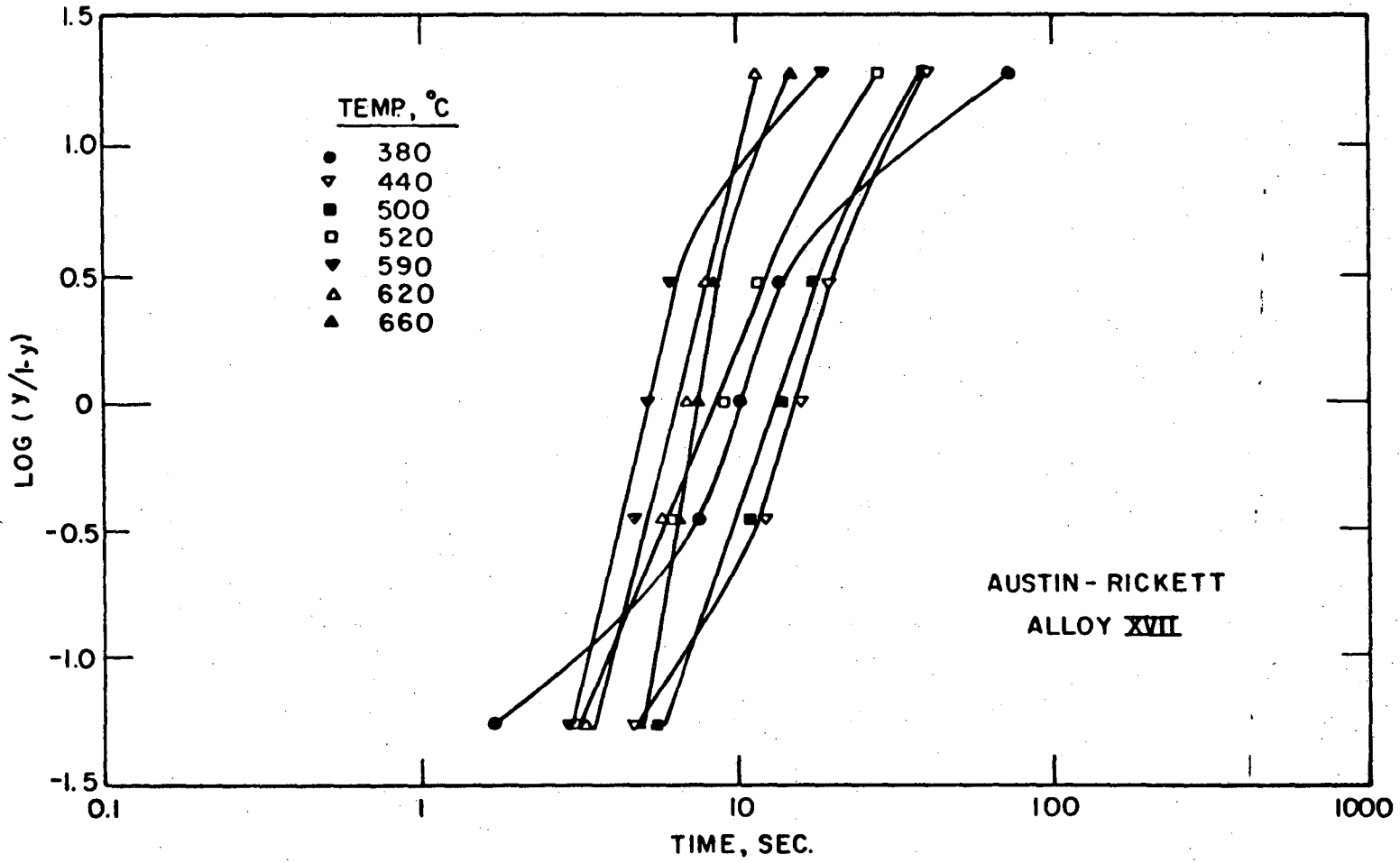
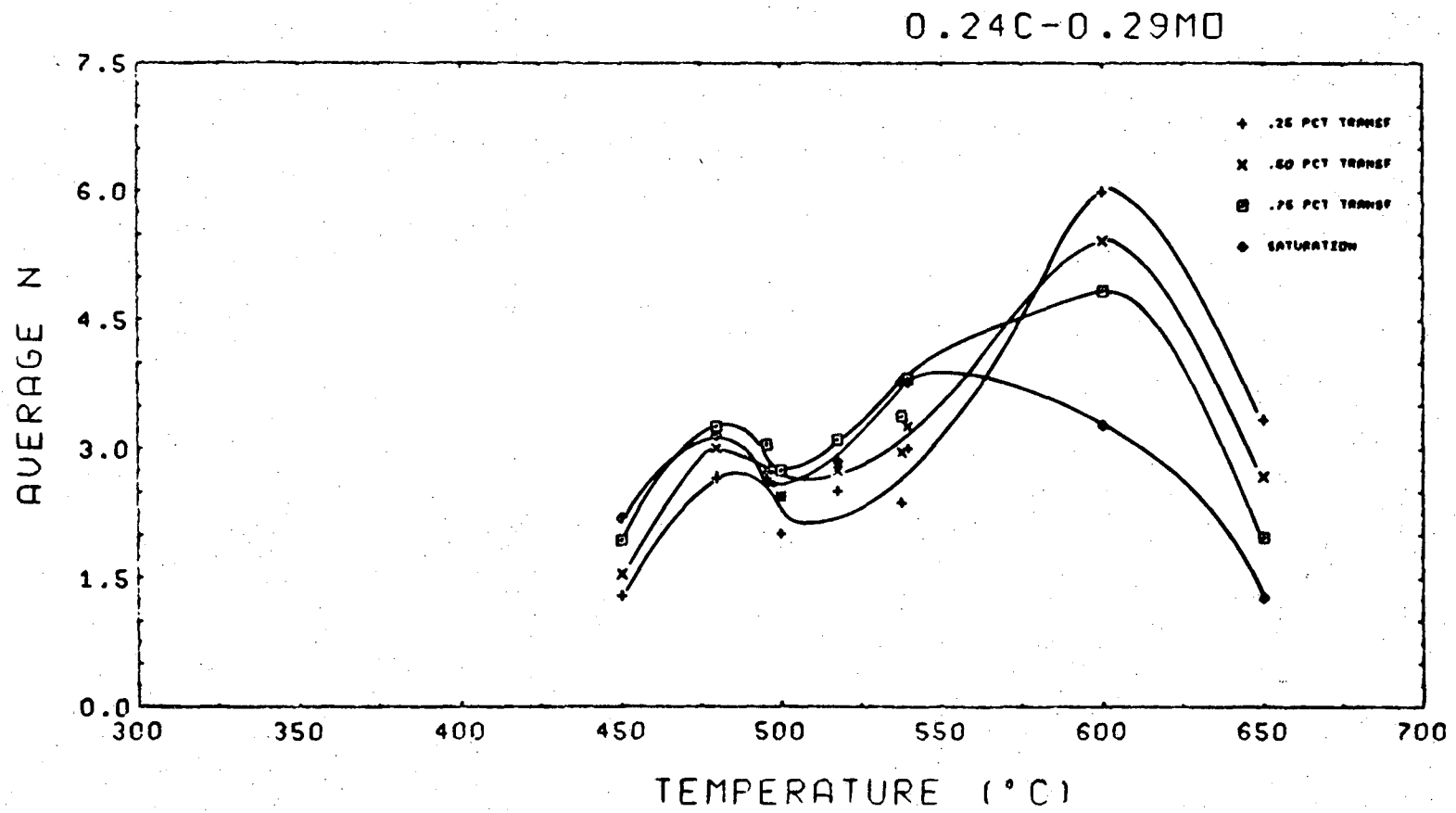


Fig. 44D

XBL 7612-11,000



-179-

00004708684

Fig. 45A

XBL 7612 7982

0.30C-0.49MD

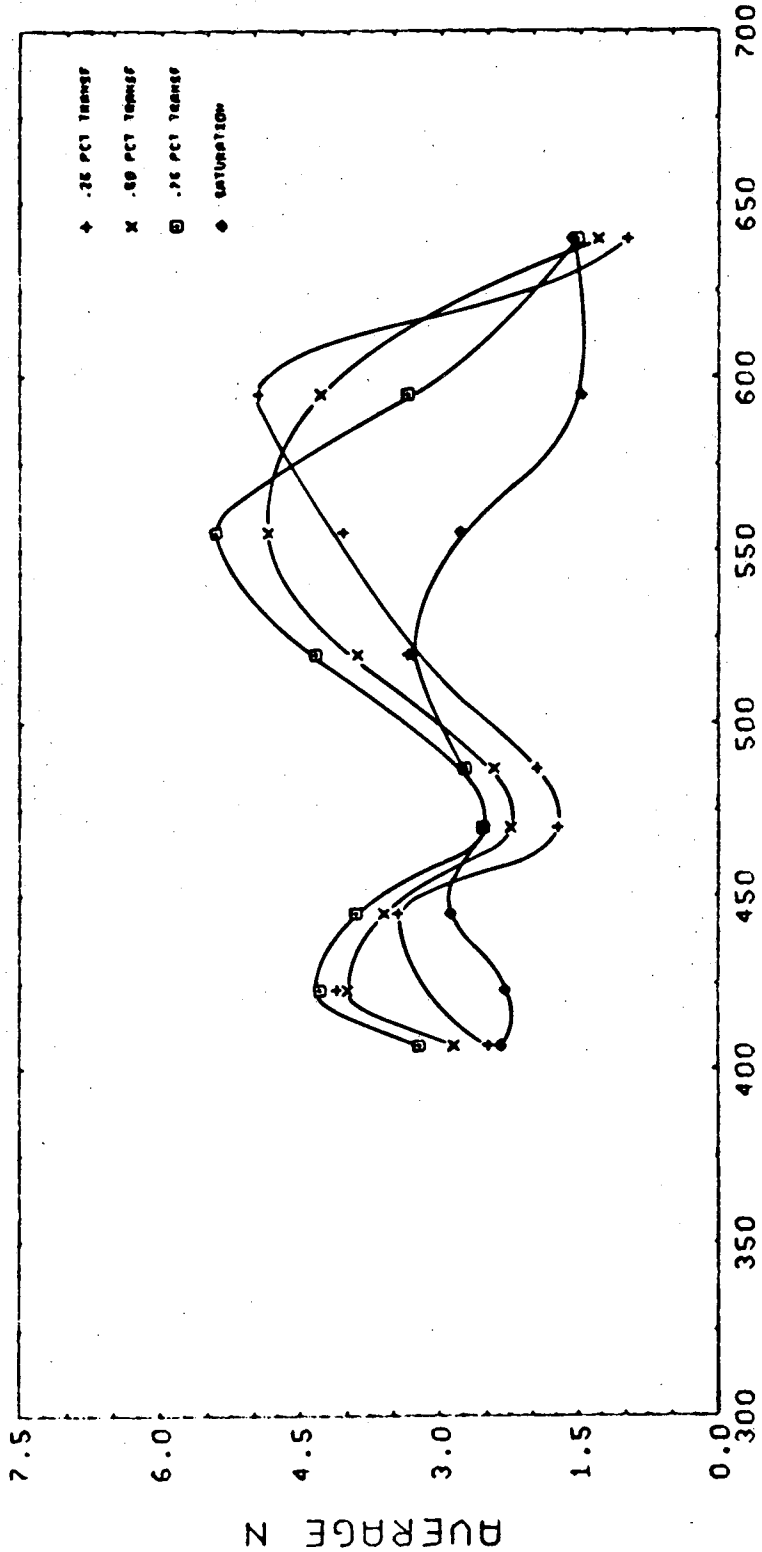
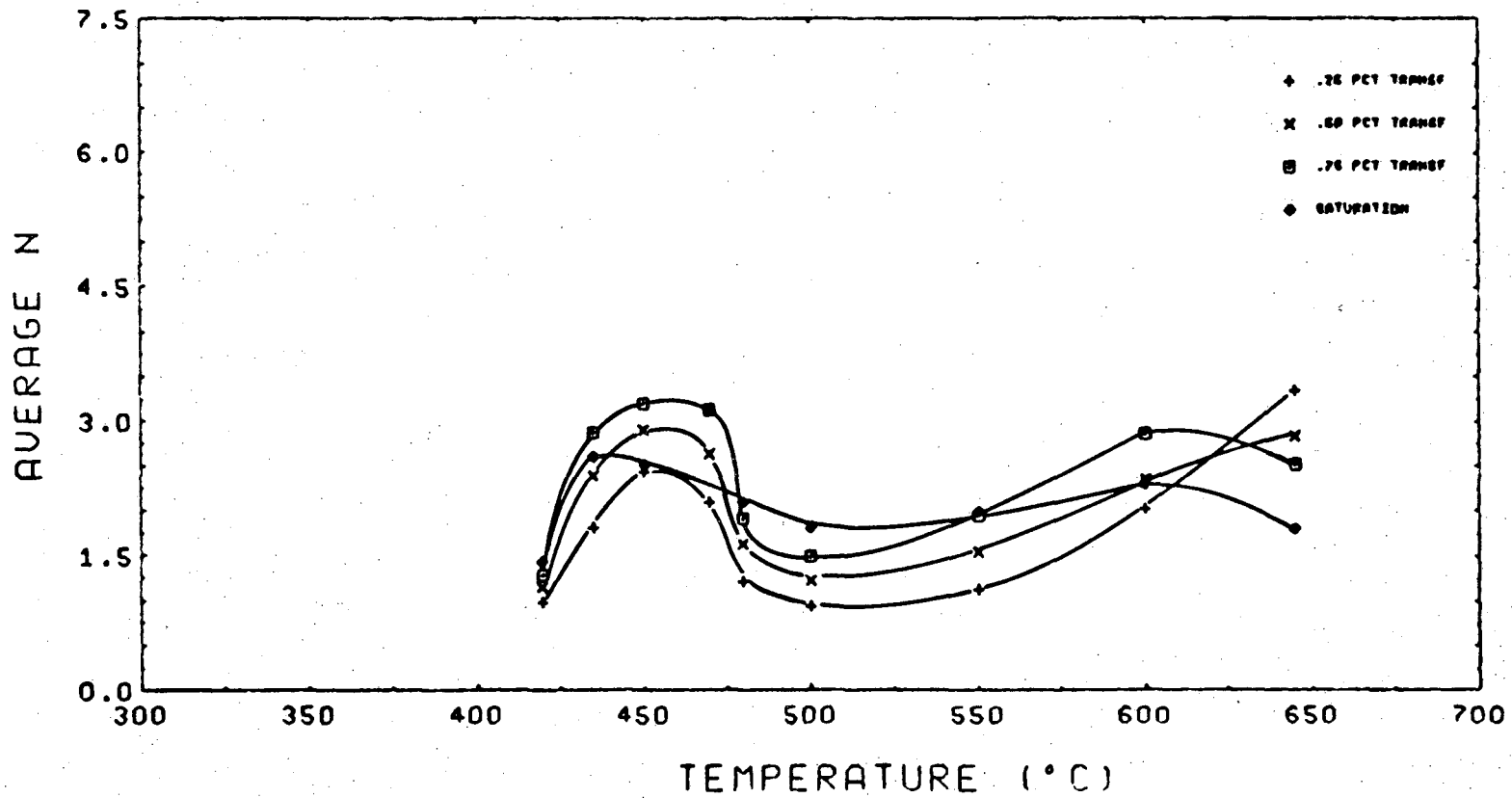


Fig. 45B

XBL7612-7983



0.23C-2.04NI



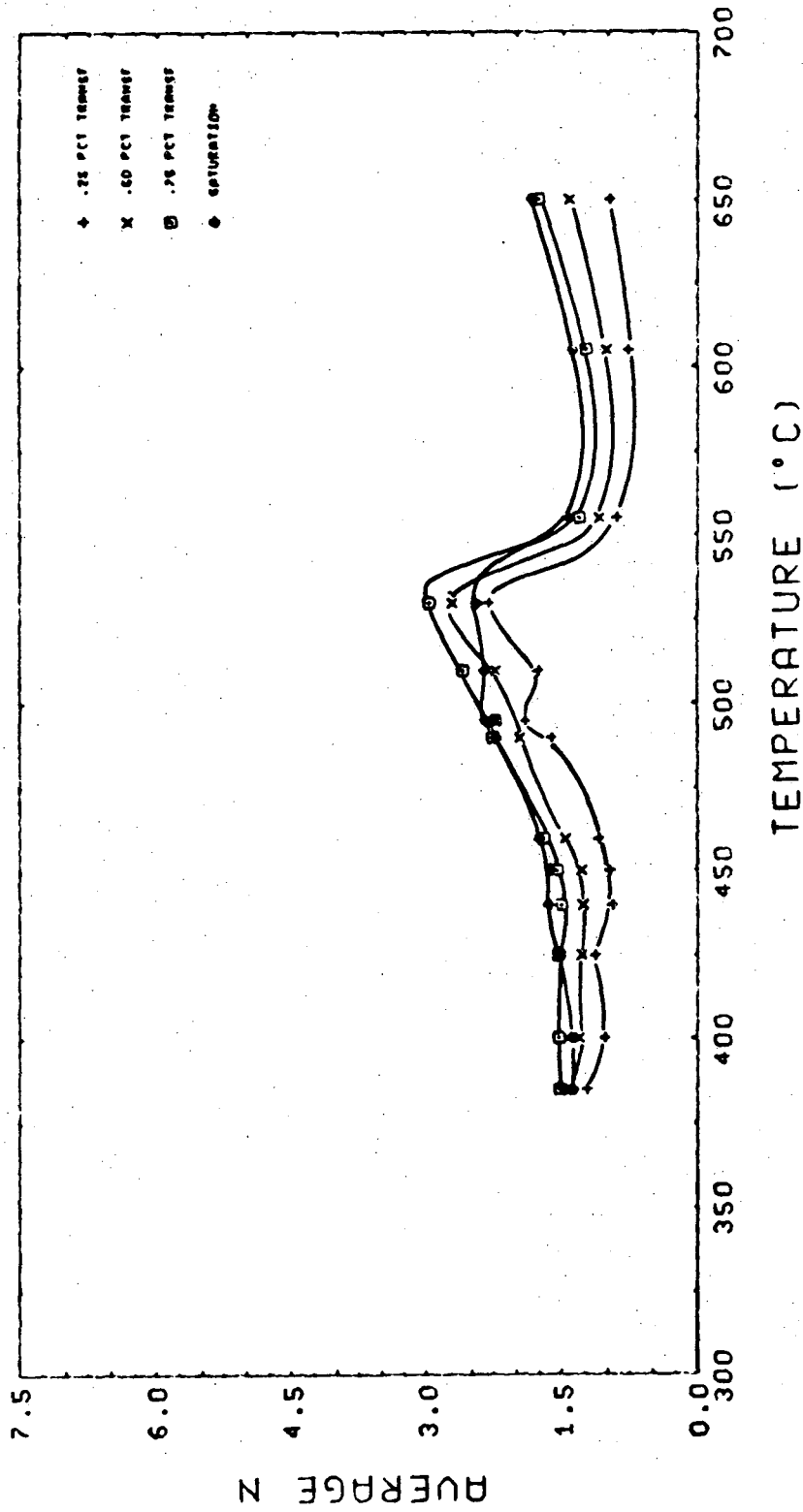
-181-

00004700685

Fig. 45C

XBL 7612-7984

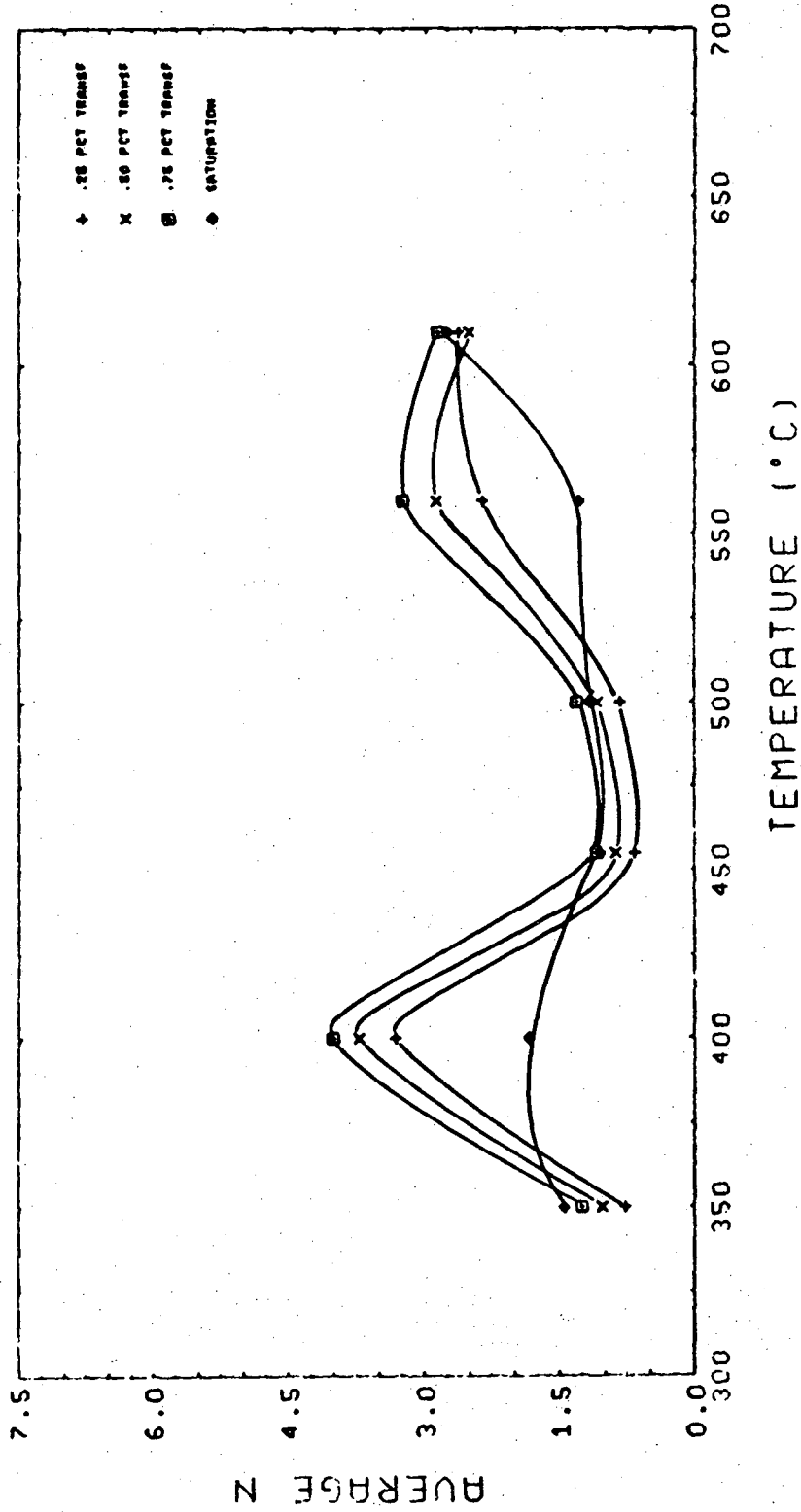
0.29C-1.00CR



XBL 7612-7985

Fig. 45D

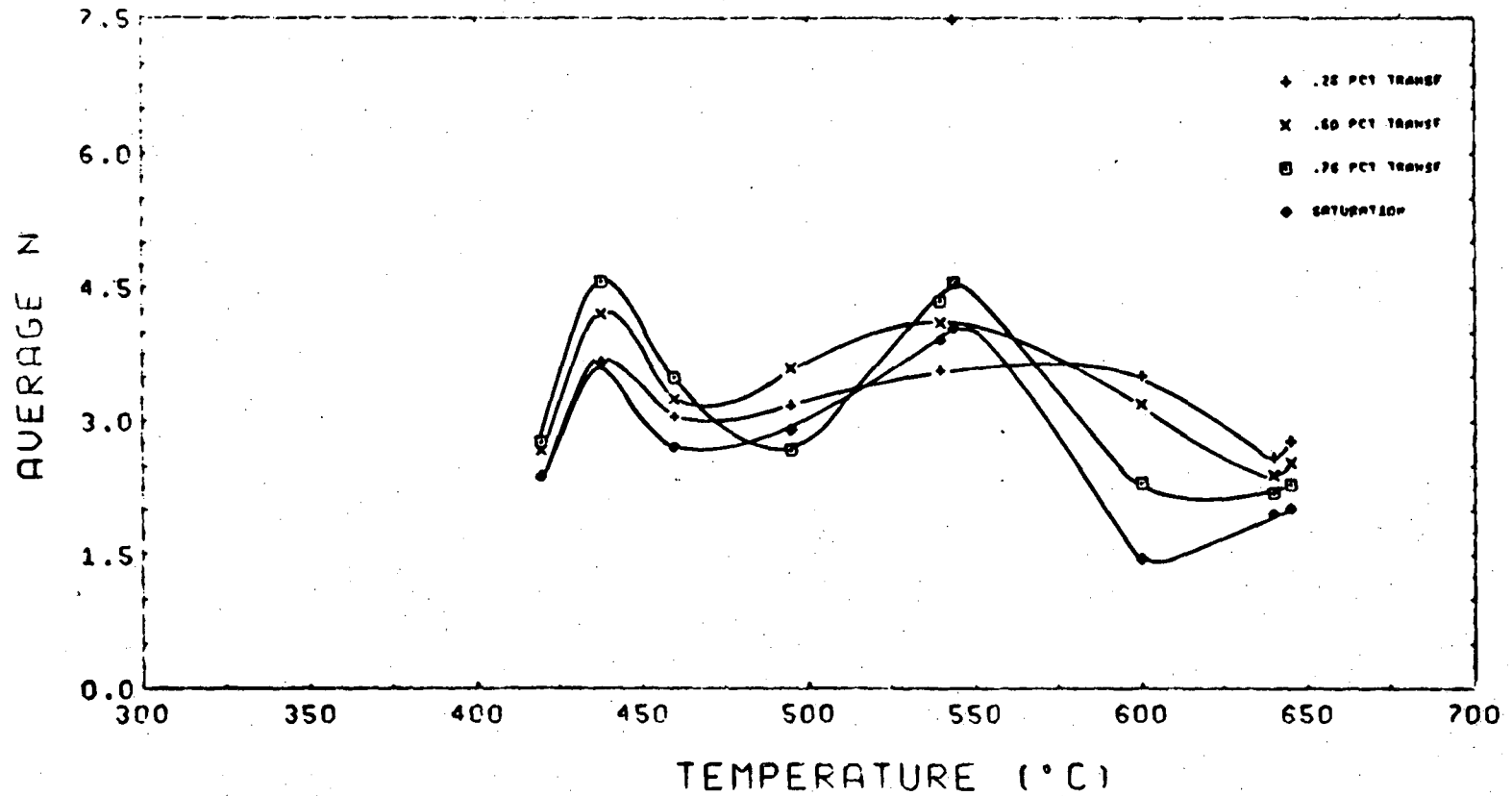
0.41C-1.67MN



XBL 7612-7986

Fig. 45E

0.25C-1.00NI-0.48MO

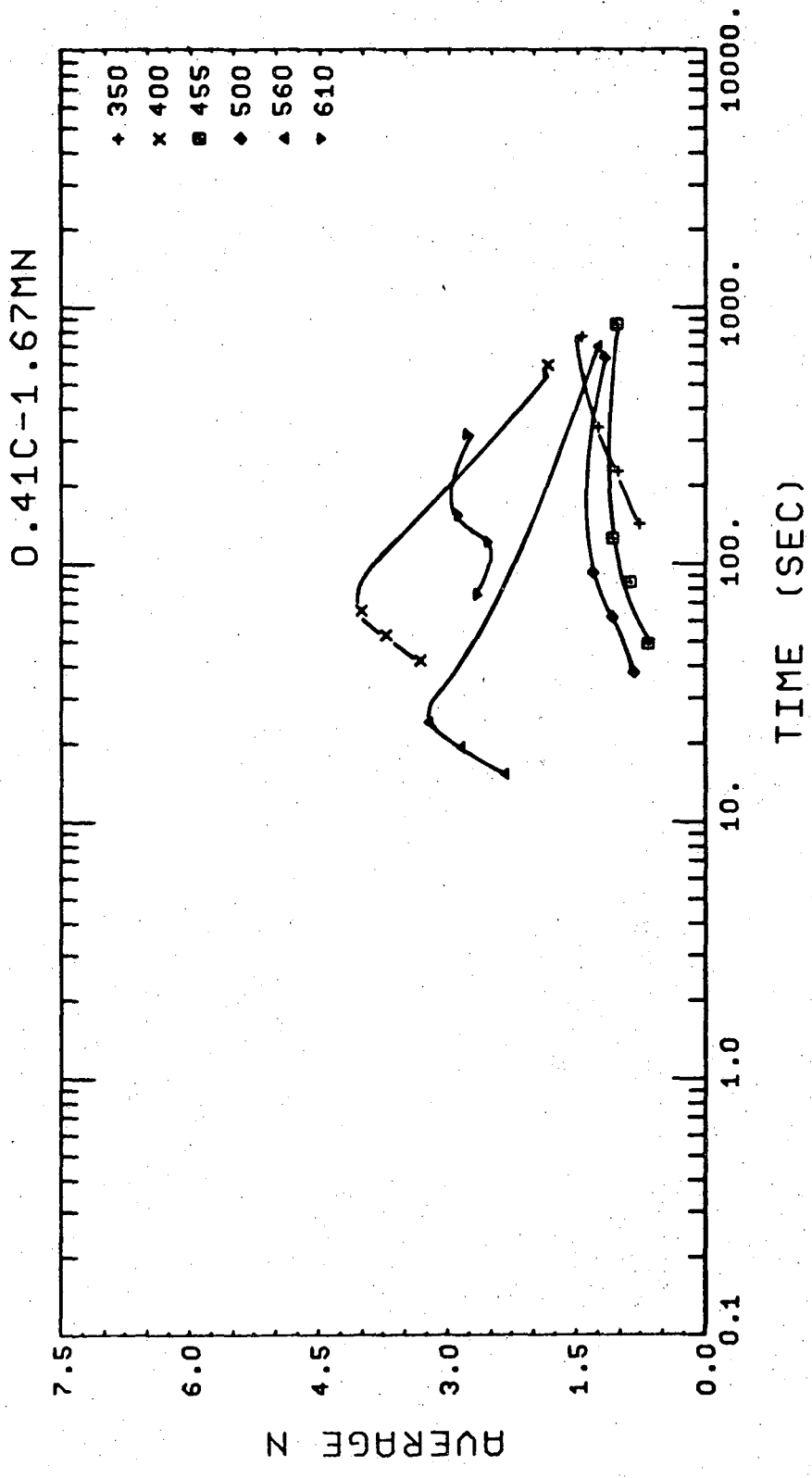


-184-

Fig. 45F

XBL7612-7987

0 0 0 0 4 7 0 8 6 8 7



XBL 7612-7989

Fig. 46A

0.30C-0.49M0

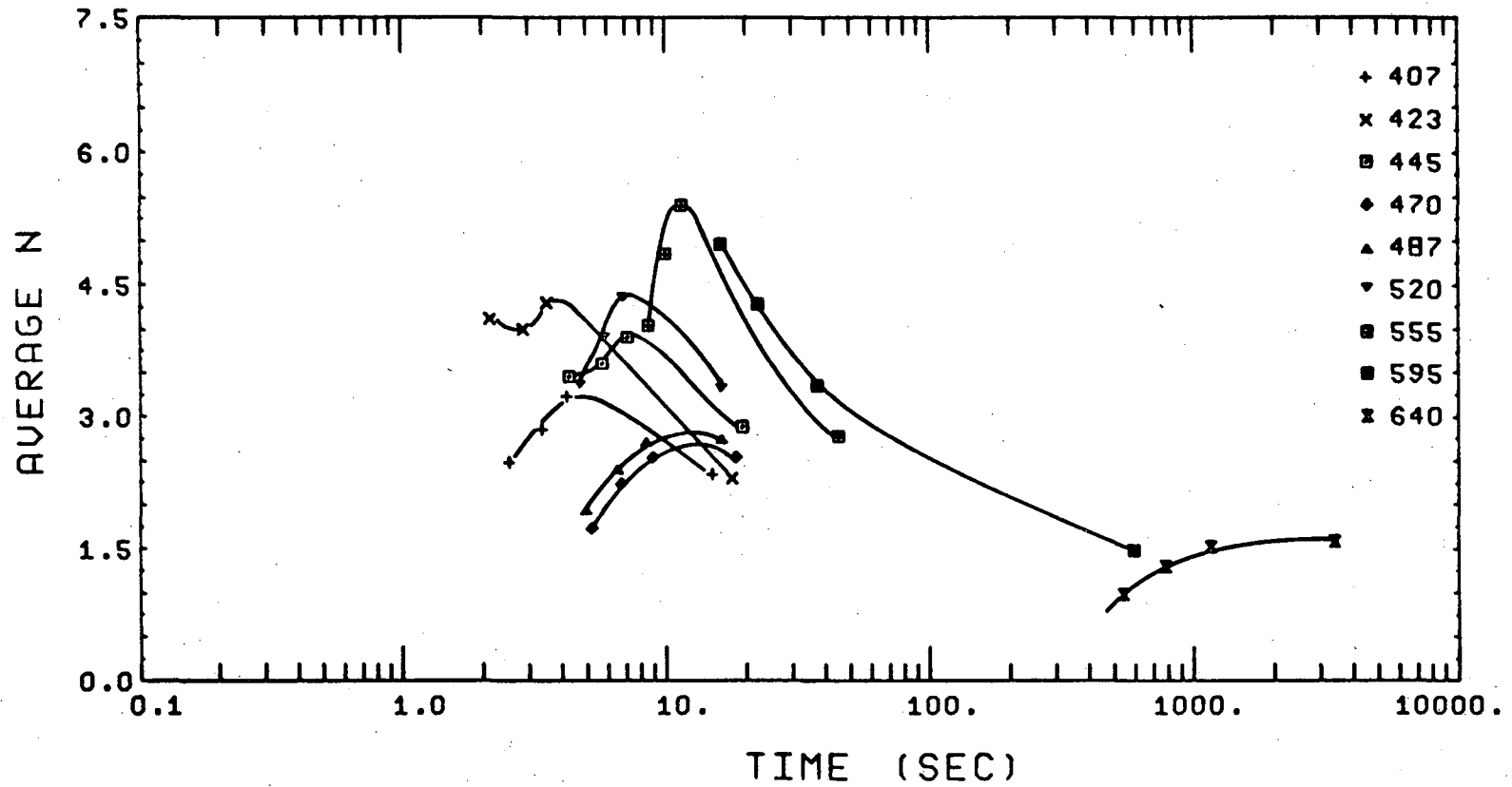
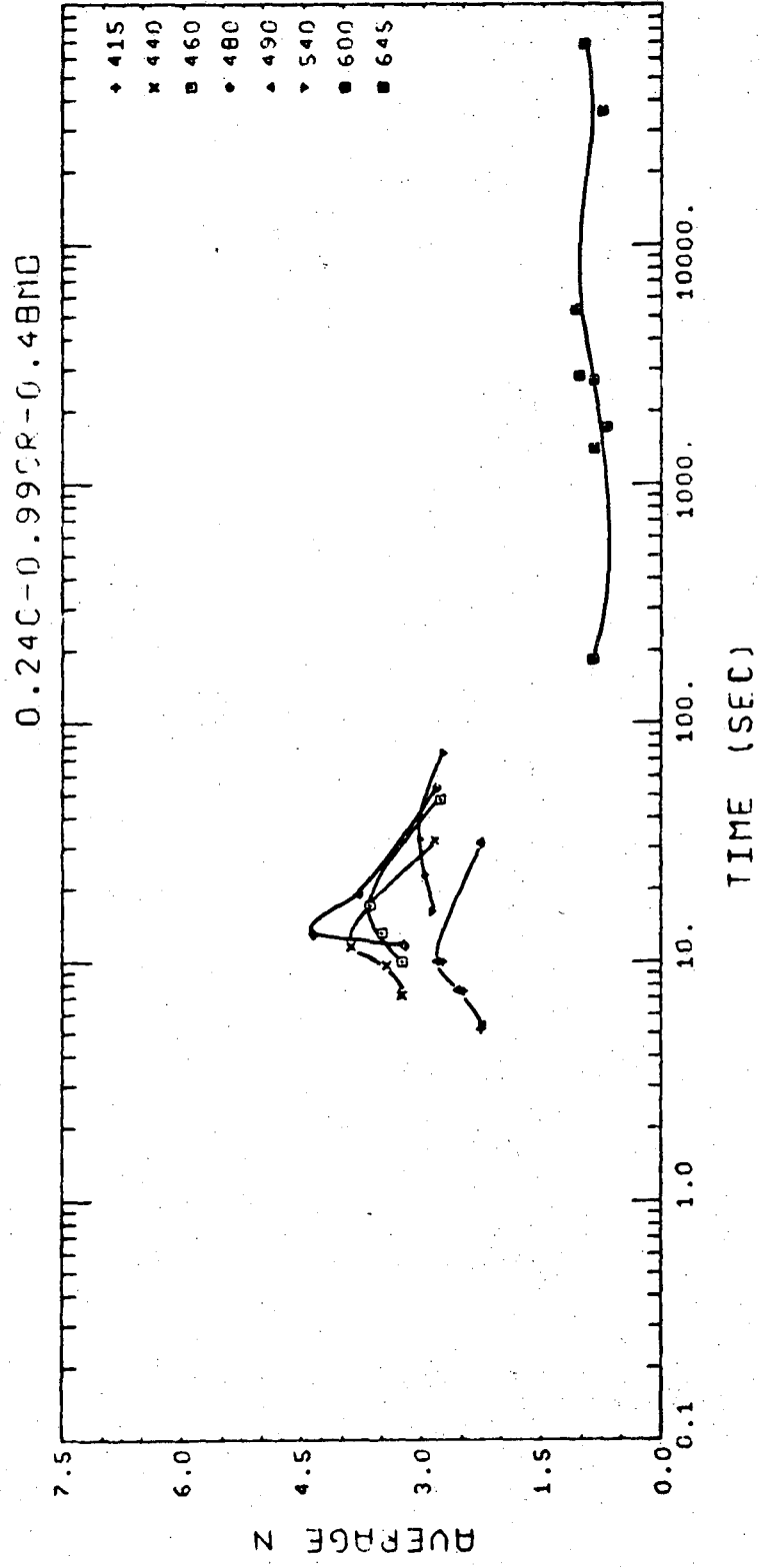


Fig. 46B

XBL7612-7988



XBL7612-7990

Fig. 46C

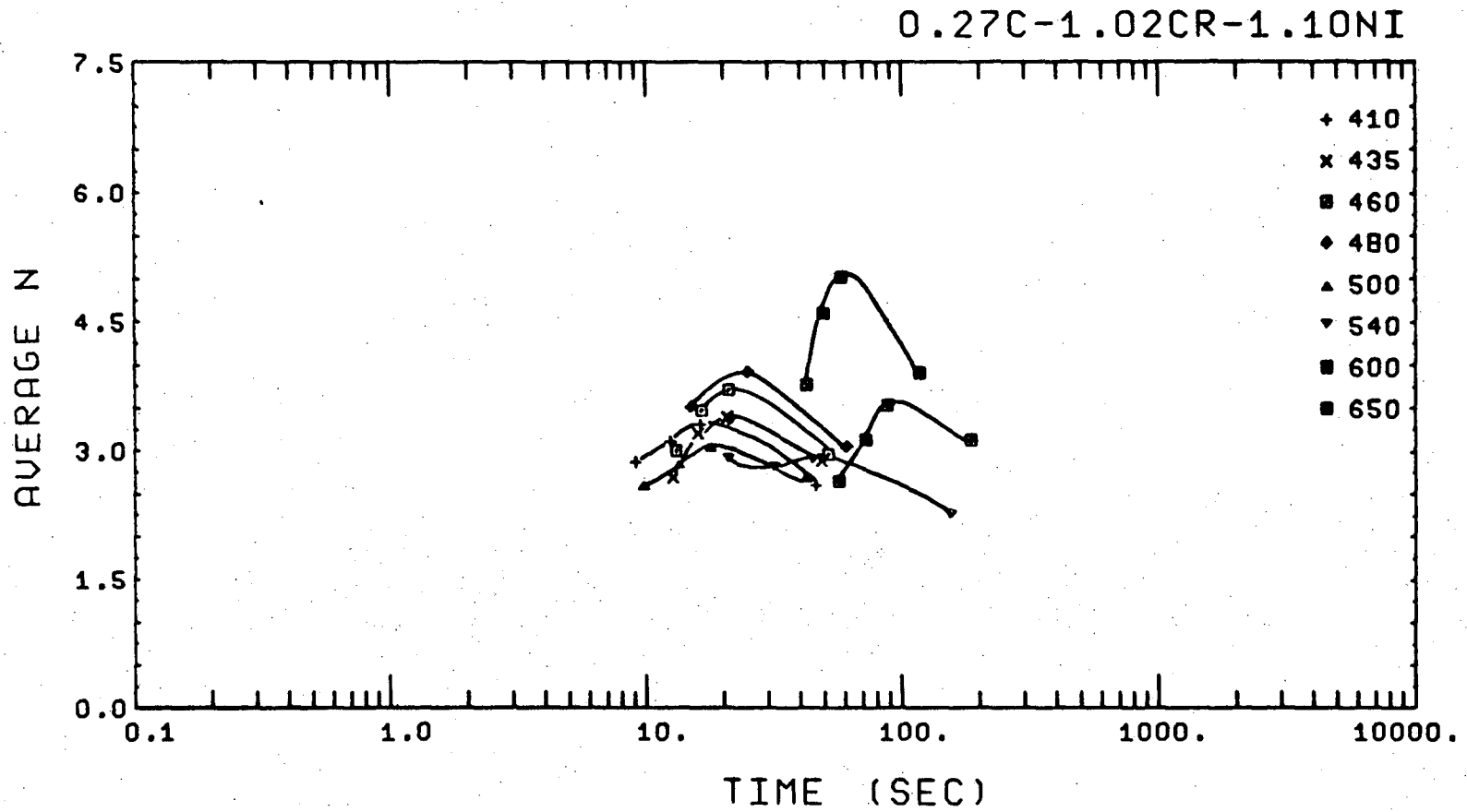


Fig. 46D

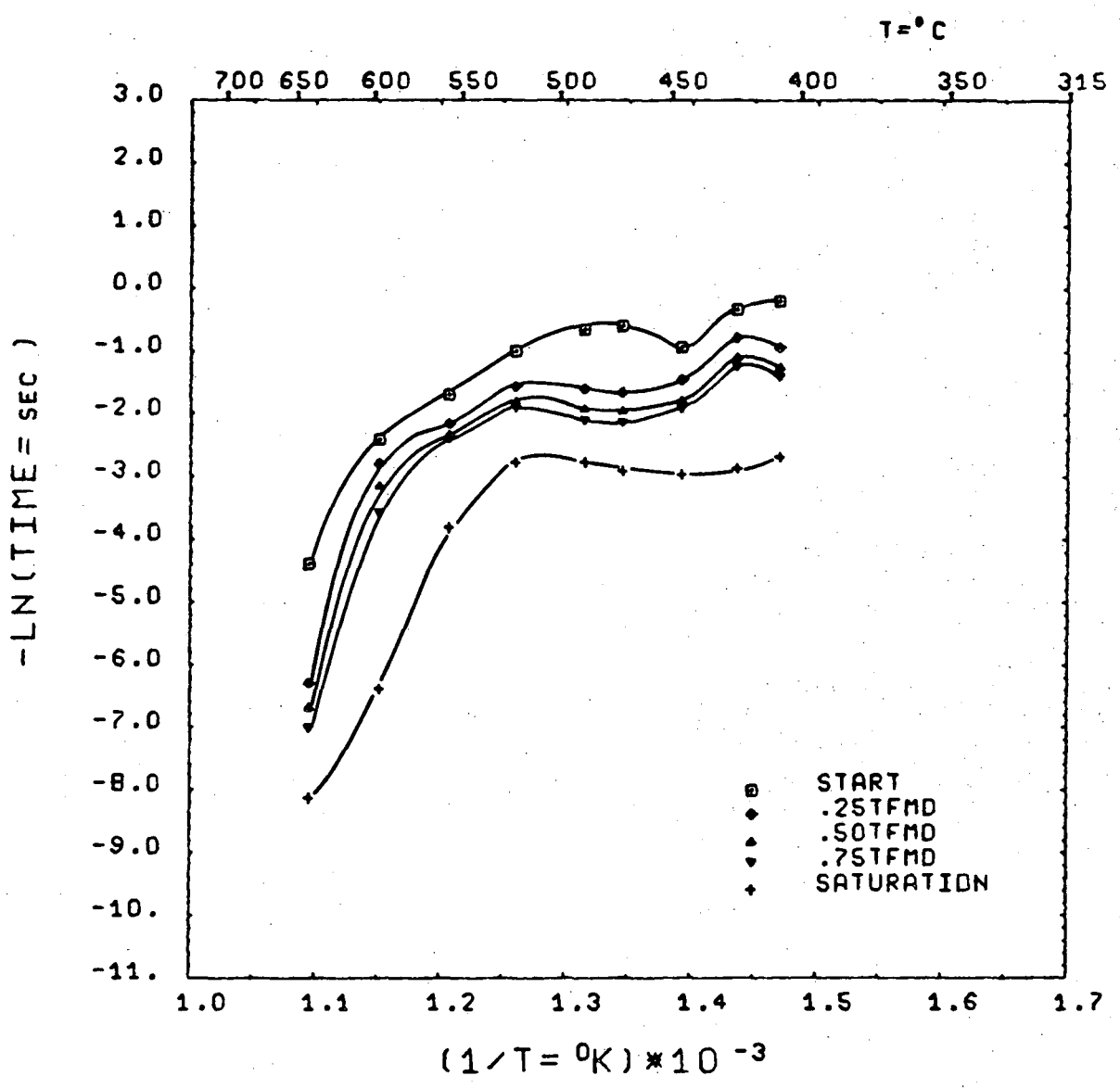
XBL7612-7991



0 0 0 0 4 7 0 8 6 8 9

-189-

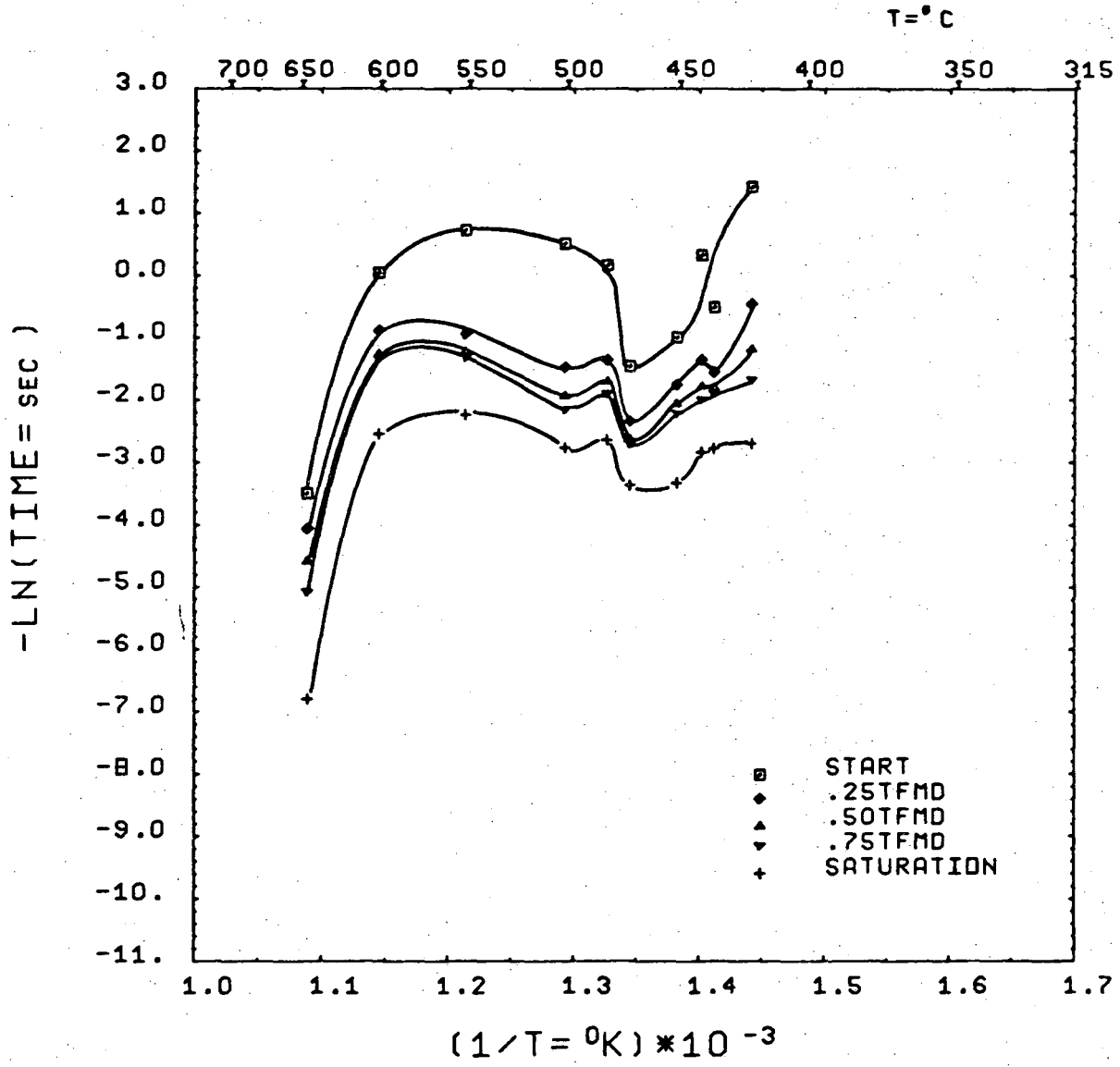
0.30C-0.49MD



XBL7612-7998

Fig. 47A

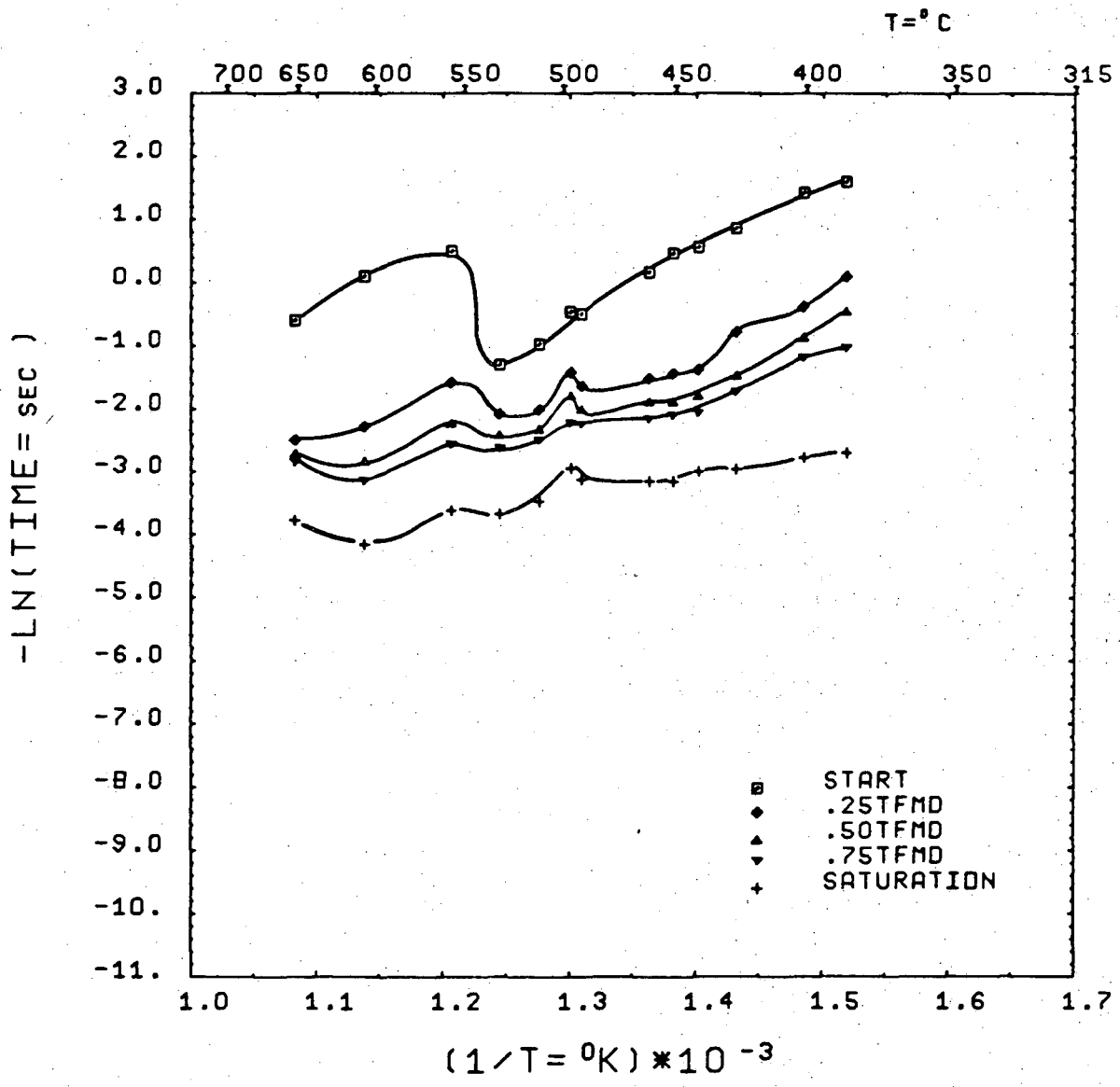
0.23C-2.04NI



XBL 7612-7997

Fig. 47B

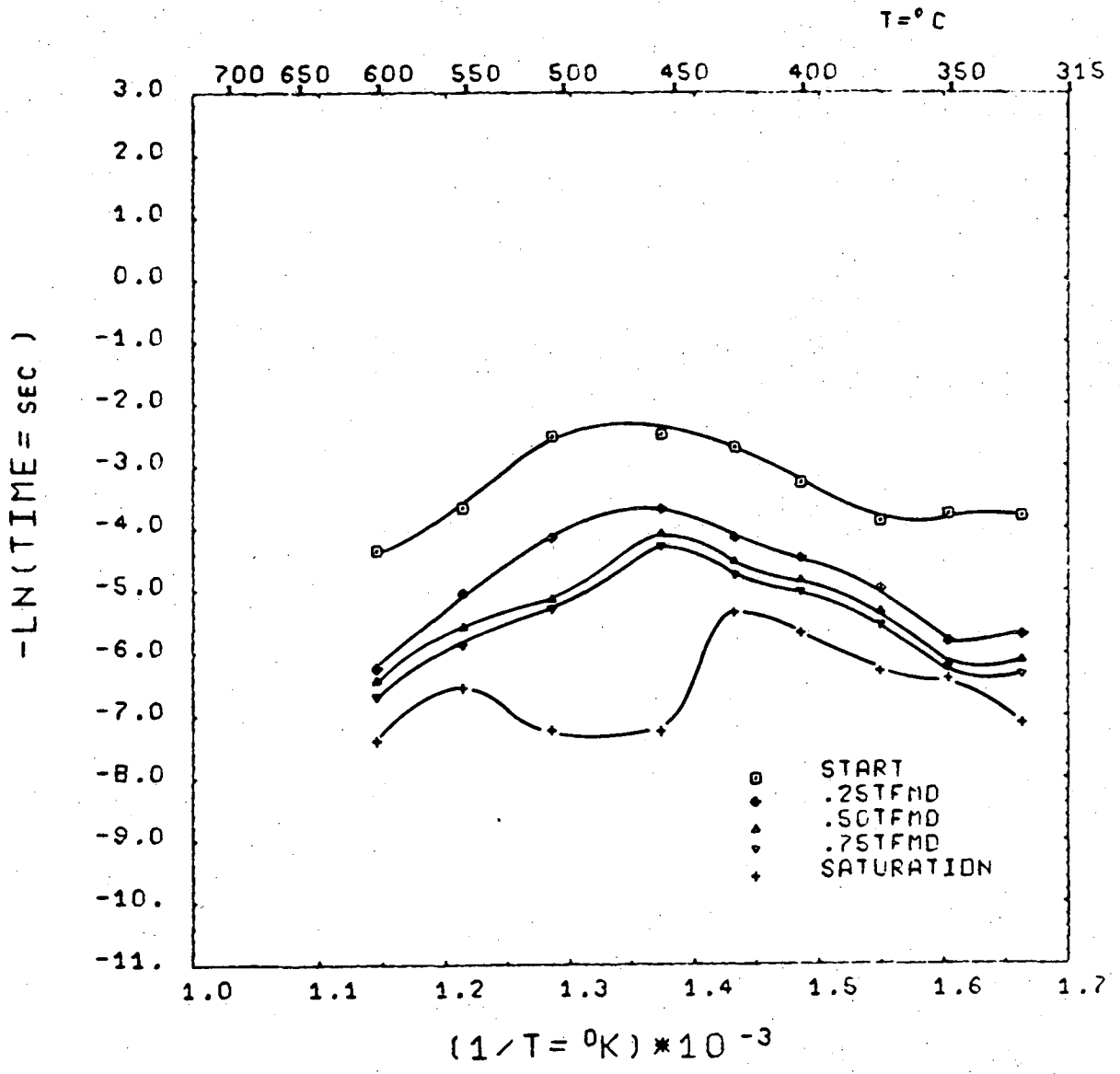
0.29C-1.00CR



XBL 7612-7996

Fig. 47C

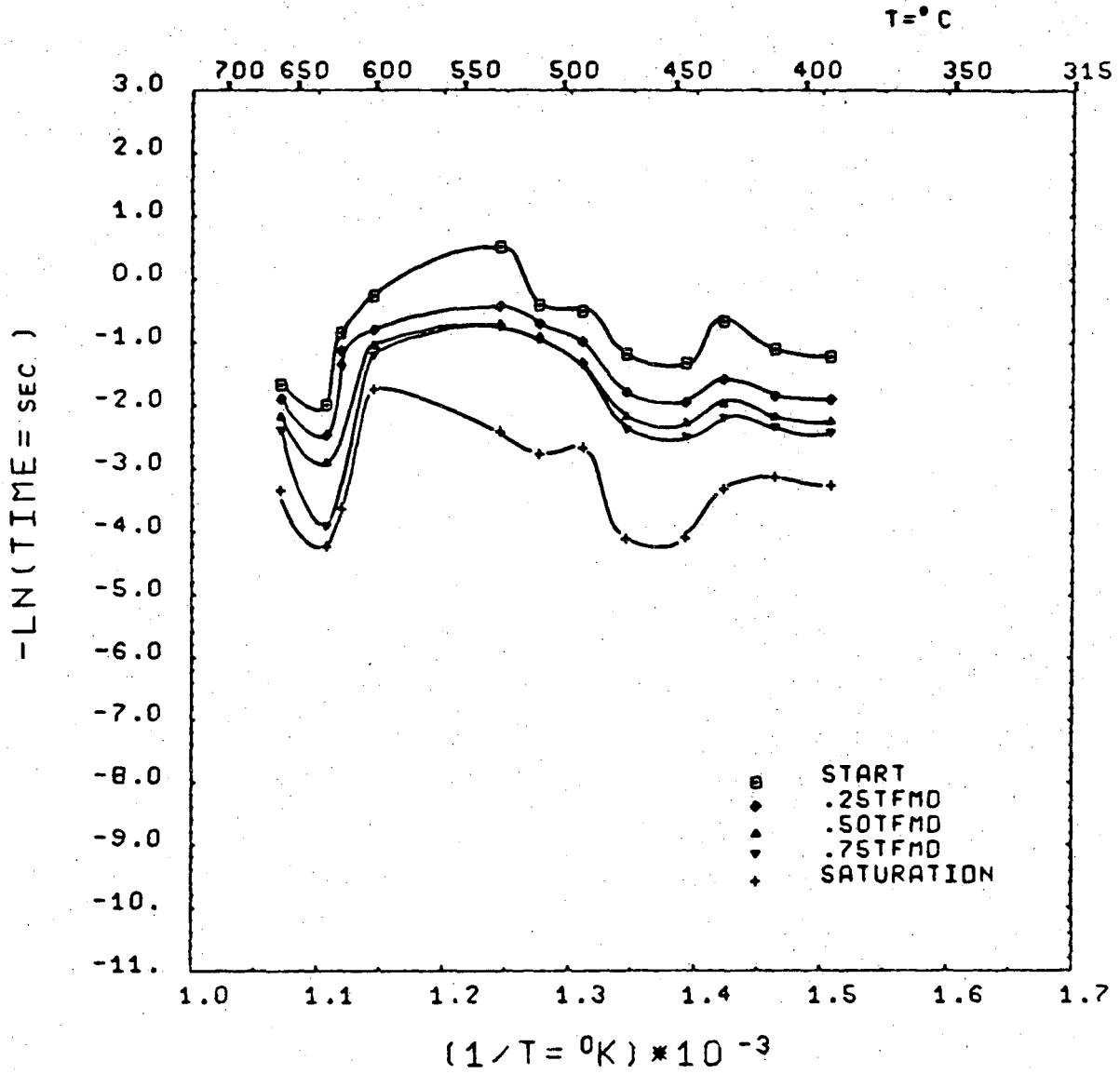
0.39C-2.59MN



XBL 7612-7995

Fig. 47D

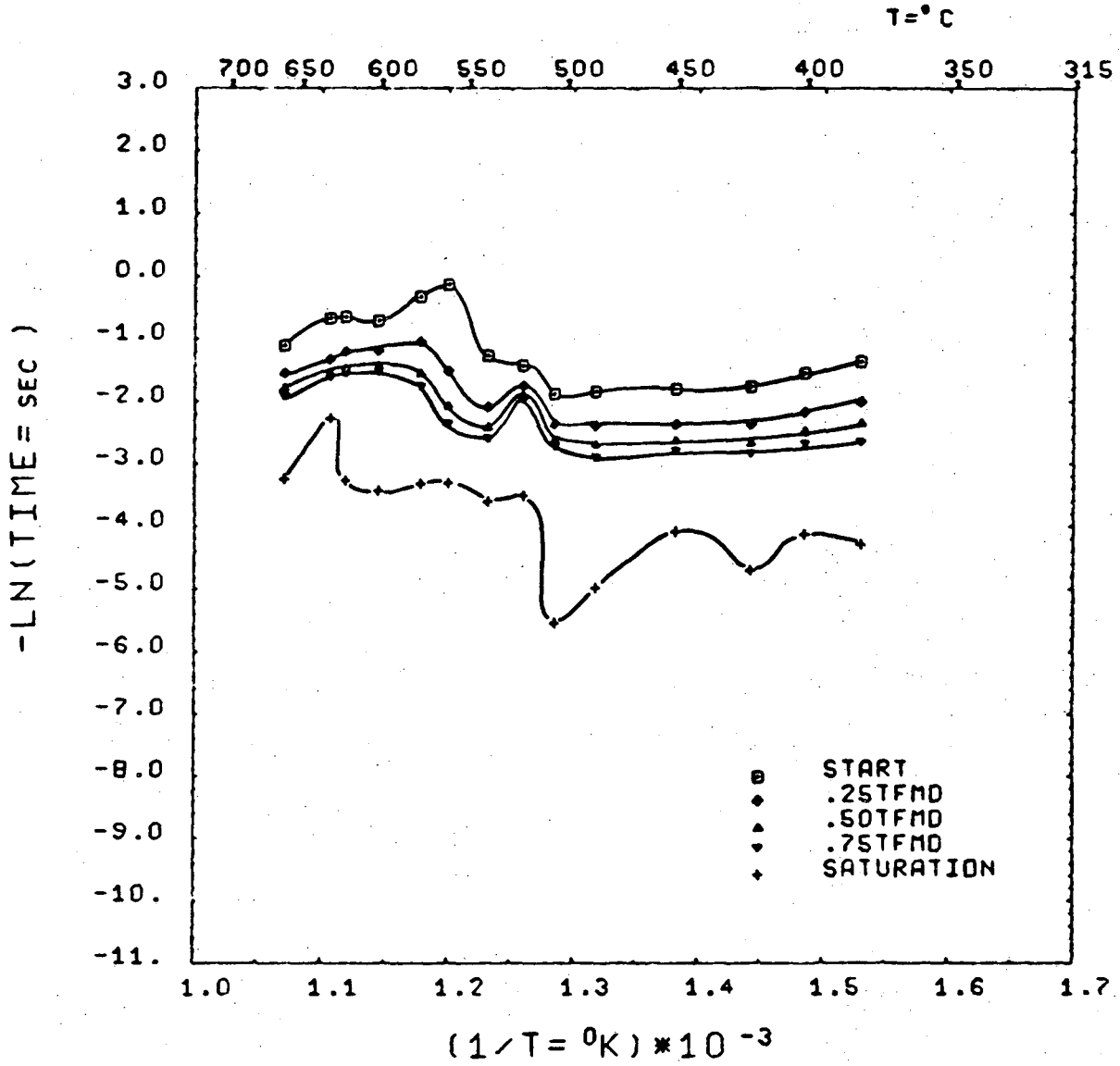
0.37C-0.87AL



XBL 7612-7994

Fig. 47E

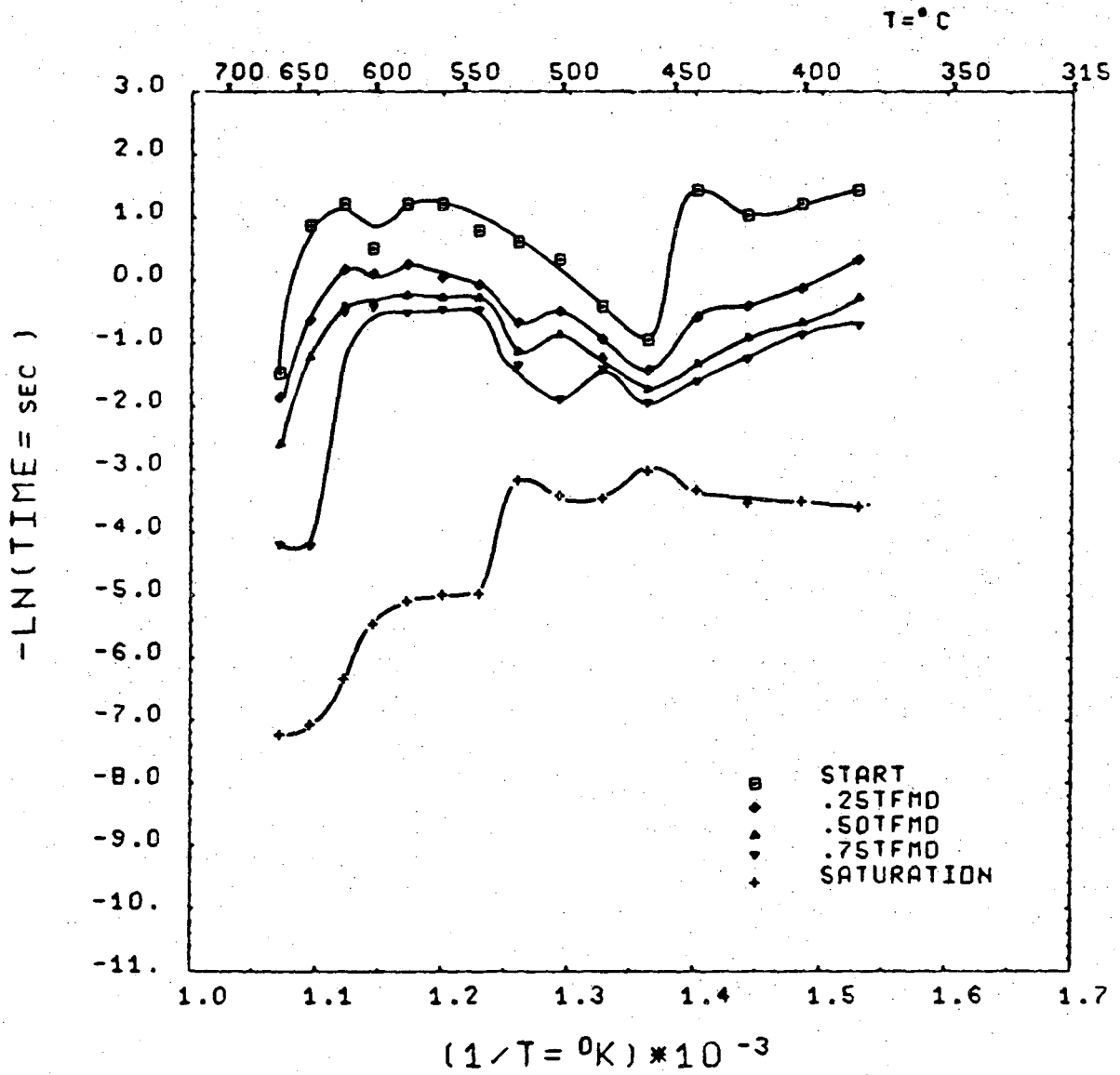
0.39C-0.94SI



XBL762-7993

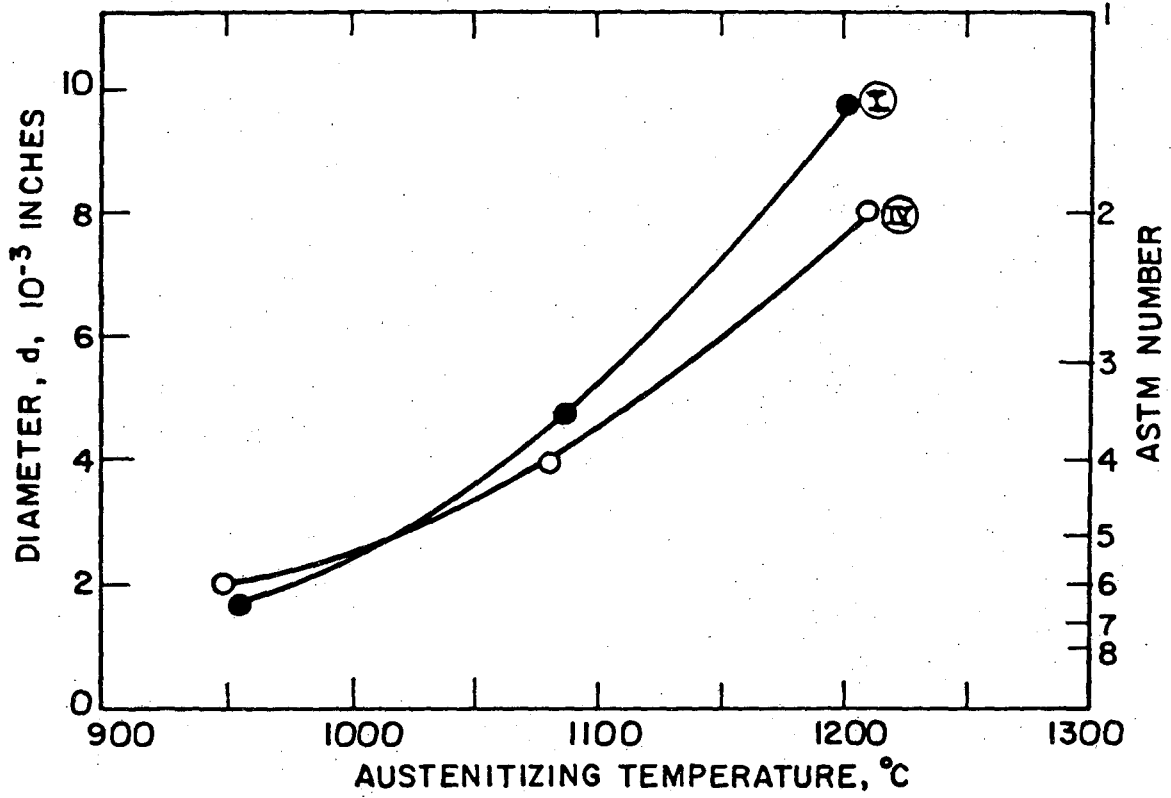
Fig. 47F

0.33C-0.52C



XBL 7612-7992

Fig. 47G



XBL 7512-9287A

Fig. 48



**OPTICAL MICROGRAPHS**

All of the micrographs were taken at 1000x magnification. Figures 49 through 75 and 78 through 85 were reduced 25% during reproduction, and figures 76 and 77 were reduced 10% during reproduction.

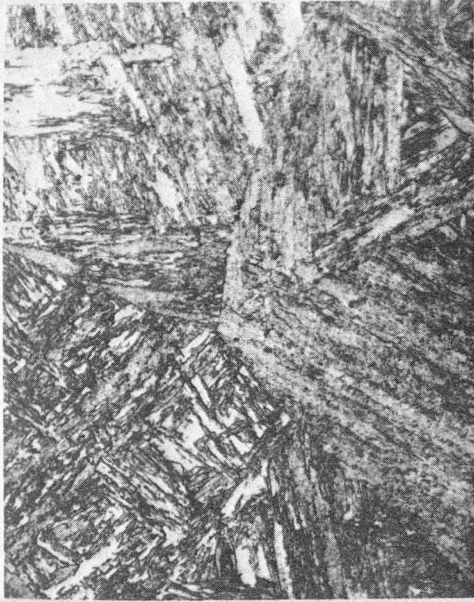


Fig. 49



Fig. 50



Fig. 51



XBB 760-11815

Fig. 52

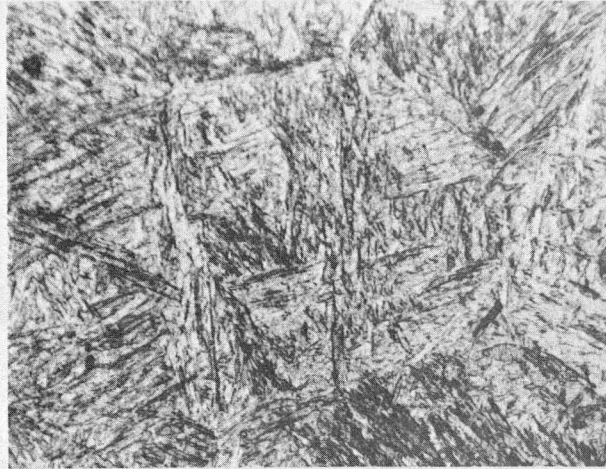


Fig. 53

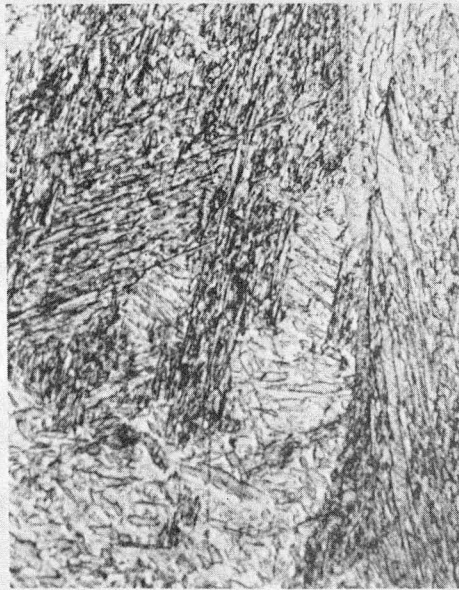


Fig. 54



XBB 760-11817

Fig. 55



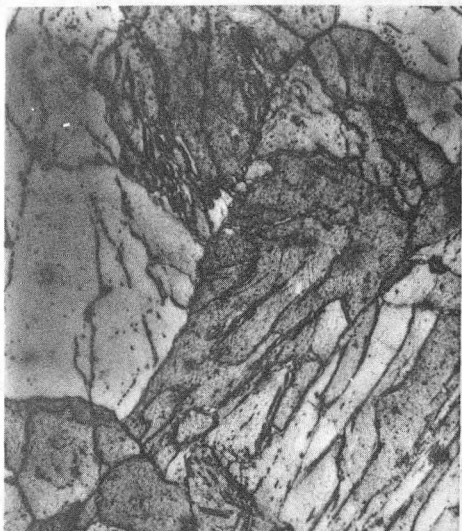


Fig. 56



Fig. 57

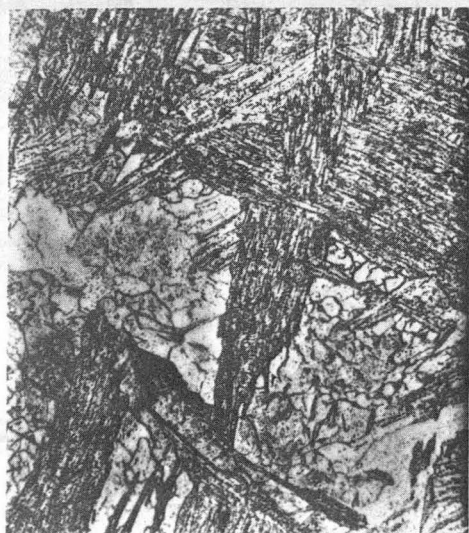


Fig. 58



XBB 7512-9080

Fig. 59

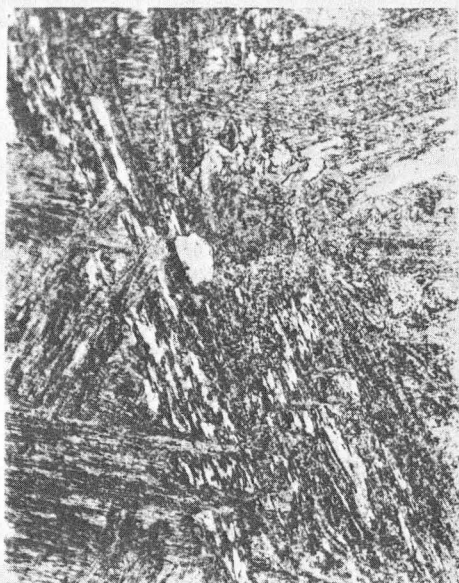


Fig. 60

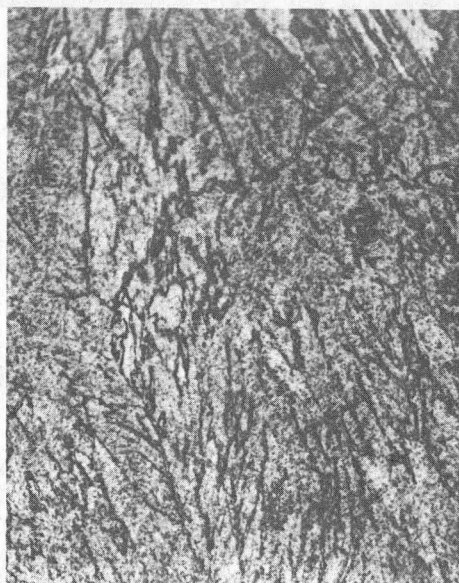


Fig. 61



Fig. 62



XBB 7512-9079  
Fig. 63

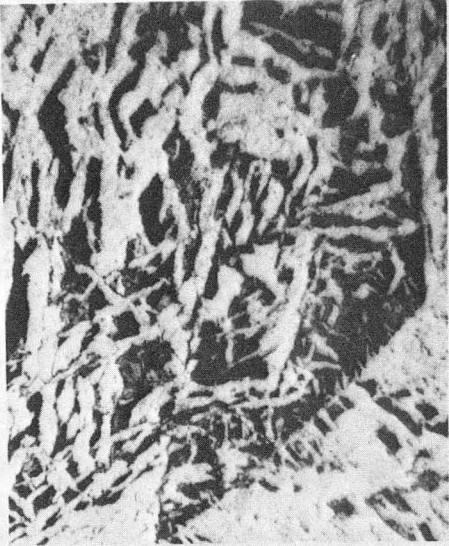


Fig. 64

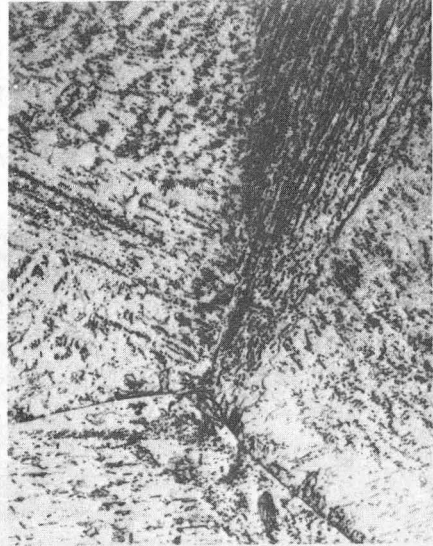


Fig. 65



Fig. 66



XBB 7512-9082

Fig. 67



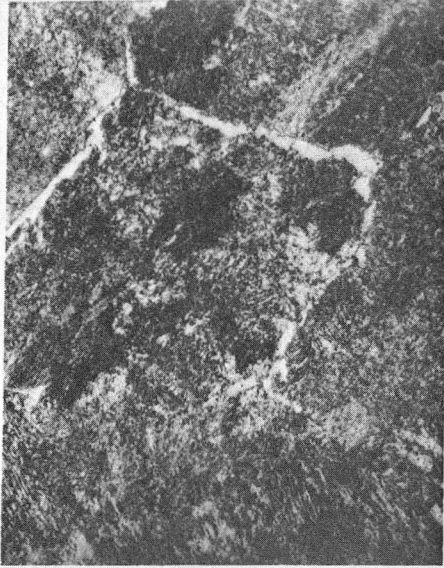


Fig. 68

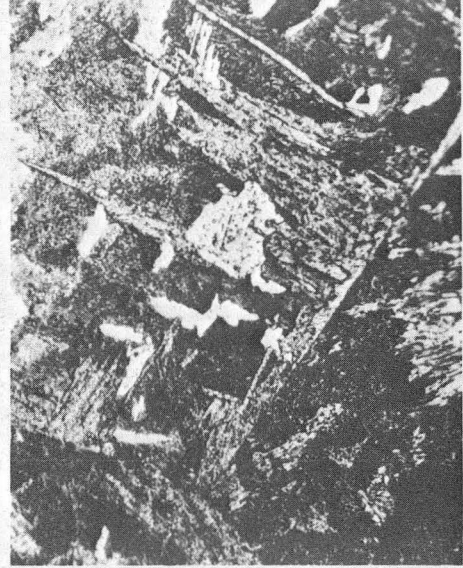


Fig. 69

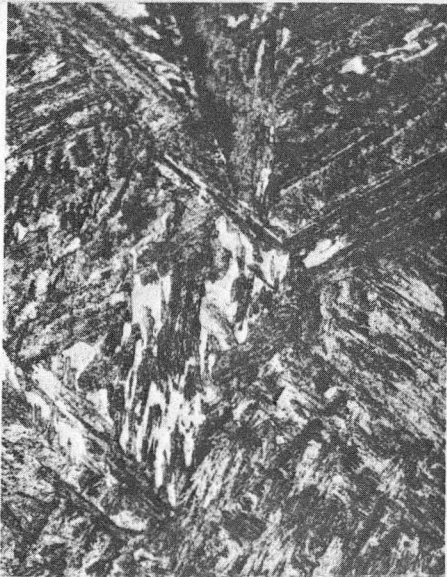
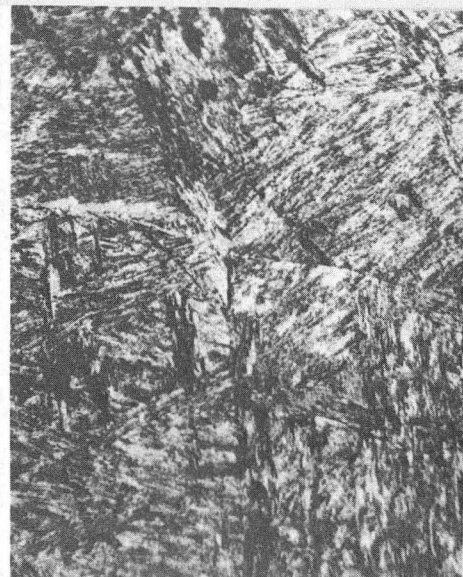


Fig. 70



XBB 7512-9081  
Fig. 71



Fig. 72



Fig. 73

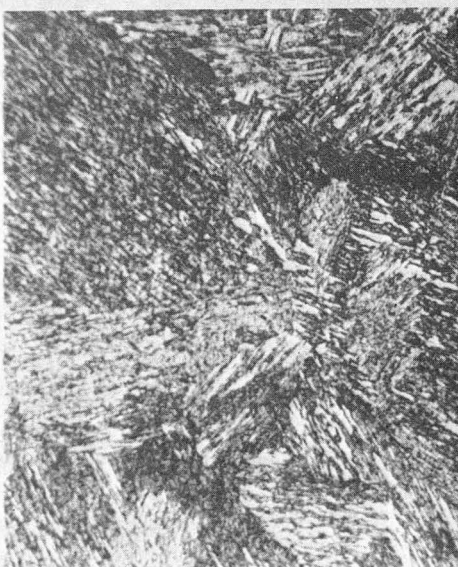


Fig. 74



XBB 760-11816

Fig. 75



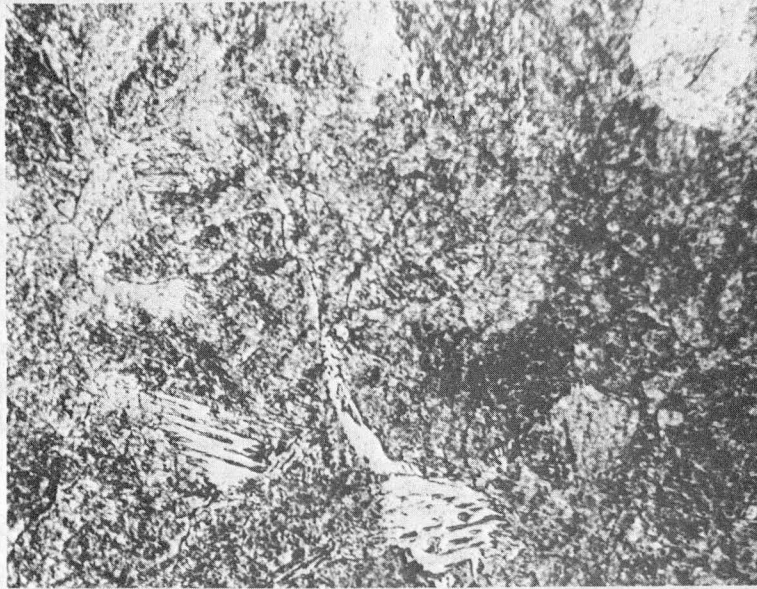


Fig. 76



XBB 760-11819

Fig. 77



Fig. 78



Fig. 79



Fig. 80



XBB 760-11818

Fig. 81





Fig. 82

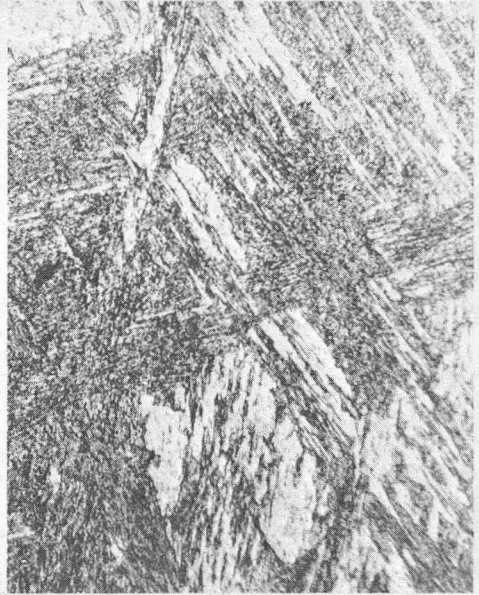
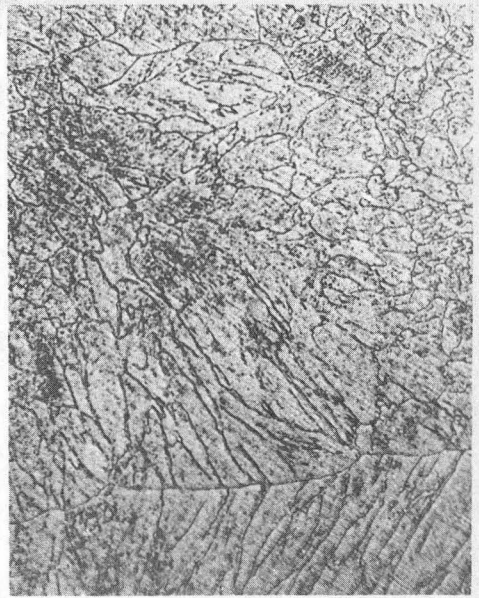


Fig.83



Fig. 84



XBB 760-11814

Fig. 85

This report was done with support from the Department of Energy. Any conclusions or opinions expressed in this report represent solely those of the author(s) and not necessarily those of The Regents of the University of California, the Lawrence Berkeley Laboratory or the Department of Energy.

TECHNICAL INFORMATION DEPARTMENT  
LAWRENCE BERKELEY LABORATORY  
UNIVERSITY OF CALIFORNIA  
BERKELEY, CALIFORNIA 94720